AN EXPERIMENTAL STUDY OF HYPERSONIC WAKES BEHIND WEDGES AT ANGLE OF ATTACK

Thesis by

Jiunn-Jenq Wu

In Partial Fulfillment of the Requirements

For the Degree of

Aeronautical Engineer

California Institute of Technology

Pasadena, California

1971

(Submitted March 26, 1971)

ACKNOWLEDGEMENTS

The author wishes to express his sincere appreciation to Professor Wilhelm Behrens for his helpful guidance during the course of this research program and to Professors Toshi Kubota and Lester Lees for their interest, suggestions and support of this research program. The author is also grateful to Messrs. P. Baloga, S. Roman, J. Van Dijk, G. Van Halewyn and H. Mazurowski of the GALCIT hypersonic wind tunnel for their assistance during the experimental tests; to Mr. G. Carlson and the staff of the GALCIT Aeronautics Shop for constructing the experimental equipment; to Mrs. Truus Van Harreveld for her assistance in data reduction; and to Mrs. Virginia Conner for the excellent typing of the manuscript.

The author wishes to thank his wife Janice for her encouragement and her participation in the processing and reduction of the experimental measurements.

This work was carried out under the sponsorship and with the financial support of the U. S. Army Research Office and the Advanced Research Projects Agency under Contract DA-31-124-ARO(D)-33, part of Project DEFENDER sponsored by the Advanced Research Projects Agency.

ABSTRACT

Experimental measurements of mean flow properties of hypersonic wakes behind wedges of 20° included angle were conducted for angles of attack up to 25° at Mach number 6, with Reynolds number based on wedge base height ranging from 7000 to 55000. The near and far wake structures were determined, including streamlines and velocity profiles, over a downstream distance of 60 base heights. The base pressure is insensitive to angle of attack within about 17°. At higher incidence, flow separation occurs on the leeward surface. The far viscous wake ($x/H \geq 4$) changes with increasing angle of attack mainly because of the increasing differences of the inviscid flow parameters at the leeward and windward edges of the viscous wake. Transition from laminar to turbulent flow moves upstream as angle of attack increases.

TABLE OF CONTENTS

Table of Contents (Cont'd)

LIST OF TABLES

LIST OF FIGURES

List of Figures (Cont'd)

List of Figures (Cont'd)

List of Figures (Cont'd)

List of Figures (Cont'd)

LIST OF SYMBOLS

H	total base height
I	an invariant along a far wake streamline $\left(= \frac{1}{\rho_e U_e H}\left[\int_{y_{e2}}^{y} \rho U(U_{e2}-U)dy + \int_{y}^{y_{e1}} \rho U(U_{e1}-U)dy\right]\right)$
M	Mach number
$P \equiv p$	Pressure
P_{t2}	Pitot pressure
$P_o \equiv P_{t\infty}$	free stream total pressure
Re	Reynolds number
T	temperature
U	streamwise velocity
V	transverse velocity
x	streamwise coordinate
y	transverse coordinate
$\bar{y}$	transformed transverse coordinate $\left(= \frac{U_e}{U_\infty}\sqrt{Re_{\infty,H}}\int_o^{y/H} \frac{\rho}{\rho_\infty} d(\frac{y}{H})\right)$
α	angle of attack
ρ	density
τ	shear stress
$\bar{\chi}$	hypersonic viscous interaction parameter $\left(= \frac{M^3\sqrt{C}}{\sqrt{Re_x}}\right)$
ψ	streamline $\left(= \int_o^y \rho\, U\, dy\right)$

Subscripts

b	base
e_1	leeward edge of viscous wake
e_2	windward edge of viscous wake
H	base height

List of Symbols (Cont'd)

o	initial condition
t	local stagnation quantity
TR	transition
1	upstream of shock
2	downstream of shock
3	downstream of second shock
∞	free stream condition

INTRODUCTION

Great efforts have been made in the last decade trying to understand hypersonic wakes. The problems encountered in hypersonic wakes and progress made up to 1964 were discussed in a paper by Lees.[1] A review of later developments was given by Lykoudis.[2] Because of the complex nature of this subject, most of the detailed flowfield studies were limited to wakes of non-lifting, two-dimensional (for example, refs. 3-6) and axisymmetric (for example, refs. 7, 8) bodies. Theoretical studies were naturally carried out at the same time (for example, refs. 9-11). In many cases reentry bodies are nonsymmetric or are flying at angles of attack.[12] Relatively little is known about hypersonic wakes of lifting bodies, for example symmetrically shaped bodies at angle of attack, even though studies have been made.[13]

There is still a lack of understanding of how sensitive the near wake is to small angles of attack, when the changes occurring in the base region affect the flow on the leeward side of the body, what effect a "large" angle of attack has on the near wake (base pressure, wake neck and rear stagnation point location, shearflow profiles), the far wake flowfield (inviscid flow, static pressure distributions, viscous wake growth and velocity profiles) and on transition from laminar to turbulent flow.

These are questions which were studied in the present experimental investigation of the flow at Mach 6 over 20 degree-wedges at angles of attack up to 25°. This body-shape was chosen because

careful near and far wake flowfield results for the same wedges at zero angle of attack were available (Batt and Kubota[6]).

In order to find out what effect an angle of attack has on the overall flowfield, a simple shock expansion model was employed to estimate the inviscid flowfield. In 1948, Kahane and Lees[14] calculated the inviscid flowfield about a two-dimensional flat plate at small angle of attack, moving at supersonic speeds. They found, somewhat surprisingly, that there was an upwash directly behind the trailing edge of the airfoil. For flows over wedges the inviscid flow is undetermined unless the base pressure is specified. Thus, for given base pressures the inviscid flow, consisting of oblique shocks and Prandtl-Meyer expansions was calculated. A typical example of the resulting inviscid flowfield is given in Figure 1 for the flow over a 20° wedge at Mach number 6 and at angle of attack of 15°.

As in the case of the flat plate at angle of attack there is an upwash, as indicated by the angle the slip line makes with the free-stream direction ($\delta_{slip} = 1.19^\circ$ in this example, for $P_b/P_\infty = 0.25\text{-}0.5$). Since in this model the flow direction behind the wake shocks is found by matching the pressures and the flow directions for the flows coming from both sides of the wedge, there is one wake pressure and one flow direction but a slip line across which velocity and temperature jump considerably ($u_{e2}/u_{e1} < 1$, $T_{e2}/T_{e1} > 1$). It is expected therefore that the viscous wake beyond the wake neck, formed from the coalescence of the free boundary layers which have separated from the wedge at or ahead of the base, differs from the symmetric wake because of the differences in inviscid flows

at the leeward and windward edges of the viscous flow. In the near wake the situation is more complicated.

Because of viscous-inviscid flow interaction near the leading edge of the models, a shock wave was observed on the leeward side even when the leeward side was inclined away from the free stream and the inviscid flow model would predict an expansion (see Figure 1). The flow on the leeward side of the wedge and in the near wake region is obviously dominated by viscous-inviscid flow interactions. At "large" angles of attack separation occurs on the leeward side.

A description of the measurements and experimental techniques is given in Section II. Section III discusses the data reduction and uncertainties in the measurements. Results are presented and discussed in Section IV, followed by a summary in Section V.

II. EXPERIMENTAL APPARATUS AND TECHNIQUES

II. 1. GALCIT Hypersonic Wind Tunnel

The experimental work reported herein was conducted in the GALCIT Hypersonic Wind Tunnel, Leg 1. A more complete description of this facility was given by Baloga and Nagamatsu.[15] This tunnel is a continuous flow, closed return device with a 5 in. x 5 in. test section and a nominal Mach number of 6. Models were placed at the center of the third port which was about 23 in. downstream of the nozzle throat. This arrangement permitted wake measurements to approximately 10 in. downstream of the model.

Reservoir pressures of 10, 35, 60 and 85 psig, with corresponding free stream Reynolds number of 0.465, 0.94, 1.42 and 1.9×10^5/in. were selected for tests. A reservoir stagnation temperature of 275° F and a dew point of -40° F (the specific humidity is smaller than 5×10^{-5}) was maintained for the present investigation, which satisfactorily eliminated condensation effects. The tunnel was warmed up for approximately two hours before any data were taken.

Static pressure and Pitot pressure surveys in the empty wind tunnel have been conducted by many investigators.[4, 5, 6, 16] Good agreement between these surveys was observed. The static pressure variations along the centerline of the tunnel conducted by Batt[6] were adopted to normalize the static pressure survey in the present tests.

II. 2. Models

Two wedges of 20° included angle which were originally used

by Batt[6] in his surveys of hypersonic wake behind wedges at zero angle of attack were used for the present test. These two models were fabricated from solid pieces of Ketos steel and had base heights of 0.15 in. and 0.3 in. respectively. The leading edges of these two models were carefully machined to a thickness of less than 0.002 in.

The wedge model with a base height of 0.3 in. is shown in Figure 2a. Four surface pressure taps and one base pressure tap all of 0.0135 in. in diameter were installed on it, and were joined by stainless steel tubing pressure leads, 0.042 in. in diameter, flush-mounted in surface grooves and led out of the side port of the tunnel. Three of the surface pressure taps were installed at one side of the wedge surface with respective distances of 0.050 in., 0.130 in. and 0.195 in. from the trailing corner. The fourth surface pressure tap was on the other side of the wedge surface and was 0.195 in. from the trailing corner. The base pressure tap was at the center of the wedge base. A metal arm, approximately 4 in. in length, with a needle on its end, was clamped on the model's shaft outside the tunnel to serve as an indicator of incidence.

The other model used was a wedge with 0.15 in. base height. This model had two base pressure taps, 0.0135 in. in diameter, installed on the centerline of the wedge base. A base pressure lead, 0.042 in. stainless steel tubing, was flush-mounted in the base groove and brought out of one of the side ports of the tunnel as shown in Figure 2b. A metal arm, approximately 2 in. in length with a needle on its end was clamped on the model's shaft outside the tunnel to serve as an indicator of incidence.

Models were installed at an incidence of 10° when the upper surface was leveled. Alignment of the models with the free stream flow was checked by the symmetric property of Pitot pressure traces in the wake at zero incidence. For the larger wedge (H = 0.3 in.), alignment at zero incidence was further checked by connecting the corresponding lower and upper surface pressure taps to each side of a silicon "U" tube, to make sure that the pressures were equal.

II. 3. Static Pressure Measurements

A conventional cone-cylinder static pressure probe was employed to measure the static pressure distribution in the wake. This probe was fabricated from a 0.032 in. stainless steel tubing with three pressure orifices being located ten diameters behind its shoulder and with a 20° cone tip. The length between tip and orifices of the static pressure probe prevented measurements in the near wake up to approximately x/H = 1.5 for the larger wedge (H = 0.3 in.) and x/H = 3.0 for the smaller wedge (H = 0.15 in.). A similar probe of 0.042 in. in diameter was designed and calibrated by Behrens.[17] Those results were applied to correct the data measured by the present probe.

A silicon micromanometer was connected to the probe to measure the static pressure. The reference pressure was maintained at about a half micron of mercury by using a diffusion pump in series with a mechanical vacuum pump. All joints were carefully sealed by using vacuum grease and glyptol to prevent possible leakage. This arrangement enabled the pressure readings to an accuracy of 0.01 mm of silicon. Because of the slow response time of the static pressure

measuring system, it was necessary to wait for a few minutes before a measurement was taken. Figure 4 shows a typical vertical static pressure trace in the proximity of minimum Pitot pressure point.

II. 4. Pitot Pressure Measurements

A stainless steel tube, 0. 032 in. in diameter, flattened to approximately 0. 040 in. x 0. 010 in. at the forward end, with a front opening of about 0. 030 in. x 0. 003 in. was used as a Pitot pressure probe. A 0 - 5 psi Statham pressure transducer which was calibrated against a mercury manometer to be 922 microvolts per psi per one volt excitation was used to convert pressure measurements to electrical signals. The reference pressure used was the same as that for the static pressure measurements (Section II. 3). In practice, the output signal from the pressure transducer was amplified to the desired voltage level, and at the same time, the position of probe was converted to an electrical signal by employing a Helipot potentiometer which was being activated by the probe positioning mechanism. A Moseley XY recorder was used to record the pressure and position signals simultaneously on a piece of 15 in. x 10 in. graph paper. The data obtained in this manner were then "read" by a digitizer which converted the data from graphical form to digital form and punched their coordinates into data cards for computer calculation. This digitizer could accurately subdivide 1 in. into about 800 units. The number of data points taken at each streamwise station ranged approximately from 100 to 300.

II. 5. Flow Visualization

The flow separations were visualized by applying a thin coat

of light machine oil on the leeward surface of the model. Normally, after starting the tunnel, the wind swept the oil and caused an oil film to accumulate in the reverse flow region, therefore clearly marked the boundary of dividing streamline. For cases with higher incidences, the model tended to block the tunnel and caused difficulty in starting the tunnel. However, this difficulty was overcome by first setting the model at a lower incidence (i.e., 10° or 15°), then gradually turning the model to the desired higher incidence. This process caused oil first to be swept to the base of the wedge, and then to travel upstream until it reached the separation point.

The results were recorded and photographed from outside the tunnel. The photographs were then read more accurately by using a comparator.

III. DATA REDUCTION AND ACCURACY ESTIMATE

III. 1. Discussion of the Measured Data

The validity of the measured data depends on the two-dimensionality of the flow, and the wake flow being free from shock waves reflecting from the tunnel walls. The problem of two-dimensionality of the flow primarily depends on the strength of the interaction caused by the existence of the sidewall boundary layer, the model and its leading edge shock waves. Similar problems were encountered by McCarthy[3] and Behrens[5] in their experiments of hypersonic wakes behind cylinders. The flow is sketched in Figure 5 which is qualitatively similar to the one given by McCarthy.[3] It is worth noting that the region of flow without interference is a function of free stream Reynolds number, model size and its angle of attack.

During the present investigation, no base fence was installed on the models, yet the measured base pressure compared favorably with those given by Batt[6] which were measured using the same models but with base fences. The agreement of the base pressures is an indication that reasonably two-dimensional flow was established in the near wake.

The wall boundary layer-model interference spreads to the center of the wake 3 to 4 inches downstream of the model (Figure 5). It becomes noticeable only at large angles of attack. Besides this disturbance there is an interference in the far wake caused by the reflection of the leading edge shock from the tunnel wall (Figure 6).

This interference could be detected by both static pressure measurements and Pitot pressure measurements. Only data without noticeable interferences were used. A summary of all data obtained in this study is given in Table I.

III. 2. Base Pressure

All base pressures were measured by using the base pressure tap installed on the models and connected to the same silicon micromanometer as that used for the static pressure measurements. Even at this low pressure, a leak correction to the measured data was estimated to be unimportant for the present pressure measuring system. No correction was made. Close agreement was found between the present data and the corresponding measurements of Batt.[6]

For the larger wedge model (H = 0.3 in.), measurements were made for both positive and negative angles of attack. The results for the same positive and negative angles of attack compare with each other within ± 3%.

III. 3. Static Pressure

Extreme precaution was taken in the static pressure measurements to minimize the undesirable leakage and outgassing effects. The static pressure probe was connected to the vacuum system with its pressure orifices sealed by tape when it was not being used. Leak corrections to the measured data were estimated, by using perfect gas law and Hagen-Poiseuille pipe flow theory, to be small, usually only a small fraction of a percent of the measured data. No correction was made.

The viscous-inviscid interaction phenomenon for this type of probe was investigated by Behrens as mentioned in Section II. 3. The pressure excess (i.e., Δp = measured pressure - actual pressure) introduced due to this type of probe was expressed in terms of the interaction parameter $\bar{\chi}$, and is given by the following relation.[17]

$$\frac{\Delta p}{p} = 0.065\,\bar{\chi} + 0.04\,\bar{\chi}^2$$

where,

$$\bar{\chi} = \frac{M^3\sqrt{C}}{\sqrt{Re_x}} \quad , \qquad C = \left(\frac{\mu_w}{\mu}\right)\left(\frac{T}{T_w}\right)$$

x = distance measured from the tip

All measured static pressure data were properly corrected by this equation before being used in the mean flow calculations. It is a well-known fact that the static pressure probe is sensitive to its "misalignment" with respect to the stream; in other words, the angle of attack of the probe has significant influence on its measurement. McCarthy[3] made a quantitative investigation of a probe similar to the one used in the present tests, but his results were limited to very small angles ($\pm 2^\circ$). Recently, Igawa* did a systematic study of cone-cylinder static pressure probes with angles of attack as high as $\pm 25^\circ$. The primary difference between the probes Igawa used and the present probe is that the present probe had three pressure orifices located at 120° intervals while Igawa's probes had two or four pressure orifices installed at various angular locations. One

* Graduate Student, GALCIT

of Igawa's important findings is that the deviation in the pressure caused by angle of attack is less than ± 4% for 5° incidence, and less than ± 10% for 10° incidence for all probes he investigated. Taking the misalignment of the probe into consideration, the uncertainty for most of the static pressure measurements was estimated to be of the order of ± 5%, or smaller for the lower angles of attack. But for the larger angles of attack and at lower free stream Reynolds number (for instance, H = 0.3, $Re_{\infty, H} = 1.4 \times 10^4$, $\alpha = 20°, 22.5°$), the uncertainty might be as high as ± 10%.

In the near wake, no static pressure measurements were taken due to the length of the probe. For the purpose of data reduction, the static pressures in this region were interpolated from the measured wake pressure and base pressure data.

After being corrected for the viscous-inviscid interaction, the static pressures were normalized with the free stream pressure, using the free stream data given by Batt.

III. 4. Pitot Pressure

The Pitot traces provide an accurate measurement of wake geometry and one important flow parameter. The Pitot probe is relatively insensitive to the flow inclinations as demonstrated by McCarthy.[3] McCarthy's results showed that for flow inclinations less than 15°, the error in the measurement was of the order of 1% and only about 4% for 25°. Errors introduced due to higher flow inclinations can be estimated from measurements in well defined flow regions of the present test, e.g., the flow on the windward side of the wedges. The flow on the windward side is very nearly

parallel to the windward side surface of the wedge. Therefore, the sum of angle of attack and wedge half angle (10°) yields the flow inclination. Knowing the free stream conditions and the angle of the windward surface with respect to the free stream, the flow behind the oblique shock may be calculated. For the highest angle of attack (25°), with a flow inclination of 35°, and a downstream Mach number of about 2, the measured Pitot pressure is about 8% less than the value calculated by the above mentioned procedure. Since most of the flow inclinations encountered in the present tests are far below 35°, the error in the Pitot pressure measurements due to misalignment of the probe is small.

Pitot pressure behind leading edge shocks

Knowing the free stream conditions and the Pitot pressure jump across an oblique shock, the shock angle and the conditions behind the shock may be calculated, including the stagnation pressure which is necessary for the calculation of the static pressure in the inviscid flow at the edge of the viscous wake (see Section III.6). Problems arise when the shock angle becomes of the order of 30°, as shown in Figure 8, where the theoretical inviscid Pitot pressure (P_{t_3}/P_{t_1}) and total pressure (P_{t_2}/P_{t_1}) downstream of an oblique shock wave are shown. These pressures for three free stream Mach numbers of 5.9, 6.0 and 6.1 are shown to demonstrate the effect of upstream Mach number on the downstream Pitot pressure. This figure indicates that the Pitot pressure (P_{t_3}/P_{t_1}) for these upstream Mach numbers has a maximum near a shock wave angle of 30°. If the angle of the oblique shock wave is in the range of 25° to

40°, evaluation of downstream total pressure from the measured Pitot pressure jump may lead to a considerable error even if the downstream Pitot pressure measurement is in error by only a few percent. A second problem occurs when the shock angle is large. The Pitot pressure measurement across the windward side leading edge shock wave near the wedge generally experiences an overshoot on the high pressure (downstream) side of the shock wave, as shown for example in Figure 7d. For the highest angles of attack addition on undershoot occurred on the lower pressure side ahead of the shock wave. The reason for these overshoot and undershoot phenomena is not known but is believed to be caused by the interaction of the oblique shock wave and the detached shock wave of the Pitot probe.

The edge shock wave on the leeward side is very weak, therefore the downstream flow conditions can be accurately evaluated from the Pitot pressure jump across these shocks. Table II summarizes the leading edge shock wave angles near the wedge for the present tests. This table was obtained by measuring the shock wave inclination which was constructed by connecting the shock wave locations and the model's leading edge as shown in Figure 6, and checked by the jump relations of the Pitot pressure where possible. The accuracy of the shock angles determined in this way is estimated to be $\pm 1^{o}$.

Streamline displacement effects of the Pitot probe in the measurements of shear layer flows and shock wave locations are assumed unimportant in the present experiments. It is estimated

that the shear layer thickness encountered in the present wake flow measurements is at least three times larger than the present probe dimension, and according to Dewey's[4] results, the displacement effects are negligible.

In the interpretation of wake geometry from the Pitot pressure trace, a pressure level half the measured jump is considered as the location of the shock wave. Bannink and Nebbeling[18] indicated that the error introduced by the displacement effect is of the order of one tenth of the probe's outer dimension and is directed towards the region of higher pressure. Accordingly, the uncertainty of the location of shock wave introduced by the displacement effect in the present experiment is estimated to be less than one percent of the wedge base height, and therefore, is a negligible source of error.

Another error of Pitot pressure measurement comes from rarefaction and viscous effects. According to the data given by Sherman,[19] this source of error is in the present tests confined to the base flow regions with subsonic speeds and low Reynolds numbers. No effort was made to correct for these errors. The estimated error may become as high as 20%, however detailed measurements were not made in the low density low speed base region.

III. 5. Location of Flow Separation on Leeward Surface

The method of obtaining the location of flow separation on the leeward surface was described in Section II. 5. The data obtained by reading the photographs and further confirmed with visual estimation are presented in Table III. The reliability of the data is not well known because of a potential error from the distortion caused by taking the photographs through a plexiglass window, especially when the closeup lens was used. No correction was made for the final results of flow separation shown in Table III.

While conducting oil-film experiments in separated and reattaching flows, Chapman et. al.,[20] in turbulent boundary layer separation found a simultaneous occurrence of two thread-like lines which were stable, repeatable, and normal to the stream direction and which were displaced streamwise a distance equivalent to several boundary layer thicknesses. The downstream oil line was located at separation. In the present experiments, the separation is laminar, and only one oil line was observed and believed to be at separation.

III. 6. Data Reduction Procedure

Flow variables

Three independent flow parameters have to be known in order to reduce the raw data to primary variables. These independent parameters were (a) measured Pitot pressure, (b) measured static

pressure or stagnation pressure determined from the slope of the shock wave, and (c) estimate of stagnation temperature. Two different procedures were employed to accomplish the data reduction; one in the viscous wake, and the other in the inviscid wake.

Total temperature surveys in the wake behind a symmetric wedge of H = 0.3 in. base height were made by Batt.[6] The results indicated that, for the adiabatic wedge, the ratio of total temperature along the wake center line to its free stream value varied from 87% on the base to 95% at X/H = 30 for the same Reynolds number range as in the present test. These results suggested that the assumption of isoenergetic flow with $T_t = T_{t,\infty}$ is a good first approximation. This assumption was used throughout the data reduction.

Reduction of viscous wake data was executed by assuming a constant static pressure across the viscous wake. (A discussion of the validity of this assumption follows below.) By combining static and Pitot pressures and taking the total temperature as a constant equal to its free stream value, other flow quantities were calculated, applying compressible flow relations.

Inviscid wake data reduction proceeded as follows: The leading edge shock wave on the leeward side was observed to be very close to a straight line within the region of interest, except from a very small portion near the leading edge of the model. Therefore, all streamlines in the inviscid wake flow on this side were assumed to suffer the same total pressure loss in passing through the oblique shock wave. Because most of the inviscid wake flow

considered here on the windward side consisted of the flow along the streamline which passed the straight portion of the windward side leading edge shock wave, the same argument as for the leeward flow applies. The total pressure losses could be determined, knowing the angle of the leading edge shock waves and the free stream conditions. Consequently, at each point in the inviscid wake the Pitot pressure, stagnation pressure and stagnation temperature were known. These quantities provide enough information to determine all flowfield variables.

In the near wake flows, the viscous regions extend beyond the wake shock waves; Pitot pressure jumps across these shock waves were used to evaluate the static pressure jumps. Since the static pressure is known inside the wake shocks, it could be calculated ahead of the shock. The boundary of application between the two data reduction procedures in the viscous and inviscid wake was determined by the fact that $P_{t\ inviscid} \geq P_{t\ viscous}$; in other words, the constant pressure data reduction procedure was applied in the viscous region toward the inviscid region until it reached a point where the total pressure had a magnitude just below the magnitude of the total pressure calculated for the inviscid flow. A typical result of the near wake calculation is shown in Figure 9 which indicates that the present data reduction scheme gives consistent results, as shown by a comparison with the results of Batt, who calculated the flow conditions by using measured Pitot pressure together with the total temperature and mass flux data measured by a hot-wire.

As mentioned, constant static pressure across the wake was assumed for the far wake data reduction. To check this assumption the inviscid data reduction scheme was used to obtain the static pressure downstream of the wake shocks. Typical results of this calculation showed that the static pressure obtained in this manner was up to 20% less than measured inside the viscous wake. Even with this discrepancy in static pressure, the final results, such as velocity, are not changed significantly. (At M = 6, an error in P_{stat} of 20% results in an error in velocity of 0.5%.)

Most of the data reduction calculations were carried out on an IBM 360/75 computer. Some of the graphs were plotted by a Calcomp Plotter,

Streamlines

Near wake streamlines were constructed by integrating the mass flux from the leeward side leading edge shock wave towards and across the viscous wake. Since the mass flux in the recirculation region is very small (see Batt[6]), the effect of the reverse flow was neglected in the present investigation and was considered as a region of zero mass flux.

Far wake streamlines were constructed in a different fashion, because no reference starting point could be reached. (The leading edge shock was outside the range of measurement.) However, the following quantity is a constant along a streamline (See Appendix):

$$I = \frac{1}{\rho_\infty U_\infty^2 H}\left[\int_{y_{e_2}}^{y} \rho U(U_{e_2}-U)dy + \int_{y}^{y_{e_1}} \rho U(U_{e_1}-U)dy\right] \quad (1)$$

This invariant along a streamline served as a principal tool for the construction of far wake streamlines. The dividing streamline could not be determined by simply examining the far wake data. The minimum velocity point at $x/H = 5$ was taken as the starting point to evaluate a streamline close to the dividing streamline. The far wake "dividing streamline" was then determined, using relation (1). Judging from the results of the near wake flowfield, the dividing streamline obtained from this assumption was somewhat lower (toward the windward side) than that obtained by the near wake calculation.

IV. RESULTS AND DISCUSSION

IV. 1. Far Wake Flowfield

The portion of the wake upstream and including the wake neck is defined as the near wake, while the wake downstream of the neck in the region where the wake shocks are formed and the pressure is constant across the wake is considered the far wake ($x/H \geq 4$).

IV. 1. 1. Pressure Field and Viscous Wake Edge Flow Parameters

Pressure Field

The static pressure measurements at the location of minimum Pitot pressure are shown in Figures 10a-10d (H = .15") and Figures 11a, b (H = .30") as functions of distance from the wedges (x/H) and as function of angle of attack for a series of Reynolds numbers ($Re_H = 7 \times 10^3$ to 5.5×10^4). The results for the large wedge (H = 0.3") are replotted on an enlarged scale in Figures 12a,b to show some details in the near wake. As discussed in Section III, the static pressure is reasonably constant across the viscous wake, so that the measurements presented here are the proper viscous wake static pressures.

In all cases tested the streamwise static pressure data indicate an initial overshoot followed by a gradual decay back to free stream conditions. Beyond $x/H \gtrsim 50$, especially at the larger angles of attack, interference effects are visible (Fig. 10a for example). The overshoot depends very strongly on angle of attack, the higher the angle of attack, the larger the overshoot.

The effect of Reynolds number on the overshoot was discussed by Batt in his symmetric wake experiments. Batt's experiments showed that the lower the Reynolds number, the higher the overshoot. Similar

results were found in the present tests as shown in Figures 13 a-c, where the pressure data are replotted as functions of x/H and Reynolds number for a given angle of attack.

These Figures show that also at angle of attack the "centerline" pressure is the higher the smaller the Reynolds number. However at the smallest Reynolds number (Re_H = 7000) at which the wake remains laminar, the pressure does not rise as fast beyond x/H = 4 as at the higher Reynolds numbers. This somewhat faster rise of static pressure at the higher Reynolds numbers is attributed to instabilities in the near wake (see Section IV. 1. 3. on transition).

The overshoot in static pressure as function of angle of attack may be explained by a simple inviscid shock-expansion model as already discussed in the introduction. First, however, the viscous wake edge results will be presented, since they also may be calculated using the same model.

Viscous Wake Edge Properties

In the far wake ($x/H \geq 5$) where the wake shocks are well formed, the Pitot pressures are at two distinct levels on each side of the viscous wake (see Figures 7a-e). The Pitot pressure levels together with the measured static pressures (and $T_o = T_{o,\infty}$) yield the viscous wake edge quantities, such as velocities, temperatures and Mach numbers. Representative results of the edge quantities as function of x/H are given in Figures 14a to 14e* for angles of attack of 5 to 25° at one Reynolds number (Re_H = 7000).

---

* The minimum velocities and Mach numbers and maximum temperatures in the viscous wake will be discussed in Section IV. 1. 2.

The edge values of velocity, Mach number and temperature on the leeward side for all angles of attack are very close to the free stream values. However on the windward side these quantities change considerably with angle of attack. The velocity and Mach number decrease and the temperature increases with angle of attack. At all angles of attack the edge velocity and Mach number increase slightly and the temperature decreases as the flow moves downstream, indicating a slow expansion of the wake flow in the region behind the wake shocks. Compared to the changes taking place inside the viscous wake these slight gradients at the edges of the viscous wake are very small.

To better illustrate the changes of the wake edge quantities as function of angle of attack, the values measured at x/H = 10 are plotted versus angle of attack (Figs. 15a-c). As shown in these figures the effect of Reynolds number is very small, yet a systematic decrease of windward velocity and Mach number with decreasing Reynolds number is perceptible.

Comparison of Experimental Wake Edge Flow Quantities with Inviscid Flow Calculations

Even though the real flow over the wedge is quite different, the simple inviscid shock expansion model, mentioned in the introduction, has been used to calculate the wake static pressure and the velocities and temperature levels outside the viscous wake. The base pressures of $P_b/P_\infty = 0.25$ and 0.5 are chosen as two guide lines of the present inviscid calculation. This choice is consistent with the present range of base pressure measurements. Since the static pressures were

found to be nearly constant across the viscous wake, the measured wake pressure levels (maximum values found in the wake) are compared with the calculated values in Figure 16. The calculated pressures certainly show the proper trend. At high Mach numbers the static pressure is the most sensitive quantity. The wake pressure level is quite insensitive to the base pressure level and also Reynolds number. The measured wake pressure level for the case $Re_H = 7000$, $\alpha = 25^\circ$ appears high. Side wall interference might have been of importance. The difference between the edge velocities is plotted as function of angle of attack and compared with the inviscid calculation in Figure 17. Close agreement between measured and calculated velocities was found. Figures 18 and 19 present the findings of inviscid calculation and the far wake measurements of Mach number and temperature levels at the two edges. The inviscid edge Mach numbers and temperatures are again quantitatively quite close to the measured values at the edges of the viscous wake.

From this inviscid calculation, the inclination of far wake dividing streamlines may be obtained and is summarized in Figure 20 as function of angle of attack. This figure also includes the results inferred from the measurements (see also Section IV. 1. 4.). Again, good agreement between experiment and theoretical model is demonstrated. Note that the wake flow inclination is directed towards the leeward side.

The close correspondence between the simple inviscid shock expansion model and the real wake flow outside the viscous wake for $M_\infty = 6$, $\alpha \leq 25^\circ$ indicates that the inviscid "far wake" flow is determined

mainly by the relative strengths of the leading edge shocks and the fact that the flows at the edges of the viscous wake have to be nearly parallel to each other, with a very weak dependence on the base flow, i.e. on base pressure and Reynolds number. Because of separation on the leeward model surface and substantive changes of the "effective body" associated with separation, this simple inviscid model might not be as good at angles larger than 25°.

IV. 1. 2. Viscous Wake Width and Minimum and Maximum Properties

The location of wake edges were determined by the intersection of the maximum transverse gradients and the wake edge levels of the Pitot pressure traces. The wake thickness was obtained by measuring the distance between these intersections on the leeward side and windward side. Figures 21a to 21d show wake thicknesses for four Reynolds numbers and two wedge base heights. At the two lowest Reynolds numbers $Re_H = 7 \times 10^3$ (H = 0.15") and 1.4×10^4 (H = 0.30") the wake widths grow nearly linearly and indicate only a very small effect of angle of attack up to $\alpha = 15°$.* However, at the two larger Reynolds numbers, $Re_H = 2.8 \times 10^4$ and 5.5×10^4, from a certain point on the wake growth is much faster than ahead of this point. This "breakaway" phenomenon has been observed before by Sato and Kuriki,[21] Behrens[5]

* There are considerable differences in the wake widths at $\alpha = 20$ and 25 degrees. The boundary layer starts to separate on the leeward wedge surface at $\alpha \leqslant 20°$. It is possible that this separation phenomenon together with the increasing shock strength changes the character of the wake, but another possibility (and more likely) is that at the large angles of attack the ever increasing sidewall boundary layer interaction might introduce strong three-dimensionalities in the wake. As shown below, also, the wake minimum Mach numbers at the same Reynolds numbers start to change at $\alpha = 20°$. Thus, at these low Reynolds numbers at which the tunnel wall boundary layers are laminar, the measurements at $\alpha \geq 20°$ should be viewed with caution.

and Batt and Kubota.[6] It is interpreted as the onset of a nonlinear instability which is also called the onset of transition, where because of the finite fluctuations the Reynolds stresses start to become important and the mean flow starts to grow faster than a laminar steady wake flow (a wake flow where the growing disturbances are still infinitesimal and therefore do not yet have an effect on the mean flow).

From these results it is concluded that in the present experiments the wakes at the two lower Reynolds numbers (Figures 21a, b) are laminar within the region shown in the graphs and that at the two larger Reynolds numbers (Figures 21c, d) at some station in the wake the onset of a nonlinear instability (transition) occurs. This onset of transition moves towards the wedge model as angle of attack is increased. A discussion of this phenomenon is given in Section IV. 1. 3.

Minimum Velocities and Mach Numbers and Maximum Temperatures

The minimum velocities and Mach numbers and maximum temperatures which are the properties on the wake centerline for the wake without angle of attack exhibit similar trends as the wake widths. They are shown in Figures 22a to 22d (velocity), 23a to 23d (Mach number) and 24a to 24d (temperature). These quantities are of course not independent from each other but are related because the total temperature was taken to be constant (equal to $T_{o,\infty}$). Therefore, only the minimum velocities will be discussed.

At the two lowest Reynolds numbers ($Re_H = 7 \times 10^3$ and 1.4×10^4) the minimum velocities change very little with angle of attack except at angles of 20 and 25 degrees. (The discrepancies of these last two cases were discussed already in the previous section

in connection with the growth of the wake widths.)

At the larger Reynolds numbers the deviation from the minimum velocity growth rate of a laminar steady wake occurs sooner than would be predicted by the growth of the wake widths. This earlier rise of the wake centerline quantities compared to the growth rate of the wake widths was already observed by Batt and Kubota in their studies of symmetric wakes. Thus, at the Reynolds numbers of 2.8×10^4 and 5.5×10^4 also the minimum velocities exhibit growth rates from a certain point on that are faster than the growth rates of laminar wakes as found at the Reynolds numbers of 7×10^3 and 1.4×10^4.

IV. 1. 3. Transition

The location of transition was determined from the sudden increase of growth rate of wake thickness (Figures 21c and 21d). For the case of zero angle of attack and with Reynolds number of 55, 000, Batt[6] found that the point of onset of transition occurred at $x/H \simeq 15$, which seemed to be in good agreement with the results of hot-wire measurements by Demetriades and Behrens.[22] Reexamining Batt's data yielded a transition point of $x/H = 13.6$.

Figure 25 presents the location of transition as function of angle of attack for two Reynolds numbers, namely, $Re_{\infty,H} = 28,000$ and $55,000$. The results indicate that, for the same Reynolds number, transition moves upstream as the angle of attack is increased. As will be shown in the next section (IV. 1. 4), the velocity gradient on the leeward side of the laminar viscous wake increases sharply as angle of attack is increased. Laminar wake profiles become more unstable when the

density vorticity product ($\rho \frac{dU}{dy}$) increases. Because the differences of the wake edge quantities increase with increasing angle of attack, and the wake thickness changes little, the quantity $\rho \frac{dU}{dy}$ increases substantially with angle of attack, thus making the wake the more unstable the larger the angle of attack.

IV. 1. 4. Far Wake Profiles and Streamlines

Mean wake profiles were calculated from the measured data. Two cases were selected for discussion: (1) $Re_H = 7 \times 10^3$, $\alpha = 15°$, $H = 0.15''$; and (2) $Re_H = 2.8 \times 10^4$, $\alpha = 15°$, $H = 0.15''$. In the first case the wake is laminar within the whole region of measurement (60 base heights). In the second case the onset of transition as defined in the last section occurs at $x/H = 16.5$.

The results of velocity profiles, Mach numbers and static temperatures are shown in Figures 26a, b, c ($Re_H = 7 \times 10^3$) and 27a, b, c ($Re_H = 2.8 \times 10^4$).

In the wake regions ($x/H < 16.5$) where both wakes are laminar the profiles at the higher Reynolds number have much steeper gradients than in the lower Reynolds number case. Also, the gradients are steeper on the leeward side than on the windward side. A comparison with the measurements of Batt and Kubota indicates that the gradients on the leeward side are not only larger than those on the windward side but are also larger than those of the symmetric wake.

These profiles also show that the nonsymmetric viscous wake is qualitatively composed of a "wake"- component and a "free shear" layer component. In the transitional wake, the profiles at $x/H = 60$

are quite close to the profile shapes of a free shear layer.

Kubota[23] and Gold[24] showed that for two-dimensional linear symmetric wake theory of laminar compressible flow the proper transverse coordinate is

$$\bar{y} = \frac{U_e}{U_\infty}\sqrt{Re_{\infty, H}}\int_0^{y/H}\frac{\rho}{\rho_\infty}\, d\left(\frac{y}{H}\right)$$

Figures 28a, b show the velocity profiles of the two cases which were discussed in this section in this transformed y-scale, since any theory also for the nonsymmetric wakes should give results in these transformed coordinates.

Far wake streamlines were obtained by the method described earlier in Section III. 6. The quantity "I" follows the notation given by Equation (1), and is an invariant along a far wake streamline as discussed in the Appendix. The initial station for the far wake streamline calculculation is x/H = 5. At this station, minimum velocity point is taken as the starting point of the approximate dividing streamline, and the values of "I" are equally divided into ten intervals between two maximum velocity points outside the viscous wake and within the wake shocks, for eleven streamlines.

Typical results of the far wake streamline calculation are presented in Figures 29a and 29b, in which the line of minimum velocity and the wake shocks are also included. The dividing streamline has a larger slope than that of the line of minimum velocity.

IV. 2. Laminar Near Wake Flow

Investigations of the near wake flow were limited by the dimension of the static pressure probe being used in the present test.

However, an approximation of static pressure in the small base flow region could be obtained by interpolating the base pressure and the downstream static pressure which were measured with the present static pressure probe.

IV. 2. 1. Base and Surface Pressures

The base pressure measurements for both wedges are presented in Figures 30a and 30b as functions of angle of attack. When the model was at small incidence, the base pressure dropped slightly with increasing angle of attack, and decreased slightly with increasing Reynolds number. But when the model was subjected to higher angles of attack, the base pressure rose noticeably, except at the lowest Reynolds number ($Re_{\infty,H} = 7000$). At Reynolds numbers above 28,000, the effect of Reynolds number seemed to disappear. At these higher angles of attack ($> 17.5^\circ$) flow separation on the leeward surface started to appear, and the surface pressure in the separated region became almost identical to the base pressure.

Figures 31a and 31b show the correlation of base pressures for the same Reynolds number, i.e., $Re_{\infty,H} = 1.4 \times 10^4$ and 2.8×10^4, but different models. The correlation is good for the case with higher Reynolds number ($Re_{\infty,H} = 2.8 \times 10^4$), and for the lower Reynolds number case at $\alpha < 17.5^\circ$ while it is not very good for larger than 17.5°. At these large angles of attack and at low stagnation pressure at which the sidewall boundary layer is laminar, for the large wedge, model-tunnel wall boundary layer interaction may be large so that substantial three-dimensionalities are introduced in the near wake flow.

IV. 2. 2. Near Wake Velocity Profiles

The near wake of the larger wedge model (H = 0. 3 in.) was chosen for the experiments in the near wake flow because of the larger size of this region and because surface pressure taps were installed on the surface of the large wedge, which made a more detailed study possible on the leeward surface. Near wake shear layer profiles were obtained by the data reduction method described in Section III.

Figures 32a, b, c, d show the near wake velocity profiles for the wedge with a Reynolds number of 5.5×10^4 and at angles of attack of $10^\circ, 15^\circ, 20^\circ$ and 25°. In these figures, velocity profiles downstream of the leeward side trailing edge describe the velocity profiles between the leeward side leading edge shock and a point inside the windward side leading edge shock, and those upstream of the leeward side corner are for velocity profiles between the model surface and the leading edge shocks. The large increase of velocity gradients on the leeward side of the viscous wake with angle of attack is evident.

The wake shocks are relatively weak on both sides of the stream. On the leeward side the velocity acceleration caused by the expansion waves is small, the velocity profiles have a relatively flat level in the inviscid region followed by a sharp drop in the viscous region, and the turning points clearly mark the location of shear layer edges. But on the windward side, although the velocity discontinuities across the wake shock remain small, the expansion waves are stronger; therefore, significant transverse pressure gradients are noticeable just after the trailing corner, and the flow is first accelerated inside the expansion

fan toward the viscous wake, then decelerated due to shear stresses in the viscous wake and compression waves as the flow turns back towards nearly free stream direction.

IV. 2. 3. Flow Separation and Near Wake Flowfield

At small angles of attack, the structure of the near wake flow is very similar to that of the symmetric wake. The boundary layers separate at both trailing edges of the wedge and coalesce at about three-quarters of a base height downstream. As the angle of attack increases, the recirculation region moves toward the leeward side. When the angle of attack was increased beyond 17.5°, flow separation on the leeward surface was observed (Table III), and the recirculation region extended from the base to the leeward surface. Even though the oil flow technique does not yield very accurate results, a distinct tendency of increase in the separated flow region was observed with increasing Reynolds numbers. This last result is in agreement with trends found in the laminar boundary layer separation experiments by Lewis et. al.[25] and is also predicted theoretically by Lees and Reeves.[26]

The structure of typical near wake flow fields at angles of attack of 10°, 15°, 20° and 25° is shown in Figures 33a-d. These figures show some important features of the wake geometry, such as shock wave location, shear layer edges, sonic line,* contour of zero velocity* and streamlines. The contour of zero velocity is constructed from the points where Pitot pressure is equal to static pressure.

* These quantities are only estimates in the region $x/H < 1$ since the static pressure could not be measured directly.

For large angles of attack, for example $\alpha \simeq 20°$, the recirculation region seems shorter than behind a wedge without angle of attack. The streamline curvature near the windward side trailing corner clearly indicates the strong pressure gradients in this region. At four or five base heights downstream of the base the flow in the viscous wake is again nearly parallel to the free stream direction as already found from the inviscid flow calculations.

V. SUMMARY OF RESULTS

Experimental measurements of mean flow properties of hypersonic wakes behind wedges of 20° included angle were conducted at angles of attack up to 25° at Mach number 6, with free stream Reynolds number based on wedge base height ranging from 7000 to 55000. The near and far wake flowfields were determined up to a downstream distance of 60 base height.

V. 1. Far Wake Flowfield

1. The overshoot in wake static pressure depends strongly on angle of attack; the higher the angle of attack, the larger the overshoot. The effect of Reynolds number on the overshoot follows the same trend as that for the symmetric wake; the lower the Reynolds number, the higher the overshoot. The effect of Reynolds number is very much smaller than that of angle of attack.

2. The viscous wake edge values of velocity, Mach number and temperature are very close to the free stream conditions for all angles of attack on the leeward side, and change considerably with angle of attack on the windward side. A weak expansion of the wake flow in the region behind the wake shocks changes the viscous wake edge conditions only very slowly as the flow moves downstream.

3. The inviscid wake flow parameters: wake static pressure, edge velocities, edge Mach numbers, edge temperatures and flow inclination in the real flow compared favorably with the simple inviscid shock expansion model for $M = 6$, $\alpha \leq 25°$. The inviscid far wake flow ($x/H \geq 4$) is mainly determined by the relative strengths of the leading

edge shocks and the fact that the flows at the edges of the viscous wake have to be nearly parallel to each other, with a weak dependence on the base flow. The viscous wake is accordingly affected by the differences in the inviscid flow on the windward and leeward sides.

4. In the laminar wake flows the wake widths, minimum velocities, minimum Mach numbers and maximum temperatures change very little with angle of attack. In the transitional wake flows, the "breakaway" phenomenon which is similar to that in the symmetric wake flow is observed, and indicates the onset of a nonlinear instability or transition.

5. The location of transition determined from the sudden increase of growth rate of wake thickness indicates that, for the same Reynolds number, transition moves upstream as the angle of attack is increased.

6. When wake flows are laminar, the velocity profiles at higher Reynolds number have much steeper gradients than those at the lower Reynolds number. Also, the maximum gradients of the flow profiles are steeper on the leeward side than on the windward side. The gradients increase with increasing angle of attack, explaining the upstream motion of transition. The fast decay of "wake component" in the transitional wake makes the profiles at $x/H = 60$ quite close to the profile shapes of a free shear layer.

7. Far wake streamlines are calculated. Wake flow inclination is directed toward the leeward side. The dividing streamline has a larger slope with respect to free stream direction than the line of minimum velocity.

V.2. Laminar Near Wake Flow

1. In general, the base pressure is quite insensitive to angle of attack within about 17.5°, especially for those cases with higher Reynolds number. But when the model is subjected to higher angles of attack, the base pressure rises noticeably, except at the lowest Reynolds number (Re_H = 7000). At Reynolds numbers above 28000, the effect of Reynolds number seems to disappear. At these higher angles of attack (> 17.5°) flow separation on the leeward surface starts to appear, and the surface pressure in the separated region becomes almost identical to the base pressure.

2. When the wedge is at small angle of attack, the structure of the near wake flow is very similar to that of the symmetric wake. The boundary layers separated at both trailing edges of the wedge and coalesce at about three quarters of a base height downstream. As the angle of attack increases, the recirculation region moves toward the leeward side of the wedge. When the angle of attack is increased beyond 17.5°, flow separation on the leeward surface is observed, and the recirculation region extends from the base to the leeward surface. Even though the oil flow technique does not yield very accurate results, a distinct tendency of upstream motion of the separation point on the leeward surface was observed with increasing Reynolds number.

REFERENCES

1. Lees, L.: "Hypersonic Wakes and Trails," AIAA J. 2:3, 417-428 (1964).

2. Lykoudis, P. S.: "A Review of Hypersonic Wake Studies," AIAA J. 4:4, 577-590 (1966).

3. McCarthy, J. F., Jr. and Kubota, T.: "A Study of Wakes behind a Circular Cylinder at M = 5.7," AIAA J. 2:4, 626-629 (1964). Also McCarthy, J. F., Jr.: "Hypersonic Wakes," Ph.D. Thesis, 1962, California Institute of Technology, Pasadena, California.

4. Dewey, C. F., Jr.: "Near Wake of a Blunt Body at Hypersonic Speeds," AIAA J. 3:6, 1001-1010 (1965).
Also Dewey, C. F., Jr.: "Measurements in Highly Dissipative Regions of Hypersonic Flows. Part II. The Near Wake of a Blunt Body at Hypersonic Speeds," Ph.D. Thesis, California Institute of Technology, Pasadena, California (1963).

5. Behrens, W.: "Far Wake behind Cylinders at Hypersonic Speeds: I. Flowfield," AIAA J. 5:12, 2135-2141 (1967); also "Far Wake behind Cylinders at Hypersonic Speeds: II. Stability," AIAA J. 6:2, 225-232 (1968).
Also Behrens, W.: "Flow Field and Stability of the Far Wake behind Cylinders at Hypersonic Speeds," Ph.D. Thesis, California Institute of Technology, Pasadena, California (1966).

6. Batt, R. G. and Kubota, T.: "Experimental Investigation of Laminar Near Wakes behind 20° Wedges at $M_\infty = 6$," AIAA J. 6:11, 2077-2083 (1968); also "Experimental Investigation of Far Wakes behind Two-Dimensional Slender Bodies at $M_\infty = 6$," AIAA J. 7:11, 2064-2071 (1969).
Also Batt, R. G.: "Experimental Investigation of Wakes behind Two-Dimensional Slender Bodies at Mach Number Six," Ph.D. Thesis, California Institute of Technology, Pasadena, California (1967).

7. Murman, E. M.: "Experimental Studies of a Laminar Hypersonic Cone Wake," AIAA J. 7:9, 1724-1730 (1969).

8. McLaughlin, D. K.: "Experimental Investigation of the Mean Flow and Stability of the Laminar Supersonic Cone Wake," M.I.T. Aerophysics Lab. Technical Report 169, Jan. 1970.

9. Pallone, A., Erdos, J. and Eckerman, J.: "Hypersonic Laminar Wakes and Transition Studies," AIAA J. 2:5, 855-863 (1964).

References (Cont'd)

10. Reeves, B. L. and Lees, L.: "Theory of Laminar Near Wake of Blunt Bodies in Hypersonic Flow," AIAA J. 3:11, 2061-2074 (1965).

11. Weiss, R. F.: "A New Theoretical Solution of the Laminar, Hypersonic Near Wake," AIAA J. 5:12, 2142-2149 (1967).

12. Henderson, A., Jr.: "Shuttle Technology for Aerothermodynamics," Astronautics and Aeronautics, Feb. 1971.

13. Schmidt, E. M. and Cresci, R. J.: "Near Wake of a Slender Cone at Large Angle of Attack," PIBAL Report No. 68-23, Polytechnic Institute of Brooklyn, July 1968.

14. Kahane, A. and Lees, L.: "The Flow at the Rear of a Two-Dimensional Supersonic Airfoil," J. of Aero. Sci. 15:3, 167-170 (1948).

15. Baloga, P. E. and Nagamatsu, H. T.: "Instrumentation of GALCIT Hypersonic Wind Tunnels," GALCIT Memorandum No. 29 (July 31, 1955).

16. Herzog, R. R.: "Nitrogen Injection into the Base Region of a Hypersonic Body," GALCIT Hypersonic Research Project, Memorandum No. 71 (Aug. 1964).

17. Behrens, W.: "Viscous Interaction Effects on a Static Pressure Probe at M = 6," AIAA J. 1:12, 2364-2366 (1963).

18. Bannink, W. J. and Nebbeling, C.: "Determination of the Position of a Shock Wave from Pitot Tube Experiments," AIAA J. 7:4, 796-797 (1969).

19. Sherman, F. S.: "New Experiments on Impact-Pressure Interpretation in Supersonic and Subsonic Rarefied Air Streams," NACA TN 2995 (1953).

20. Chapman, D. R., Kuehn, D. M. and Larson, H. K.: "Investigation of Separated Flows in Supersonic and Subsonic Streams with Emphasis on the Effect of Transition," NACA Report 1356 (1958).

21. Sato, H. and Kuriki, K.: "The Mechanism of Transition in the Wake of a Thin Flat Plate Placed Parallel to a Uniform Flow," JFM II:3, 321-352 (Nov. 1961).

References (Cont'd)

22. Demetriades, A. and Behrens, W.: "Hot Wire Measurements in the Hypersonic Wakes of Slender Bodies," GALCIT Internal Memo No. 14, California Institute of Technology, Pasadena, California, May 1963; also Demetriades, A.: "Hot Wire Measurements in the Hypersonic Wakes of Slender Bodies," AIAA J. 2:2, 245-250 (1964).

23. Kubota, T.: "Laminar Wake with Streamwise Pressure Gradient-II," GALCIT Internal Memo 9, California Institute of Technology, Pasadena, California, April 1962.

24. Gold, H.: "Laminar Wake with Arbitrary Initial Profiles," AIAA J. 2:5, 948-949 (1964).

25. Lewis, J. E., Kubota, T. and Lees, L.: "Experimental Investigation of Supersonic Laminar, Two-Dimensional Boundary-Layer Separation on a Compression Corner with and without Cooling," AIAA J. 6:1, 7-14 (1968).

26. Lees, L. and Reeves, B. L.: "Supersonic Separated and Reattaching Laminar Flows: I. General Theory and Application to Adiabatic Boundary Layer-Shock Wave Interactions," AIAA J. 2, 1907-1920 (1964).

APPENDIX

An Invariant Along a Far Wake Streamline

Consider a two-dimensional unsymmetric wake flow as sketched in Figure A. 1. If the pressure gradients in the x- and y- directions can be neglected, the governing differential equations are:

Continuity:

$$\frac{\partial \rho U}{\partial x} + \frac{\partial \rho V}{\partial y} = 0 \qquad \text{(A. 1)}$$

Momentum:

$$\rho U \frac{\partial U}{\partial x} + \rho V \frac{\partial U}{\partial y} = \frac{\partial \tau}{\partial y} \qquad \text{(A. 2)}$$

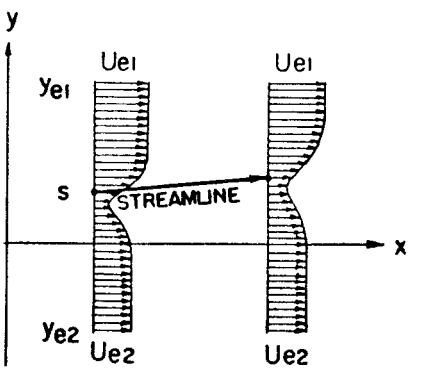

Fig. A. 1

where,

x, y streamwise and transverse coordinates

U, V velocity components

τ shear stress

The boundary conditions are:

$$\begin{aligned} &\text{as } y \to y_{e1}, \quad U \to U_{e1}, \quad \tau \to 0 \\ &\quad y \to y_{e2}, \quad U \to U_{e2}, \quad \tau \to 0 \end{aligned} \qquad \text{(A. 3)}$$

Multiply Eq. (A. 1) by $(U-U_{e1})$ and add to Eq. (A. 2). Then, integrate with respect to y from y = s to $y = y_{e1}$, and apply the boundary conditions (A. 3), gives,

$$\int_s^{y_{e1}} \frac{\partial}{\partial x}\left[\rho U(U_{e1}-U)\right]dy - \rho V(U_{e1}-U)\Big|_{\text{at } y=s} = -\tau(x, s) \qquad \text{(A. 4)}$$

Using the similar technique and integrating from $y=y_{e2}$ to y = s gives,

$$\int_{y_{e2}}^{s} \frac{\partial}{\partial x}\left[\rho U(U_{e2}-U)\right]dy + \rho V(U_{e2}-U)\Big|_{\text{at } y=s} = \tau(x, s) \qquad (A.5)$$

Adding Equations (A.4) and(A.5), yields

$$\int_{y_{e2}}^{s} \frac{\partial}{\partial x}\left[\rho U(U_{e2}-U)\right]dy + \int_{s}^{y_{e1}} \frac{\partial}{\partial x}\left[\rho U(U_{e1}-U)\right]dy = \rho V(U_{e1}-U_{e2})\Big|_{\text{at } y=s} \qquad (A.6)$$

or

$$\frac{d}{dx}\left[\int_{y_{e2}}^{s} \rho U(U_{e2}-U)dy + \int_{s}^{y_{e1}} \rho U(U_{e1}-U)dy\right] = \rho(U_{e1}-U_{e2})\left(V-U\frac{\partial s}{\partial x}\right)\Big|_{\text{at } y=s} \qquad (A.7)$$

The right hand side of Eq. (A.7) vanishes if the following relation holds.

$$\frac{\partial s}{\partial x} = \frac{V}{U} \qquad (A.8)$$

and this relation means that

$$y = s(x)$$

is a streamline. Consequently, along the streamline $y = s(x)$, Eq. (A.7) can readily be integrated as follows

$$\int_{y_{e2}}^{s} \rho U(U_{e2}-U)dy + \int_{s}^{y_{e1}} \rho U(U_{e1}-U)dy = A \qquad (A.9)$$

where A is a constant which depends only on the streamline.

The whole equation (A.9) may be normalized by freestream conditions. For example, divide Eq. (A.9) by $\rho_\infty U_\infty^2 H$, then relation (A.9) becomes,

$$\frac{1}{\rho_\infty U_\infty^2 H}\left[\int_{y_{e2}}^{s} \rho U(U_{e2}-U)dy + \int_{s}^{y_{e1}} \rho U(U_{e1}-U)dy\right] = I \qquad (A.10)$$

where,

$$I = \frac{A}{\rho_\infty U_\infty^2 H}$$

TABLE I. TEST SUMMARY

H (inches)	P_o (psig)	$Re_\infty H$	M_∞	α (degrees)	DATA MEASURED †		VALID DATA †	
					PITOT	STATIC	PITOT	STATIC
0.15	10	7000	6.02	5	70	70	70	70
				10	70	70	70	70
				15	70	70	60*	60
				20	70	70	45*	45
				25	70	70	25	25
	35	14000	6.04	5	10	10	10	10
				10	10	10	10	10
				15	10	10	10	10
	60	21000	6.06	5	10	10	10	10
				10	10	10	10	10
				15	10	10	10	10
	85	28000	6.08	5	10	10	10	10
				10	70	70	70	70
				15	70	70	70*	70
0.30	10	14000	6.02	5	35	35	30**	30
				10	35	35	20*	20
				15	35	35	15**	15
				20	35	35	10**	10
				22.5	35	35	7	7
				25	15	none	5	none
	85	55000	6.08	10	35	35	35	35
				15	35	35	30	30
				20	35	35	20*	20
				22.5	35	35	15*	15
				25	35	35	15*	10

NOTES : † shows last downstream station (x/H)

* windward side flow is partially interfered by the reflected leading edge shock wave

** windward side flow is interfered by the reflected leading edge shock wave, however, the flow is undisturbed in the vicinity of minimum velocity and on leeward side

TABLE II. SUMMARY OF LEADING EDGE SHOCK ANGLES

α (degrees)	H (inches)	0.15				0.3	
	P_o (psig)	10	35	60	85	10	85
	$Re_\infty H \times 10^{-4}$	0.7	1.4	2.1	2.8	1.4	5.5
0	SYMMETRIC (BATT)					19.2	18.4
5	WINDWARD	24.3	24.2	24.0	24.0	24.8	
	LEEWARD	16.5	15.3	15.0	14.8	17.5	
10	WINDWARD	29.0	29.0	28.8	28.8	30.0	28.5
	LEEWARD	14.0	13.2	13.0	13.2	15.0	14.2
15	WINDWARD	34.8	34.0	34.0	34.0	36.0	36.8
	LEEWARD	12.6	12.2	12.0	11.7	11.8	10.8
20	WINDWARD	40.0				41.2	41.0
	LEEWARD	12.0				12.3	10.6
22.5	WINDWARD					45.0	44.2
	LEEWARD					12.0	12.0
25	WINDWARD	47.0				47.2	47.2
	LEEWARD	12.0				12.0	12.0

TABLE III. LOCATION OF FLOW SEPARATION ON LEEWARD SIDE SURFACE OF 20° WEDGES DETERMINED BY FLOW VISUALIZATION

(% Chord from Leading Edge)

H (in.)	0.15				0.3			
Po (psig)	10	35	60	85	10	35	60	85
$Re_{\infty H} \times 10^{-4}$	0.7	1.4	2.1	2.8	1.4	2.8	4.1	5.5
α \ M_∞	6.02	6.04	6.06	6.08	6.02	6.04	6.06	6.08
17.5		100		100	100	98	100	100
20.0	96	96			95	95	94	93
22.5	90	90		90	88	87	82	70
25.0	89	86	80	75	80	66	64	60
27.0						55	40	37
30.0	70	55	45	45				

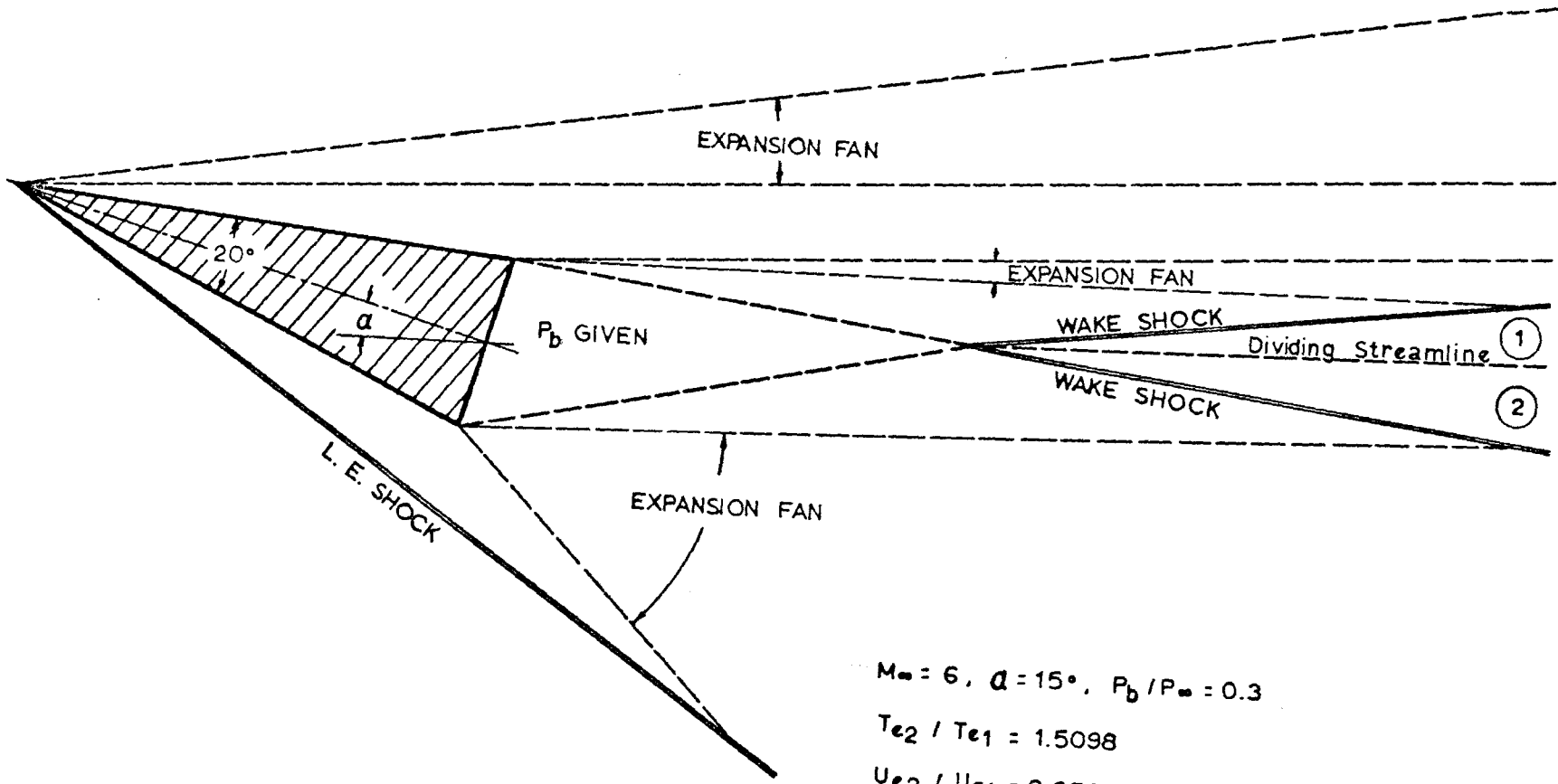

Fig. 1. TYPICAL RESULTS FROM INVISCID FLOW MODEL (SHOCK - EXPANSION THEORY)

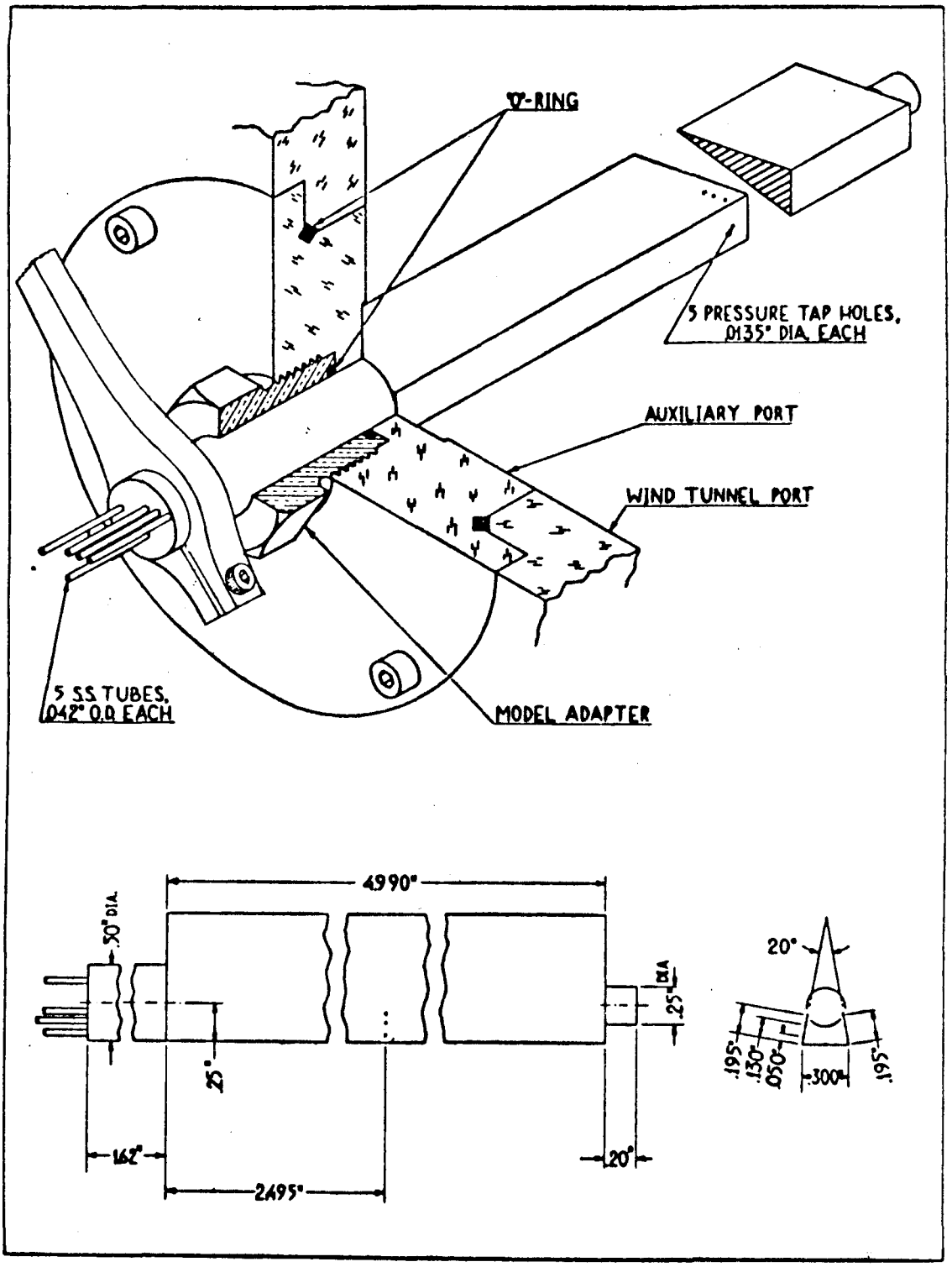

Fig. 2a MODEL DESIGN - H = 0.3 in.

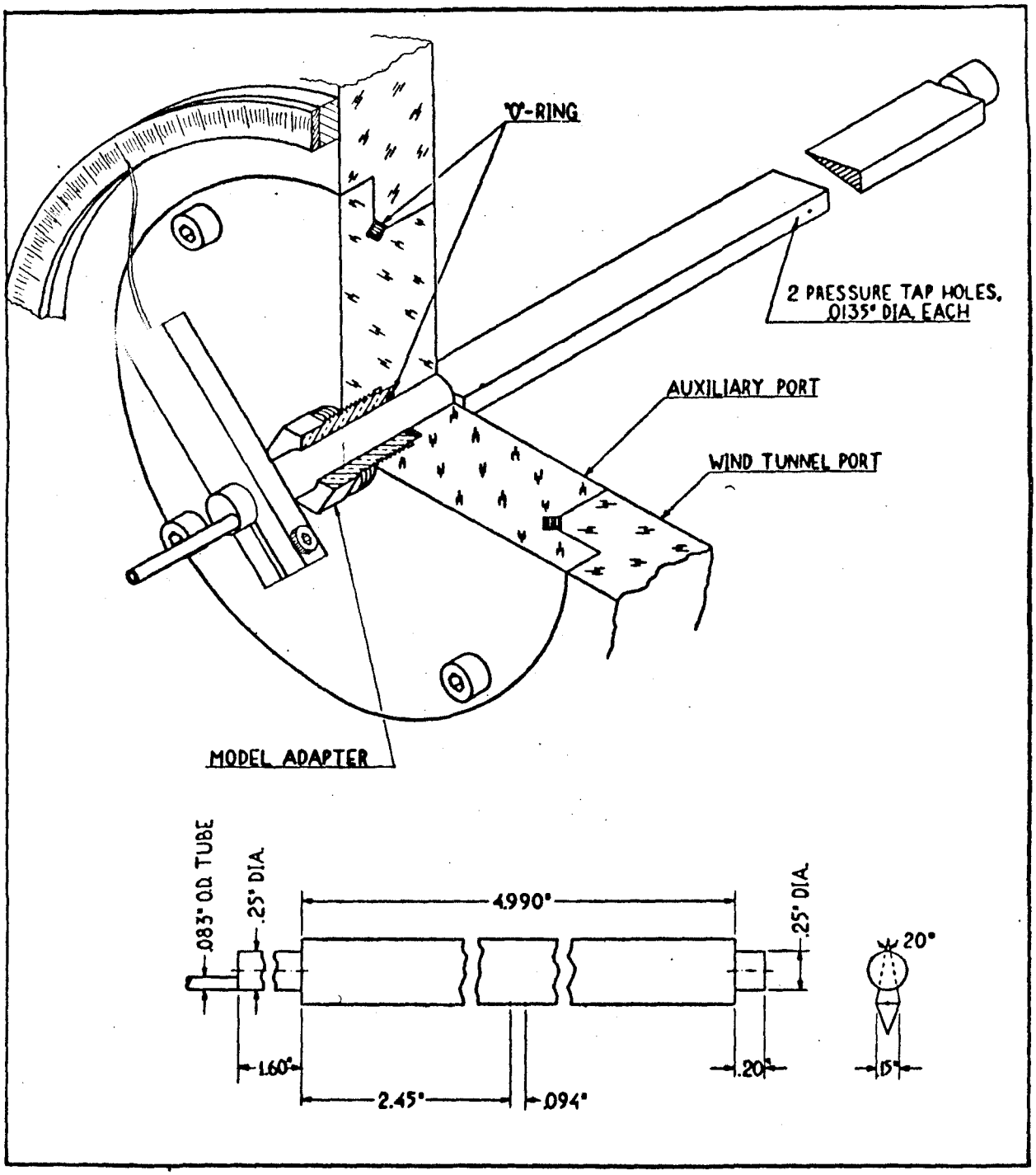

Fig. 2b MODEL DESIGN - H = 0.15 in.

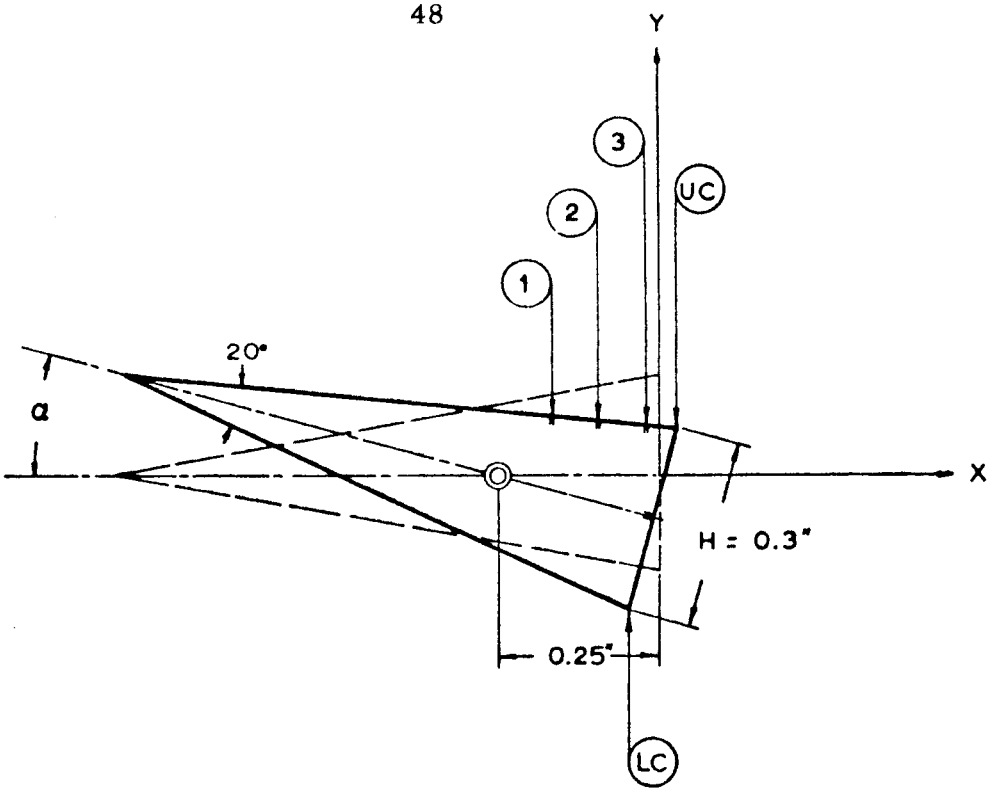

(a) 20° WEDGE MODEL - H = 0.3 in.

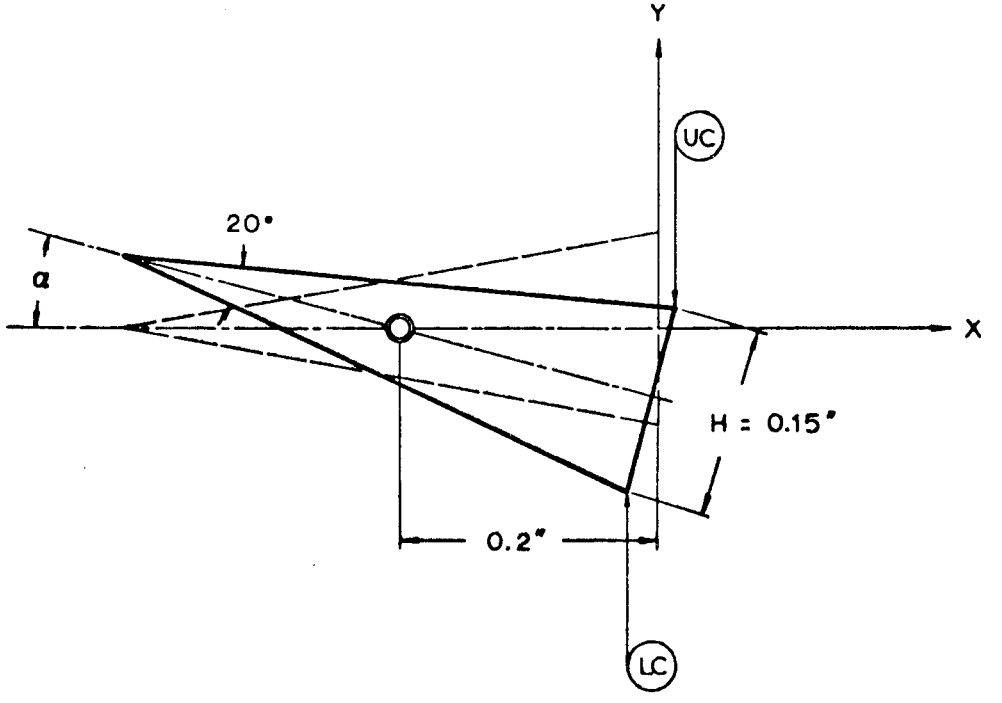

(b) 20° WEDGE MODEL - H = 0.15 in.

Fig. 3. COORDINATE SYSTEM

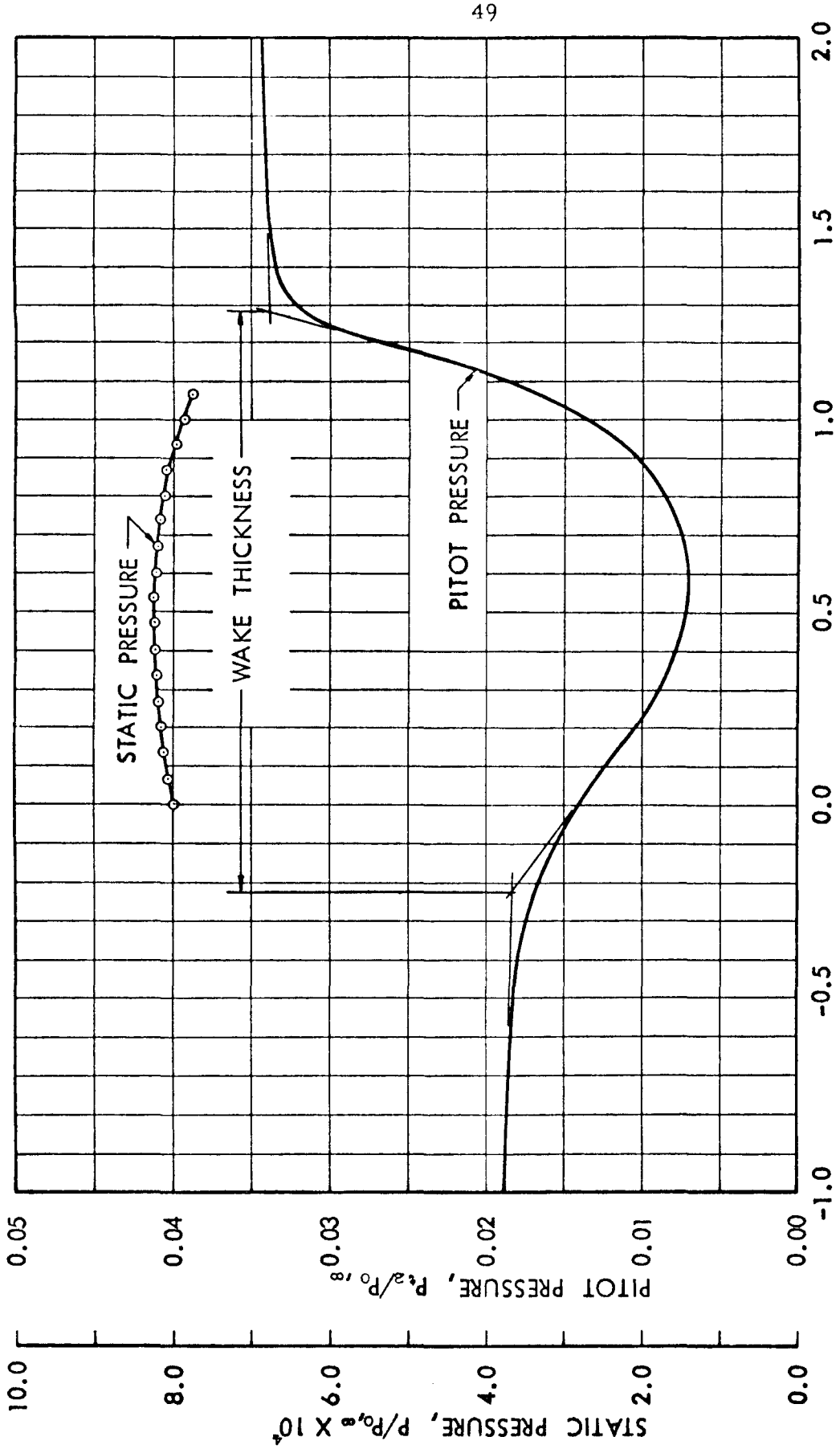

Fig. 4. TYPICAL RAW DATA

20° WEDGE, H = 0.15", $\alpha = 15°$, $P_0 = 10$ psig, $Re_{\infty H} = 0.7 \times 10^4$, x/H = 30

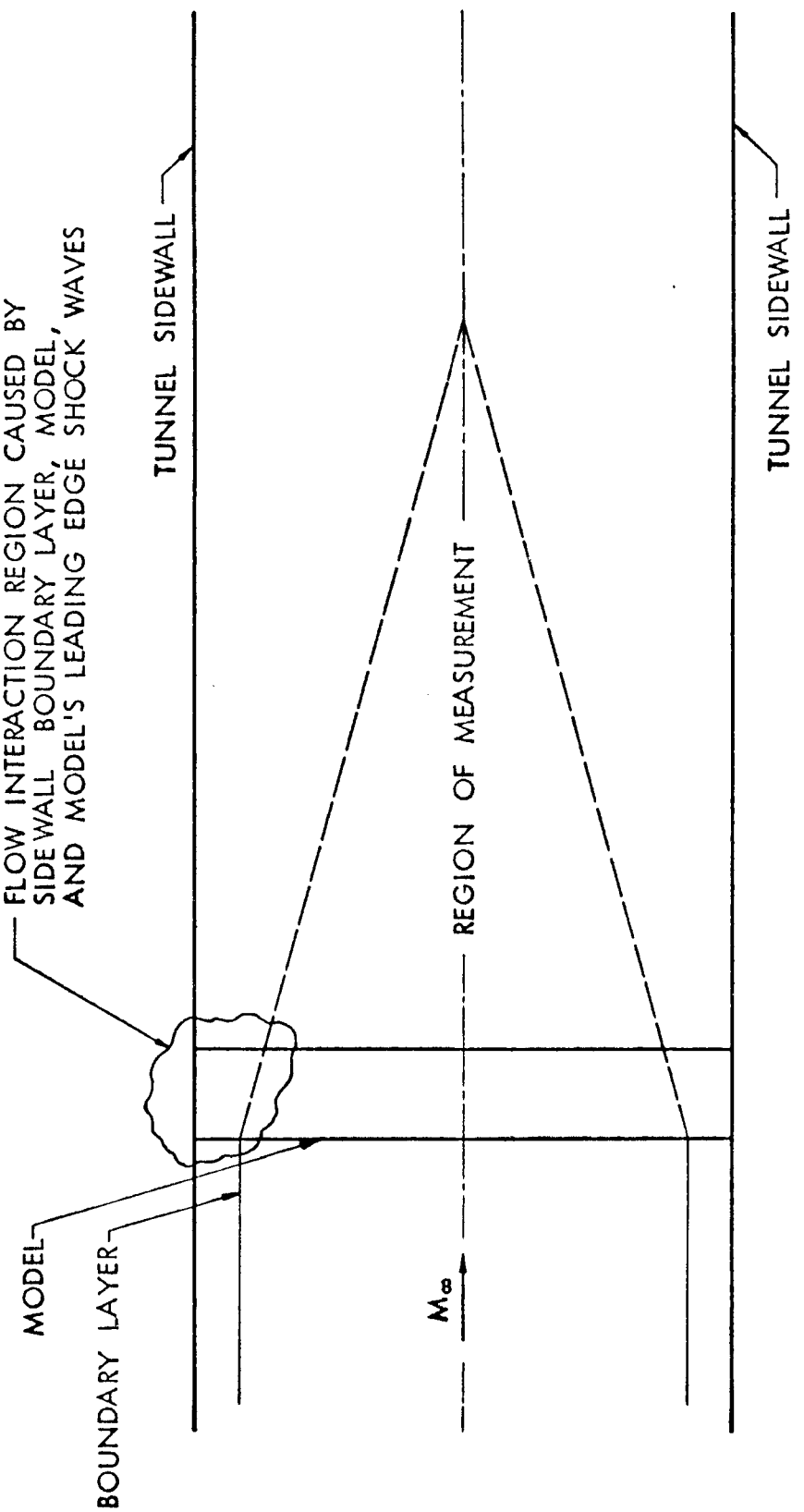

Fig. 5. SKETCH OF TWO-DIMENSIONAL REGION OF TEST

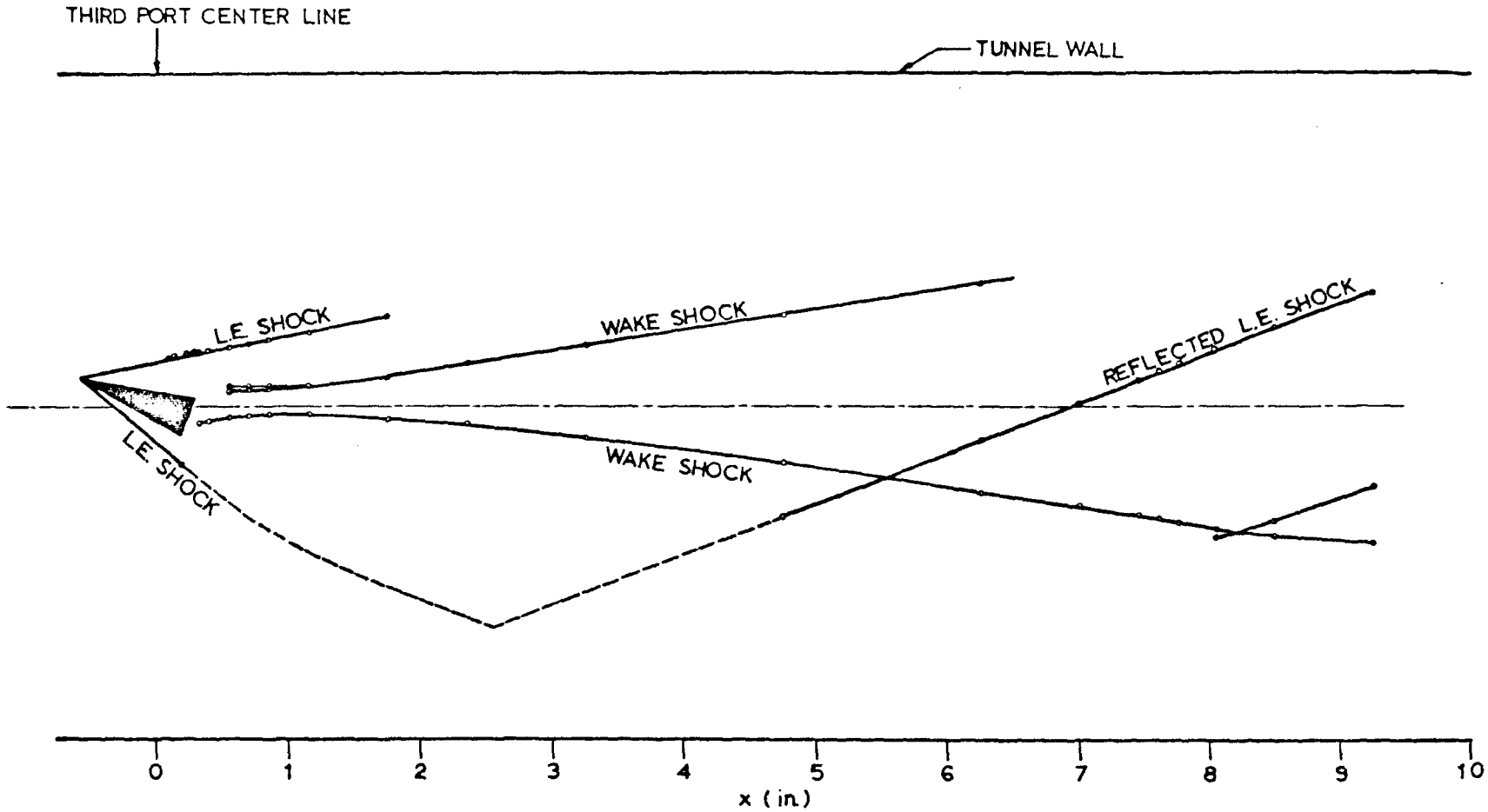

$H = 0.3$ in., $\alpha = 20°$, $P_o = 85$ psig, $Re_{\infty} H = 55000$, $M_{\infty} = 6.08$

Fig. 6. SHOCK WAVES INSIDE THE TUNNEL

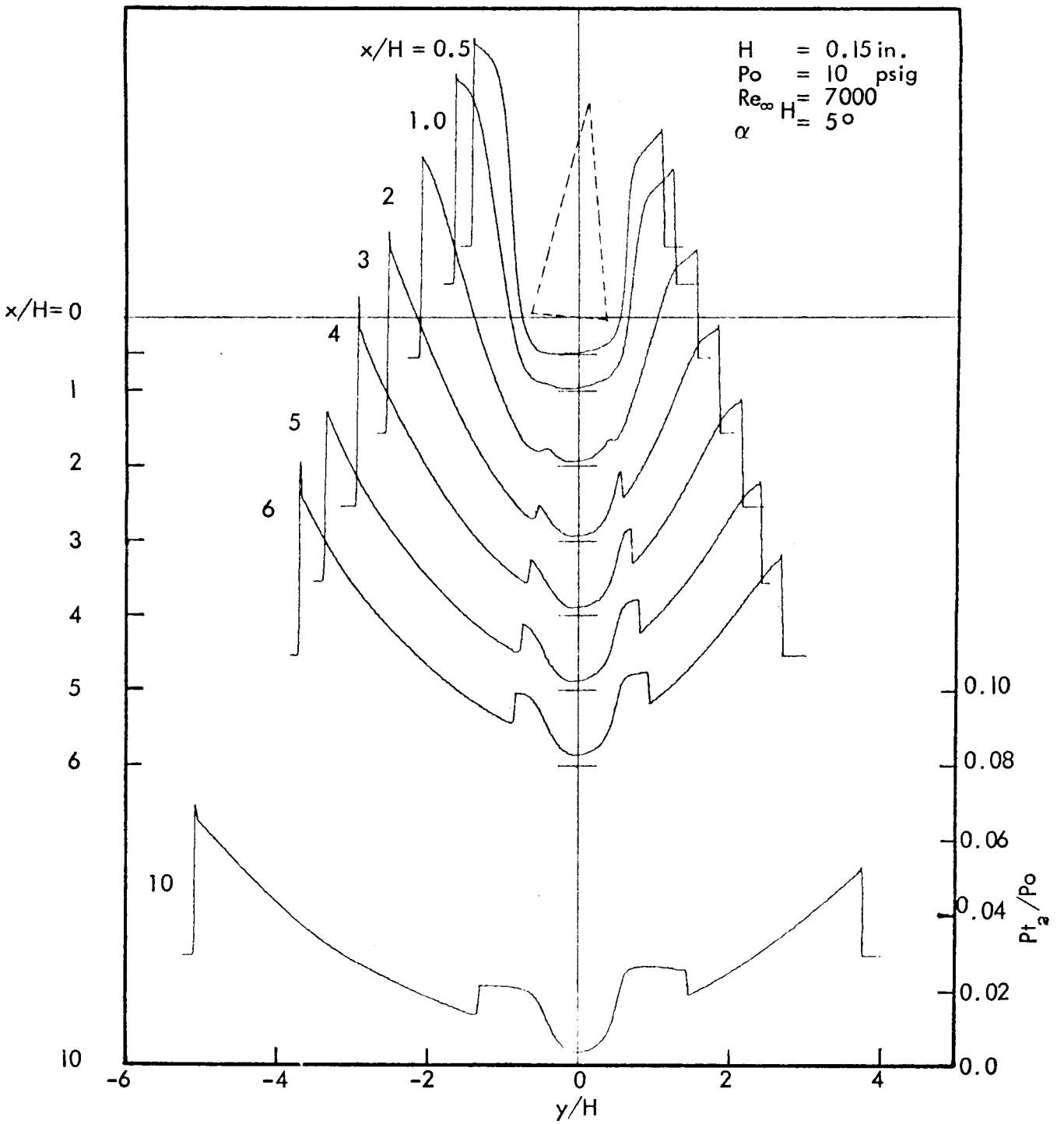

Fig. 7a PITOT PRESSURE TRACES

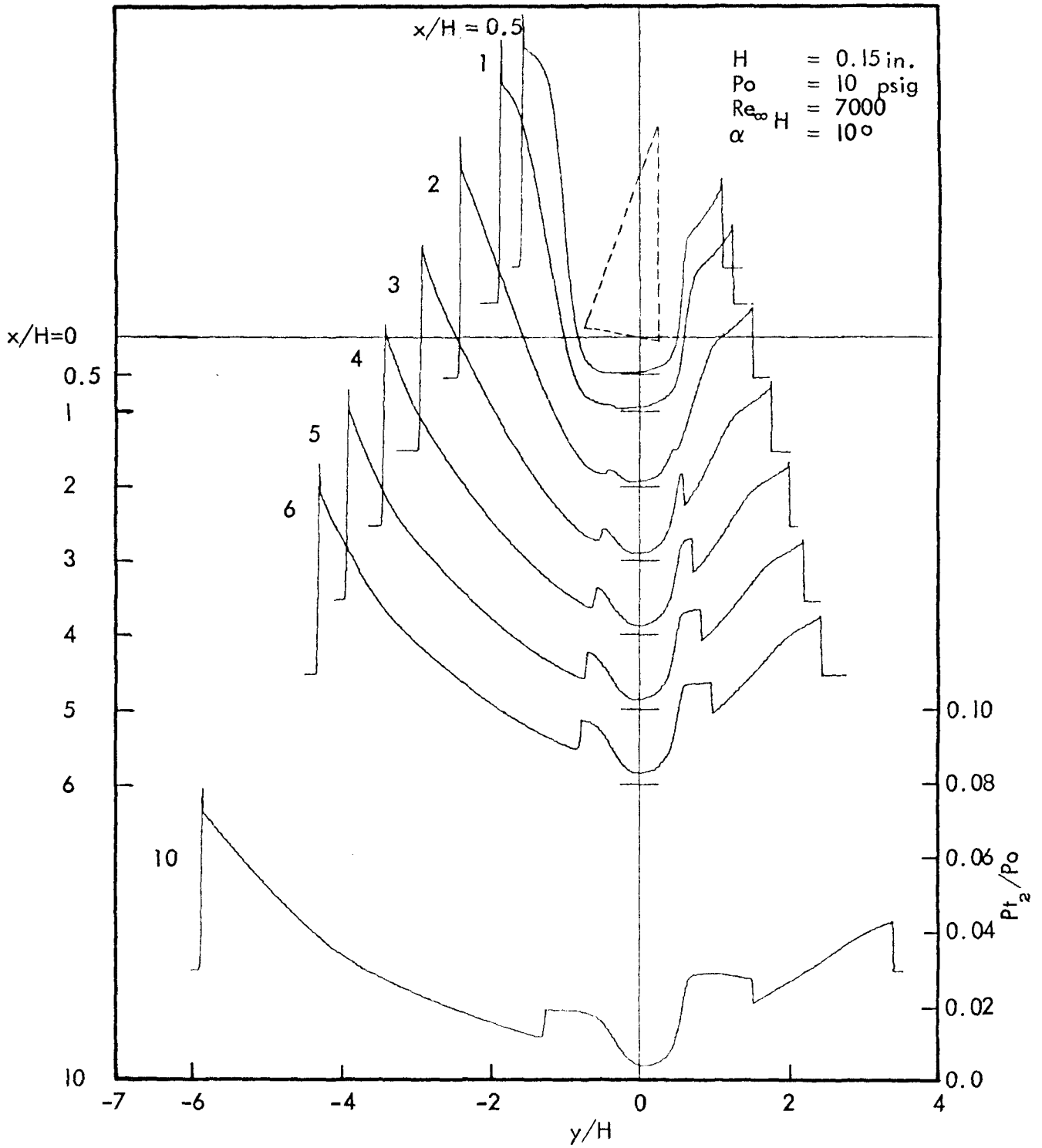

Fig. 7b PITOT PRESSURE TRACES

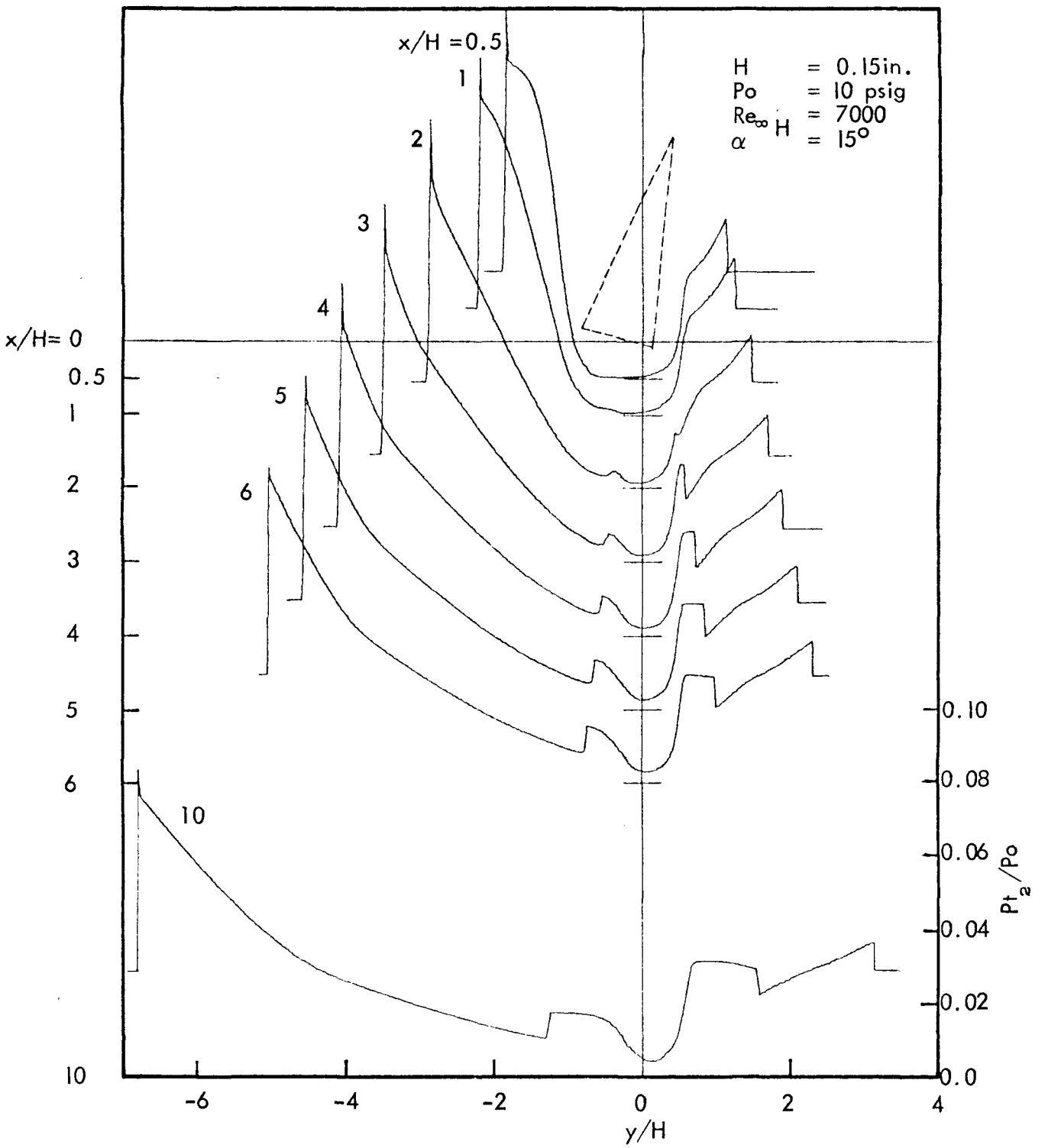

Fig. 7c PITOT PRESSURE TRACES

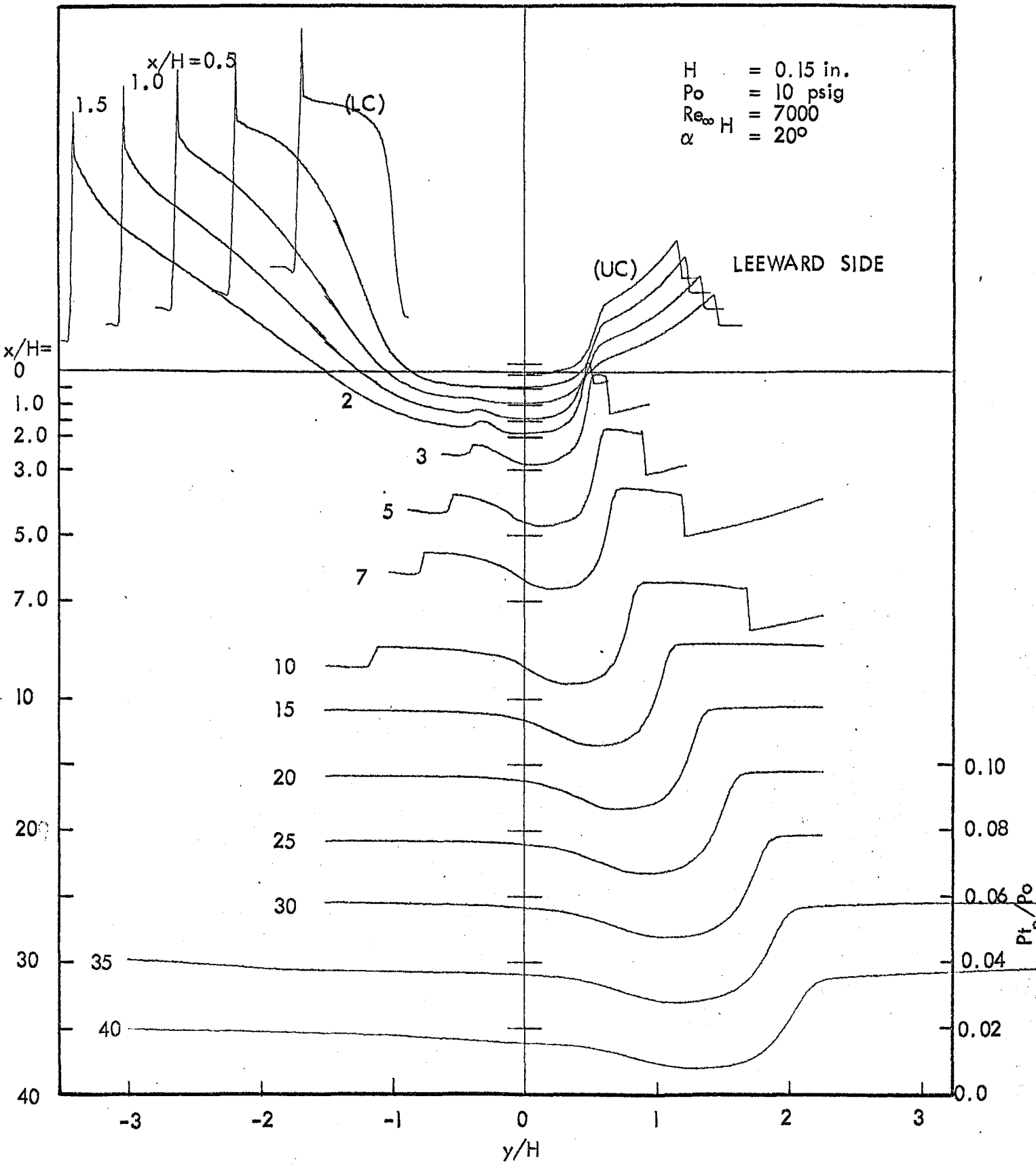

Fig. 7d PITOT PRESSURE TRACES

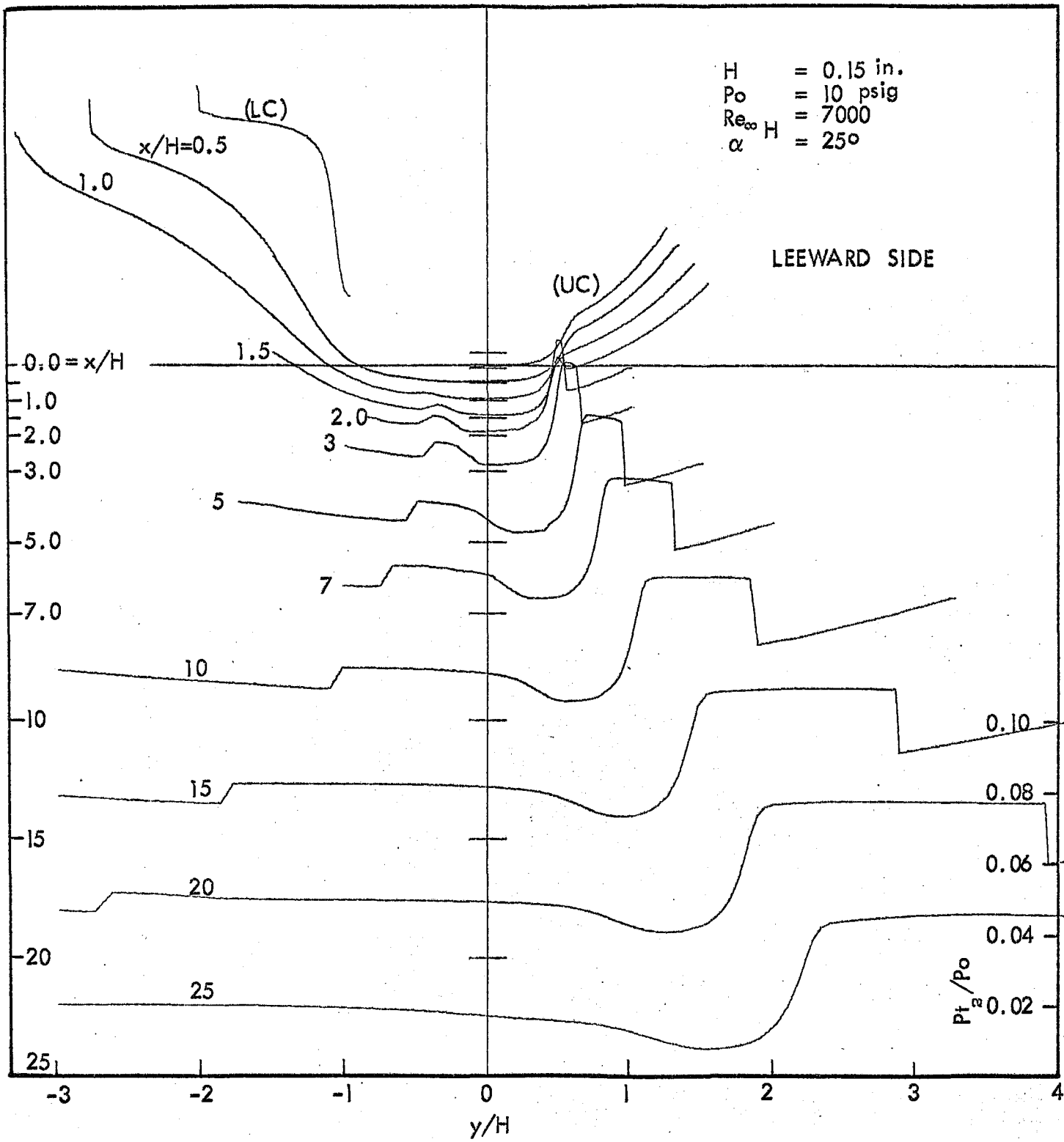

Fig. 7e PITOT PRESSURE TRACES

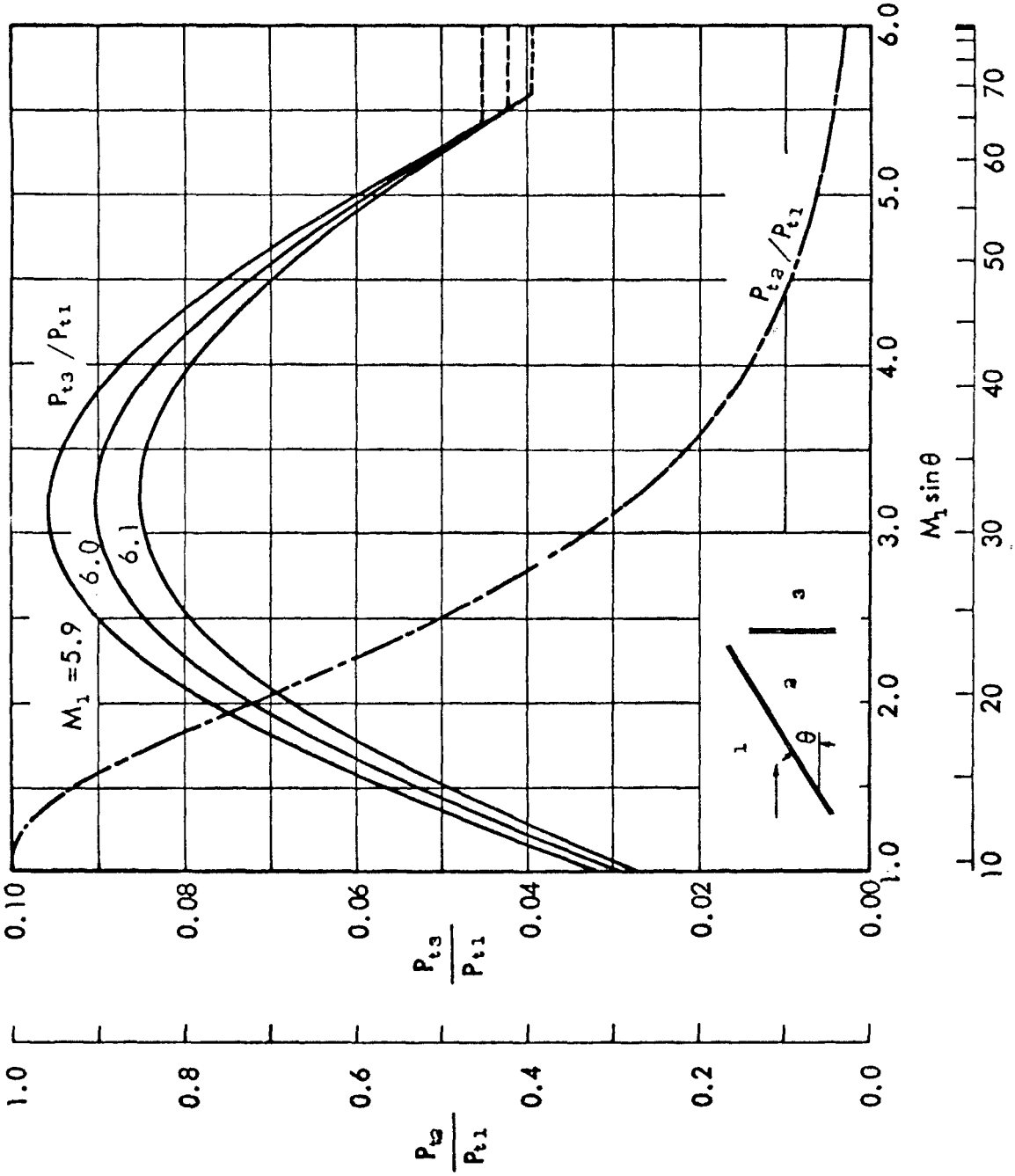

Fig. 8 VARIATION OF PITOT PRESSURE AND TOTAL PRESSURE ACROSS OBLIQUE SHOCK WAVES WITH NORMAL COMPONENT OF UPSTREAM MACH NUMBER

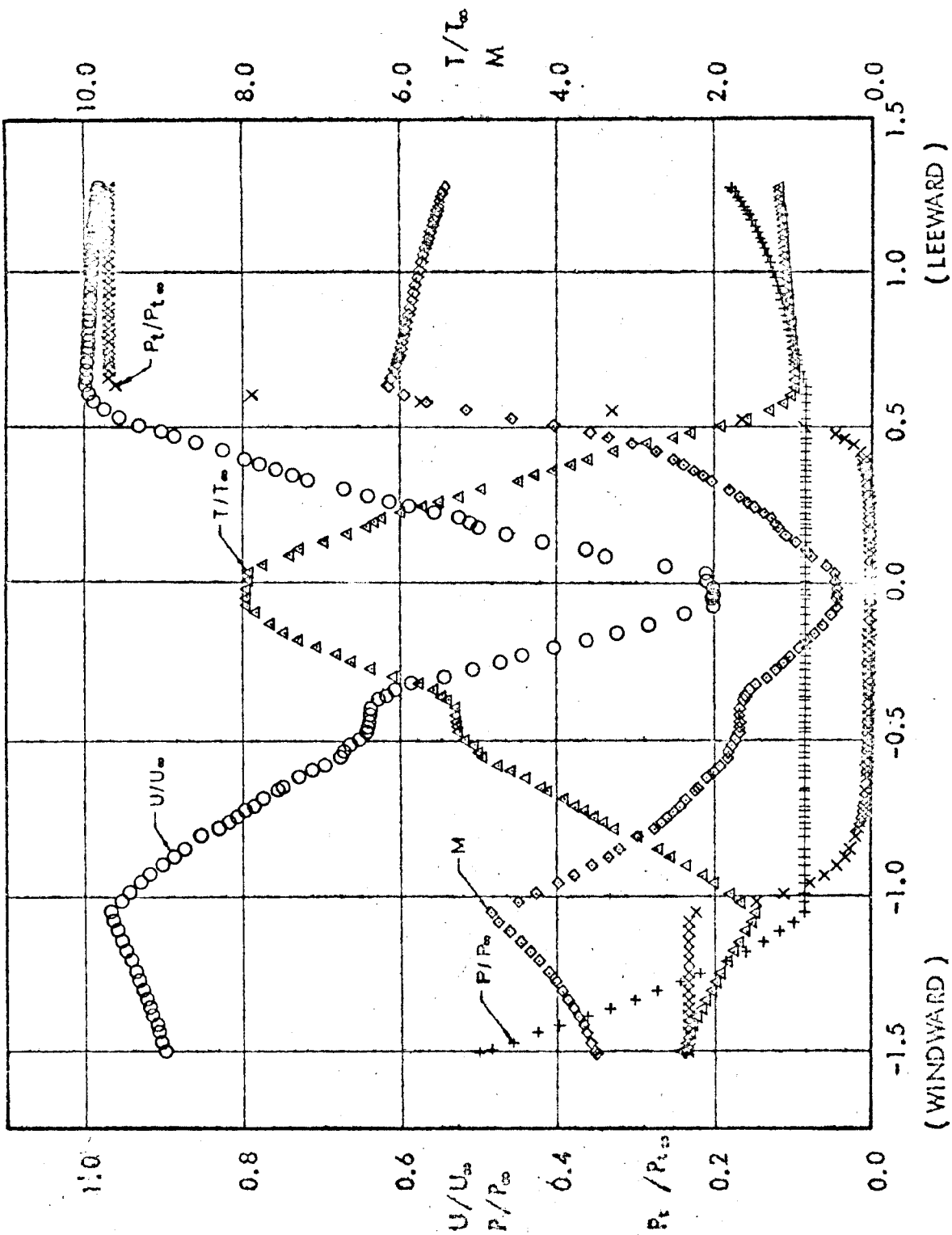

Po = 10 psig, H = 0.15 in., $\alpha = 15^{\circ}$, $x/H = 1.0$, $M_{\infty} = 6.02$

Fig. 9 TYPICAL NEAR WAKE PROFILES (NO REVERSE FLOW)

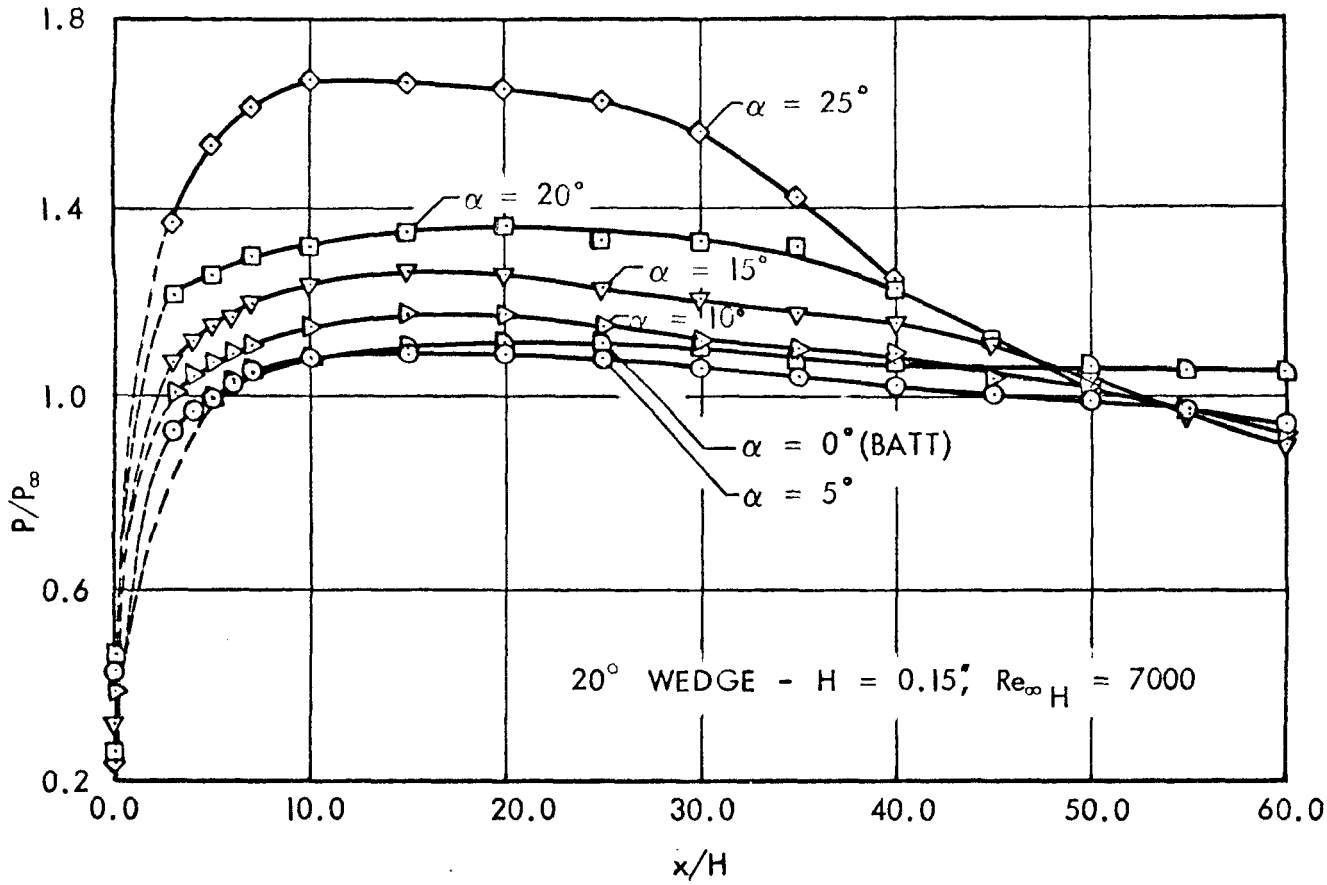

Fig. 10a STREAMWISE STATIC PRESSURE TRACES

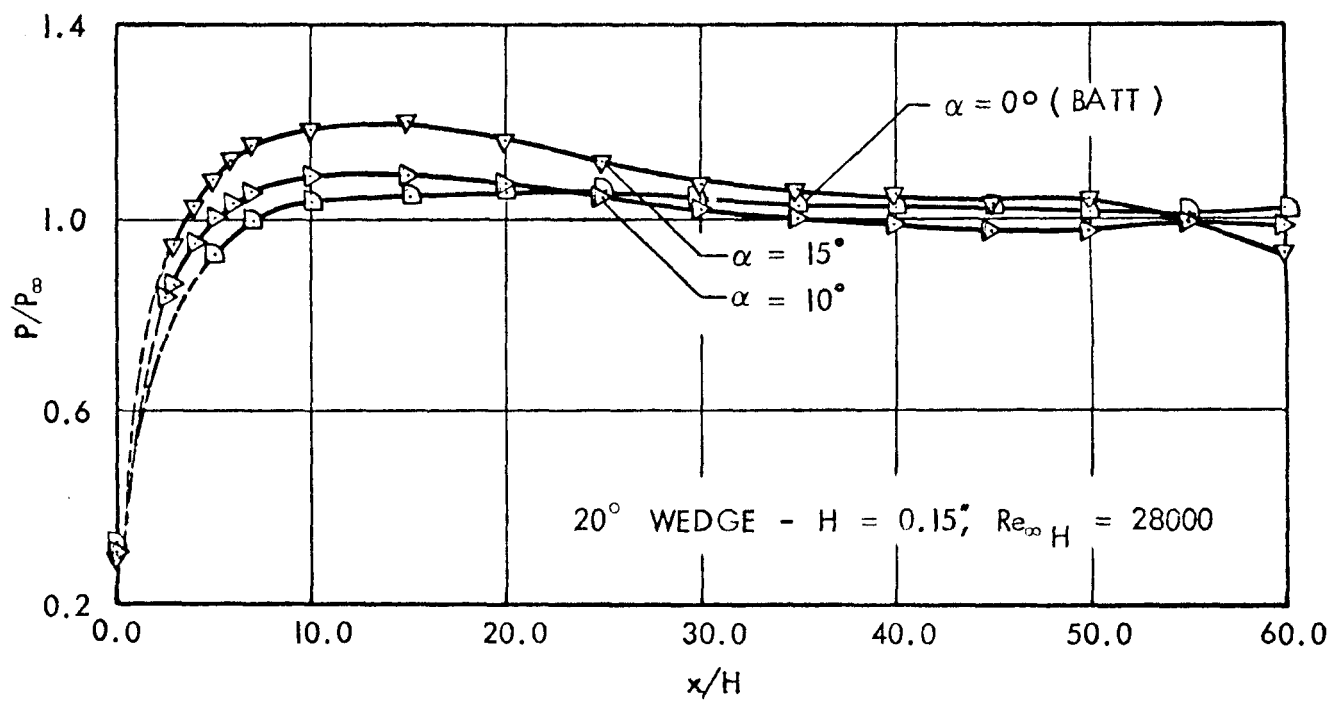

Fig. 10b STREAMWISE STATIC PRESSURE TRACES

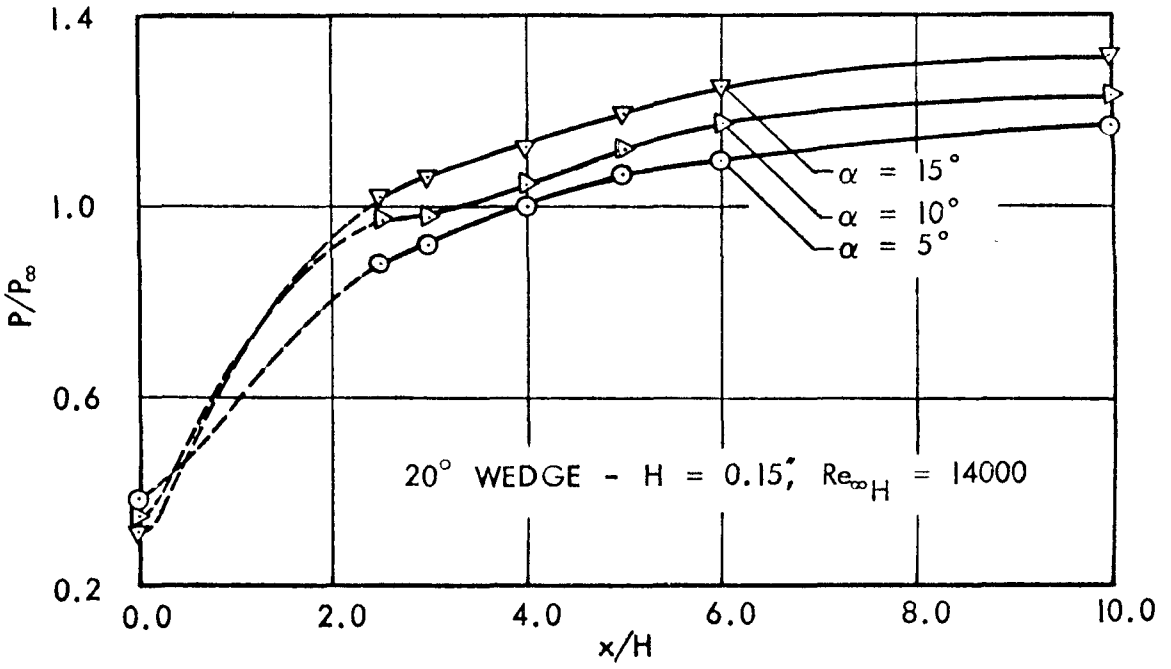

Fig. 10c STREAMWISE STATIC PRESSURE TRACES

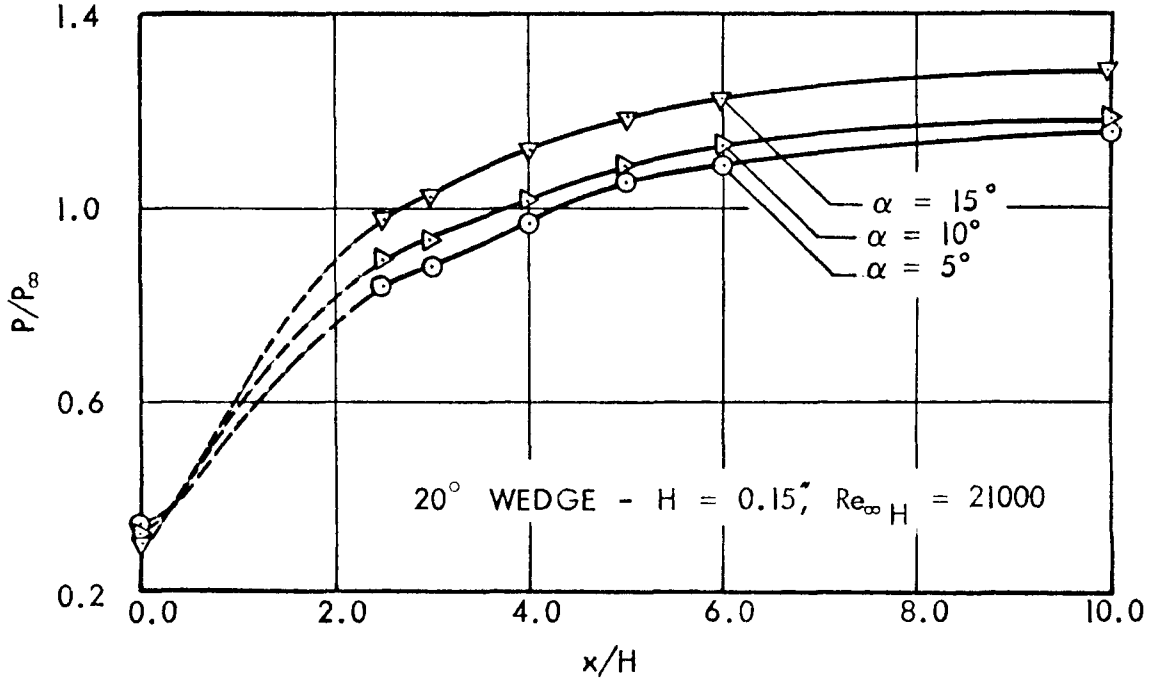

Fig. 10d STREAMWISE STATIC PRESSURE TRACES

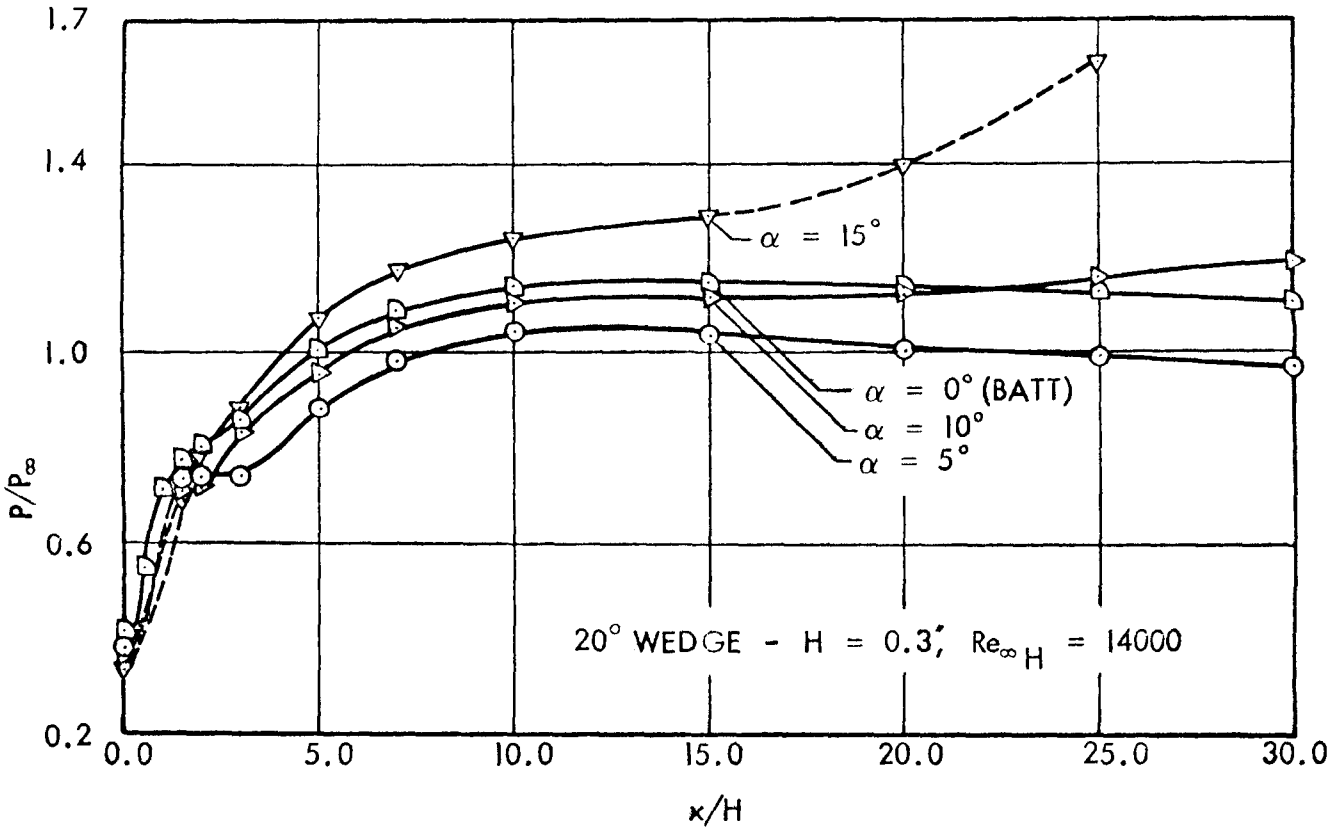

Fig. 11a STREAMWISE STATIC PRESSURE TRACES

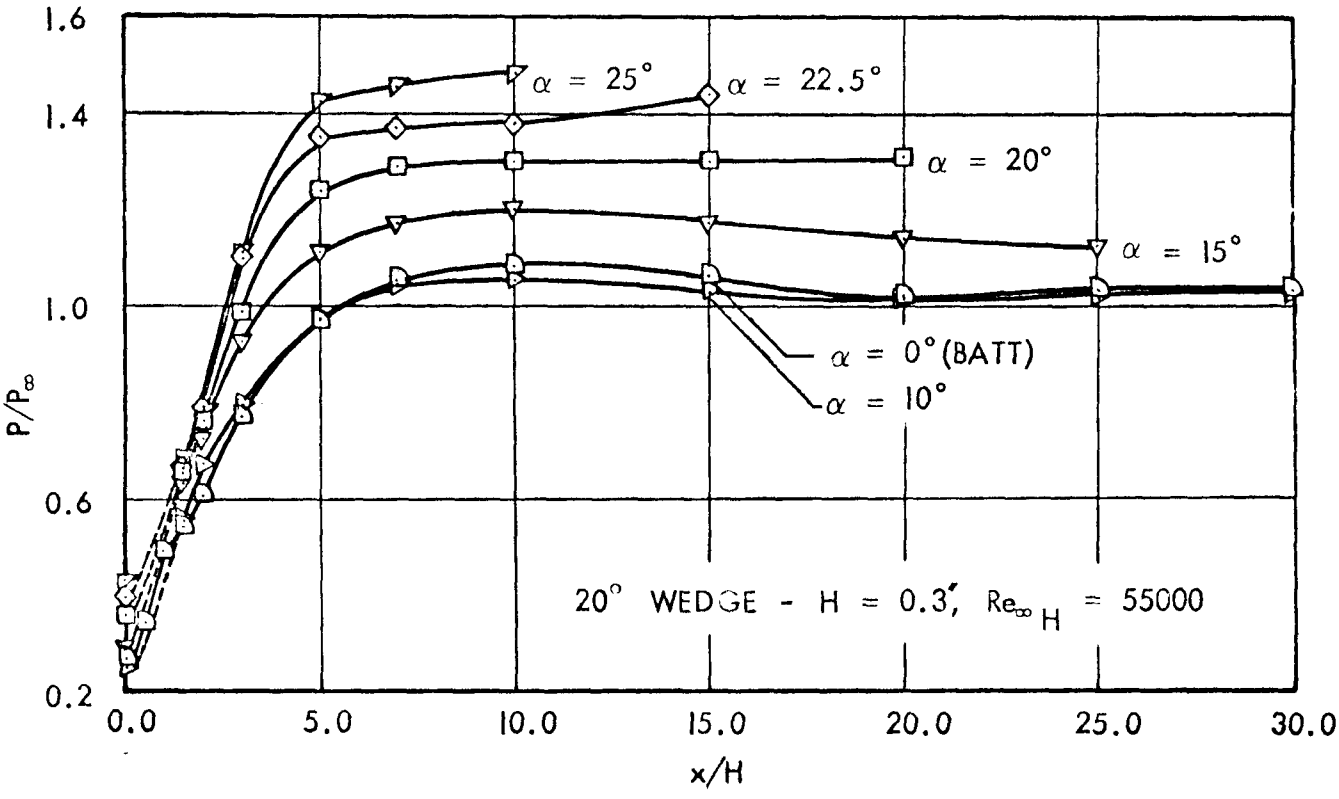

Fig. 11b STREAMWISE STATIC PRESSURE TRACES

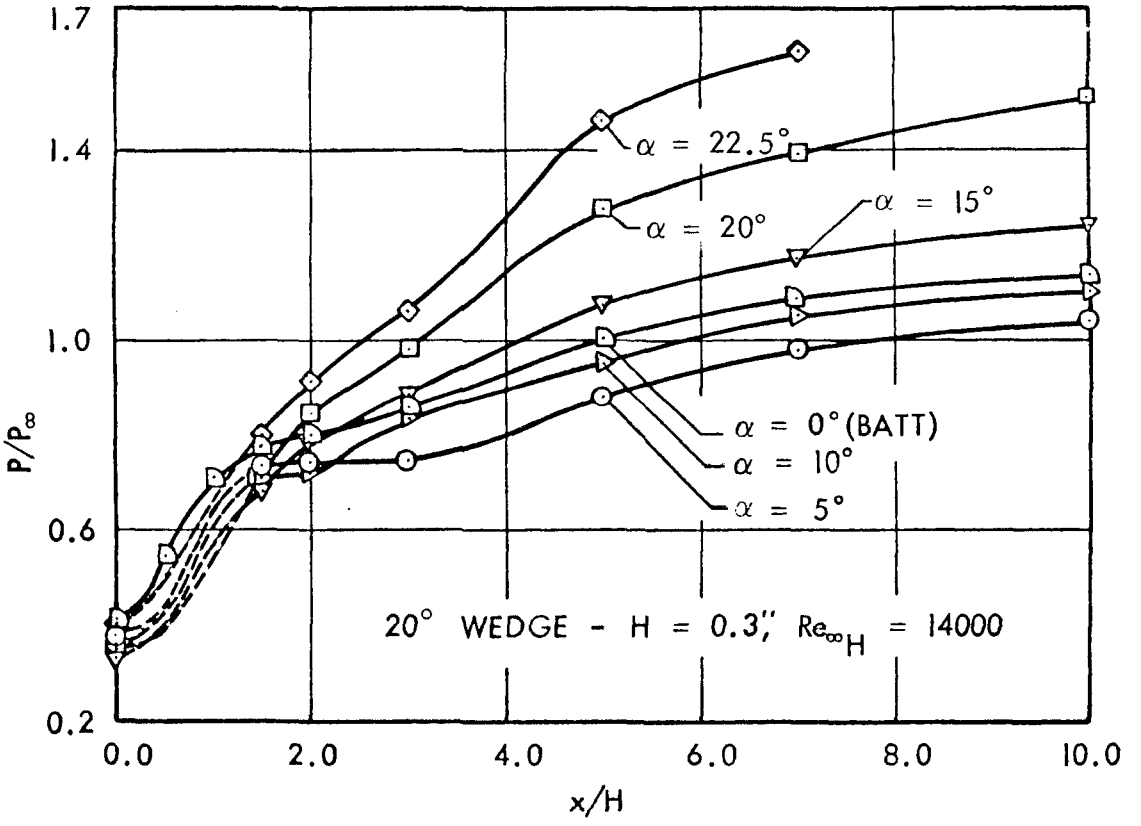

Fig.12a STREAMWISE STATIC PRESSURE TRACES

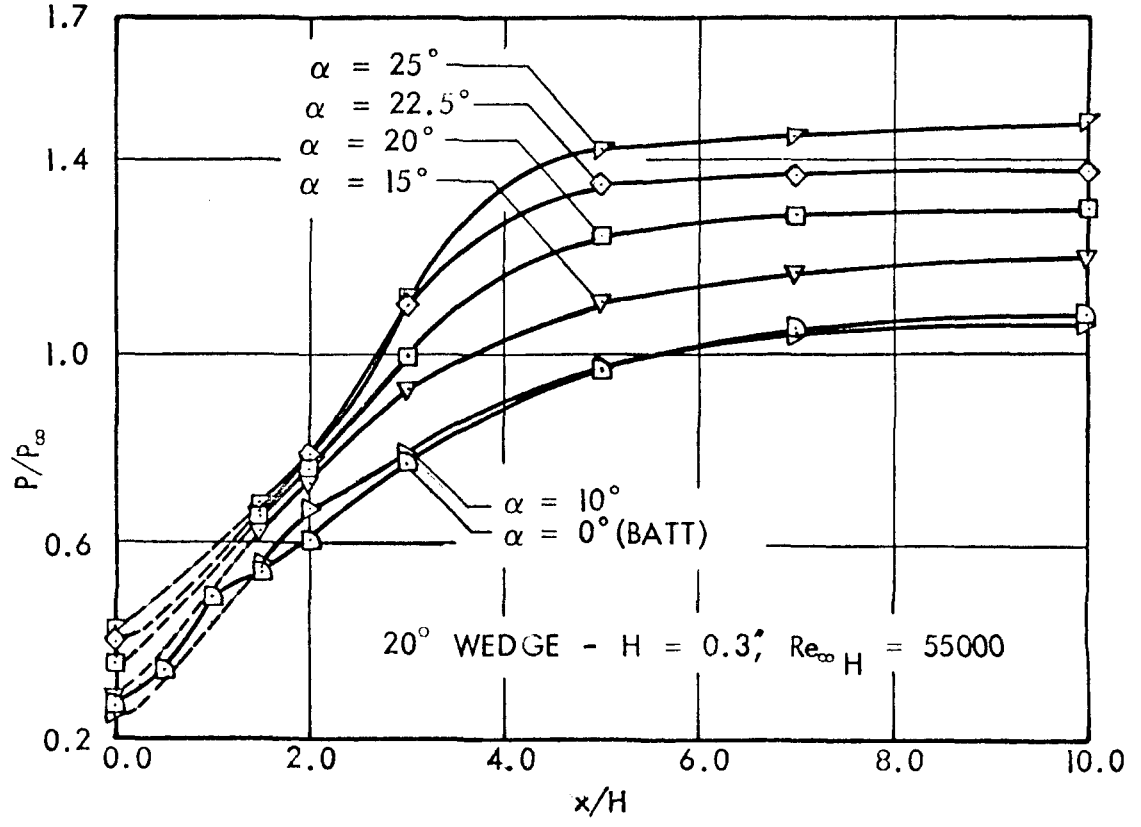

Fig. 12b STREAMWISE STATIC PRESSURE TRACES

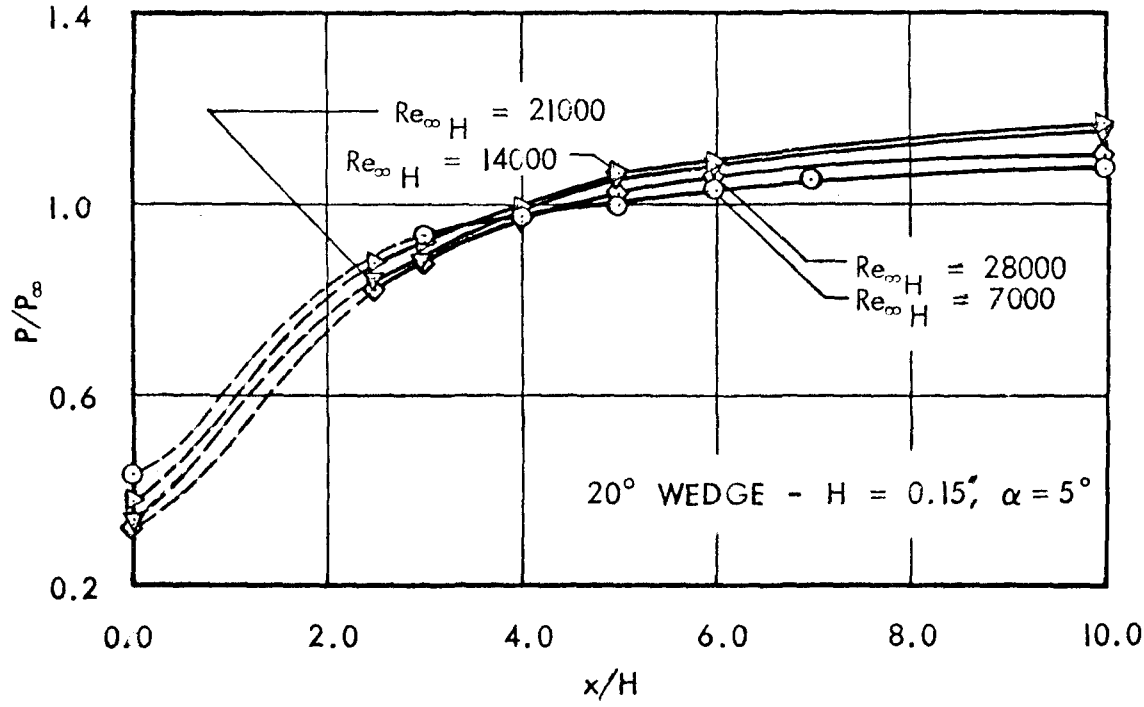

Fig. 13a STREAMWISE STATIC PRESSURE TRACES AT VARIOUS REYNOLDS NUMBERS

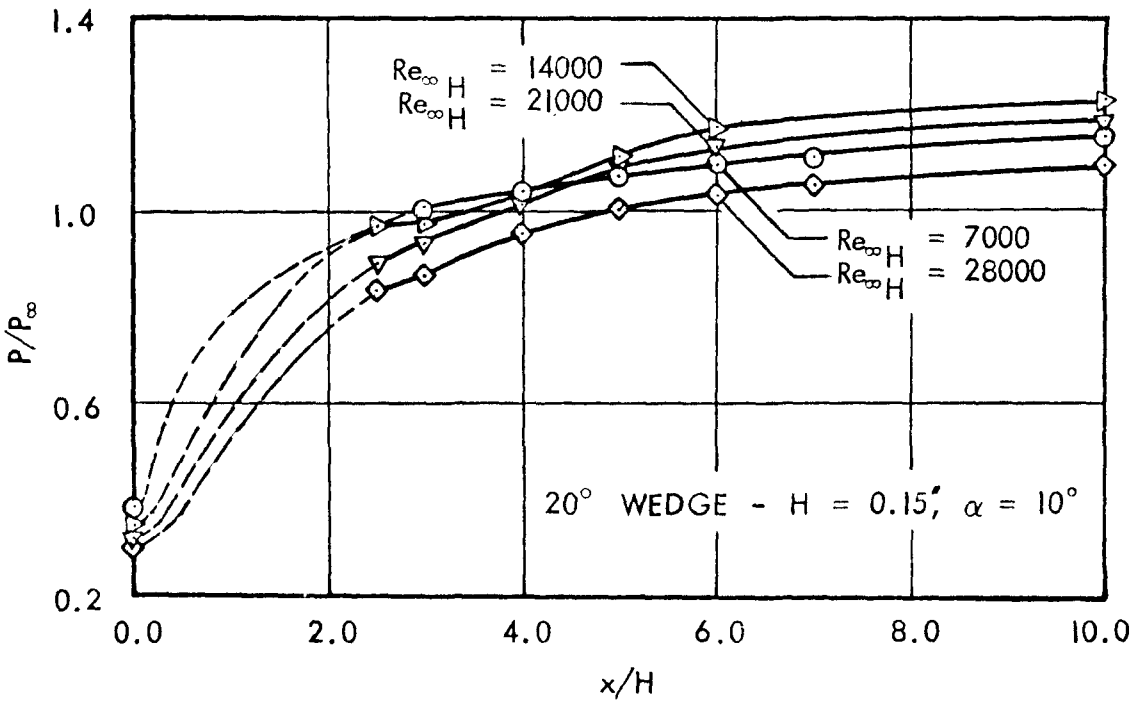

Fig. 13b STREAMWISE STATIC PRESSURE TRACES AT VARIOUS REYNOLDS NUMBERS

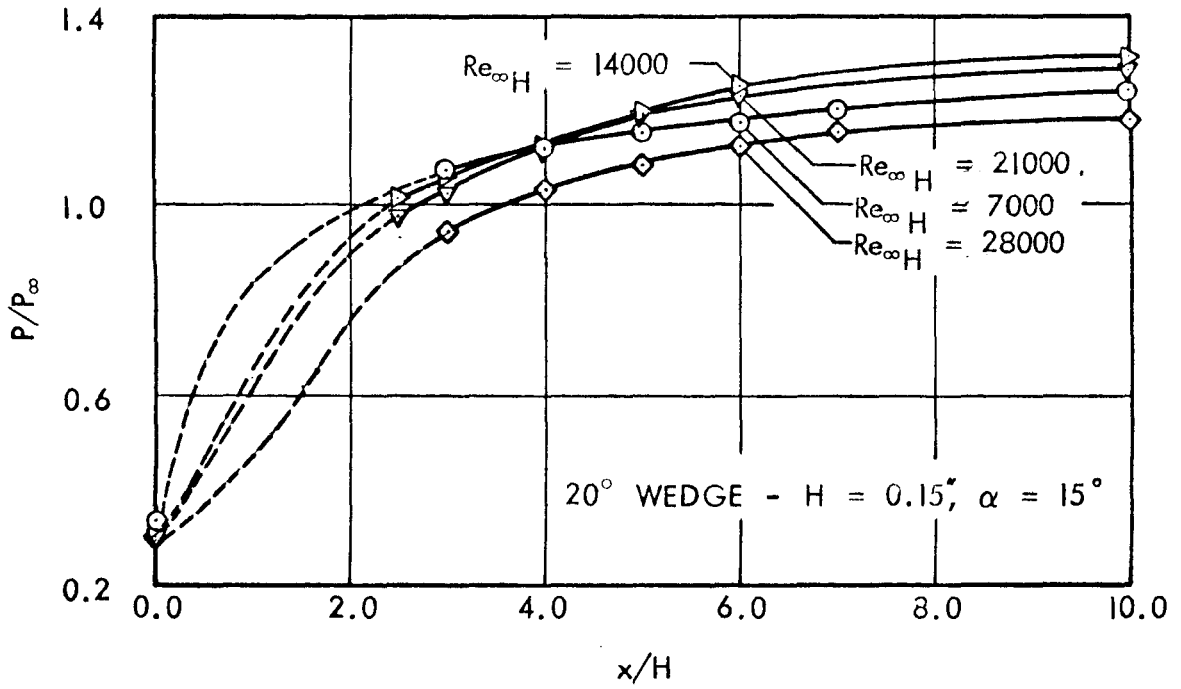

Fig. 13c STREAMWISE STATIC PRESSURE TRACES AT VARIOUS REYNOLDS NUMBERS

MODEL : $H = 0.15$ in.

$\alpha = 5°$

TEST CONDITION :

$P_o = 10$ psig $\quad M_\infty = 6.02$

$Re_{\infty H} = 0.7 \times 10^4$

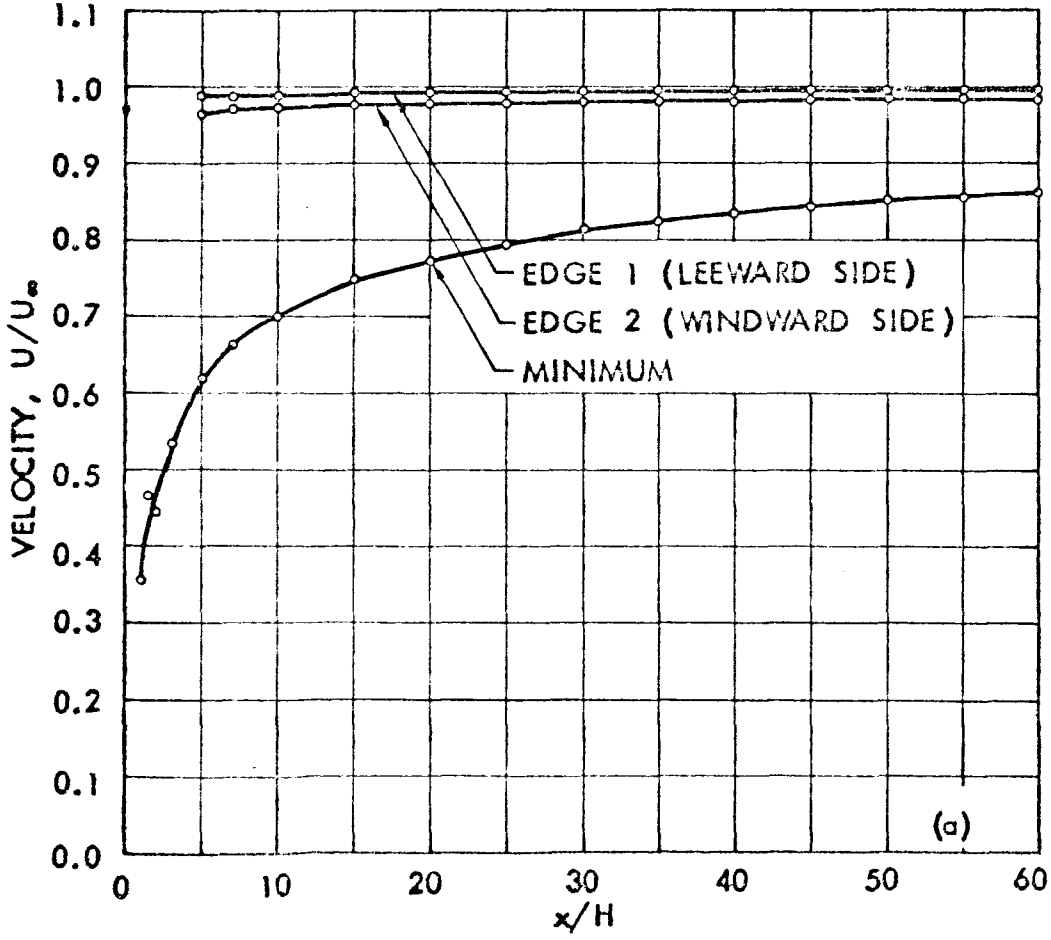

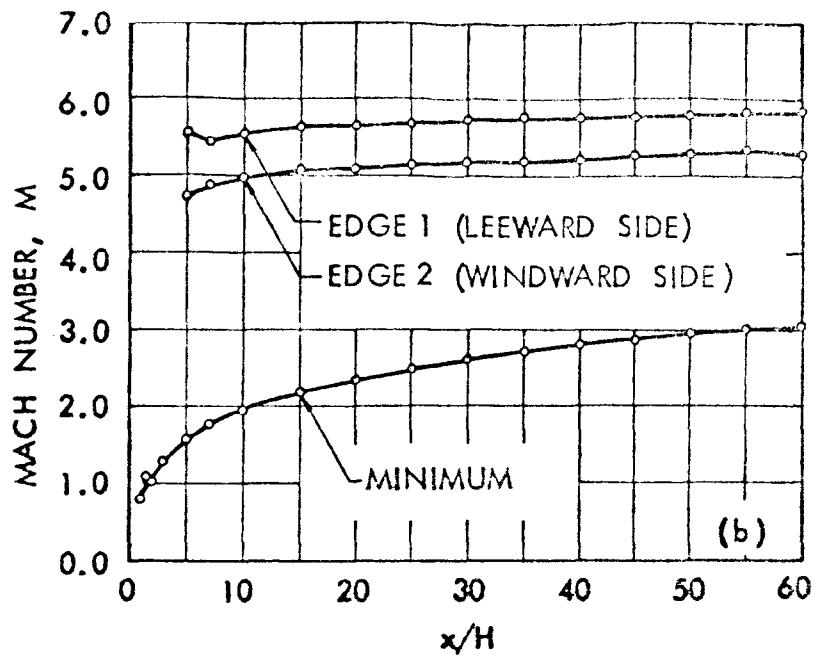

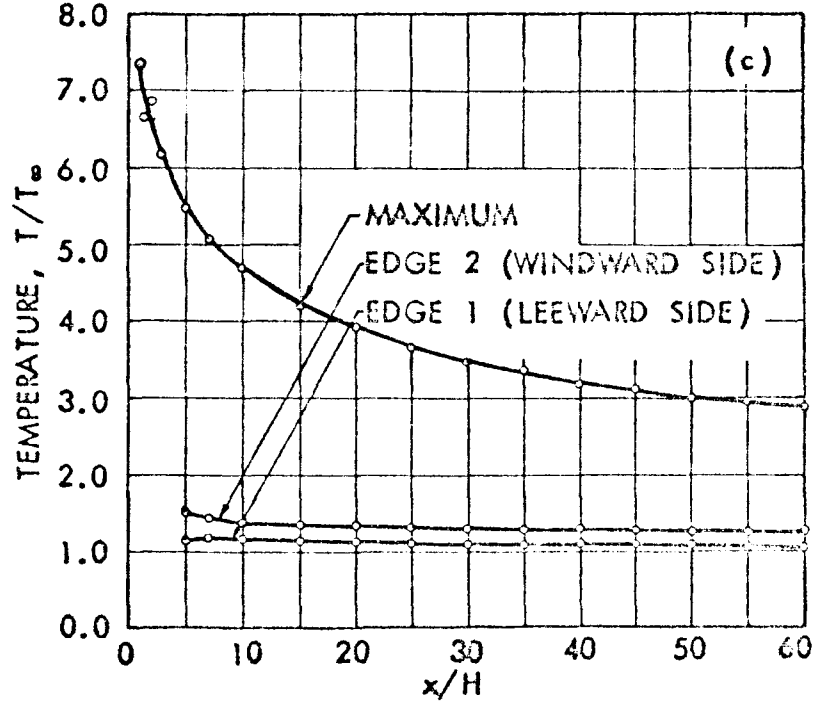

Fig. 14a STREAMWISE FLOW CHARACTERISTICS

MODEL : H = 0.15 in.

α = 10°

TEST CONDITION :

P_o = 10 psig M_∞ = 6.02

$Re_{\infty H}$ = 0.7 x 10^4

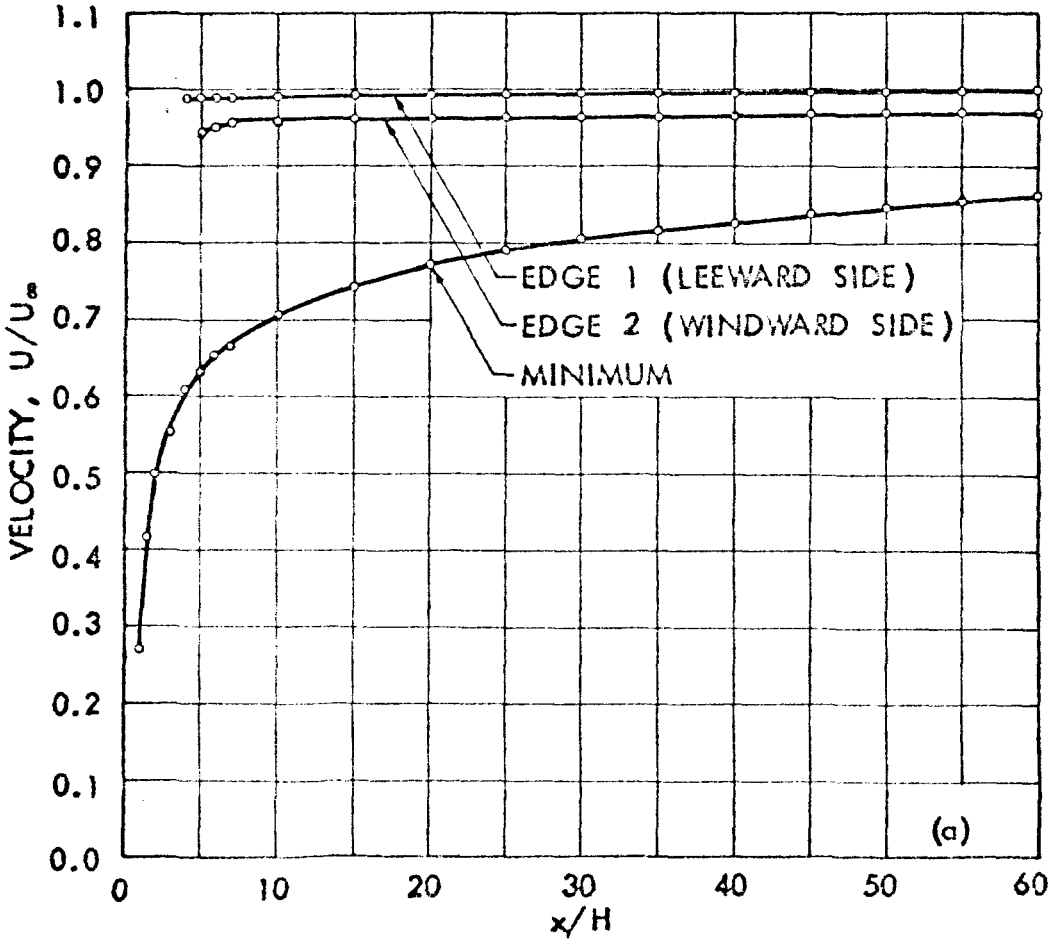

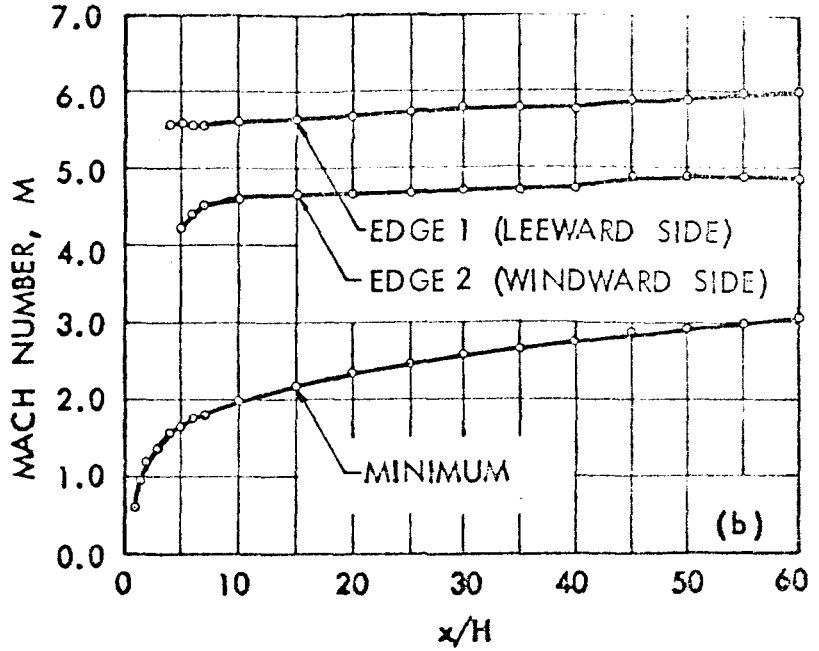

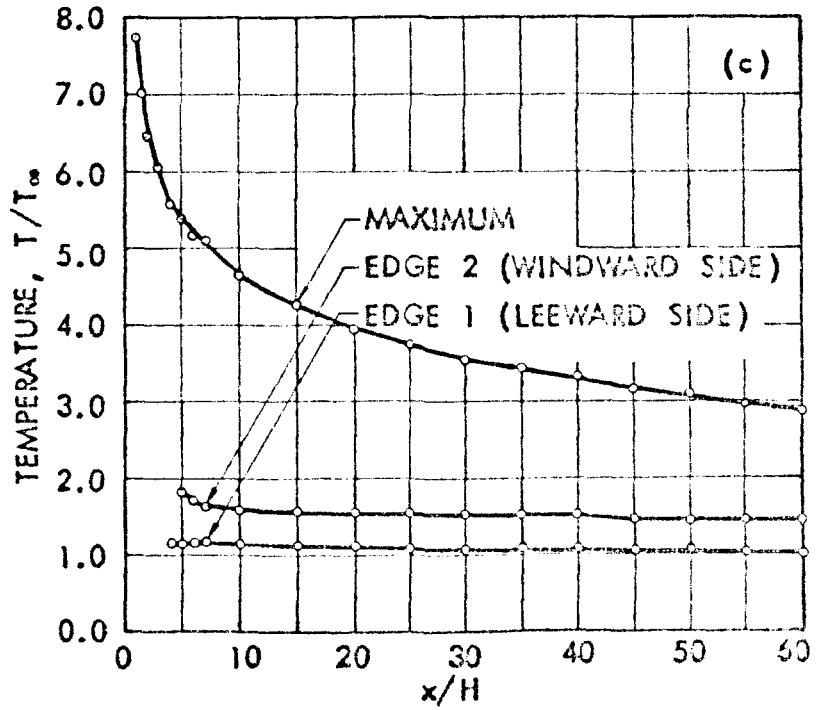

Fig. 14b STREAMWISE FLOW CHARACTERISTICS

MODEL : $H = 0.15$ in.

$\alpha = 15°$

TEST CONDITION :

$P_o = 10$ psig $\quad M_\infty = 6.02$

$Re_{\infty H} = 0.7 \times 10^4$

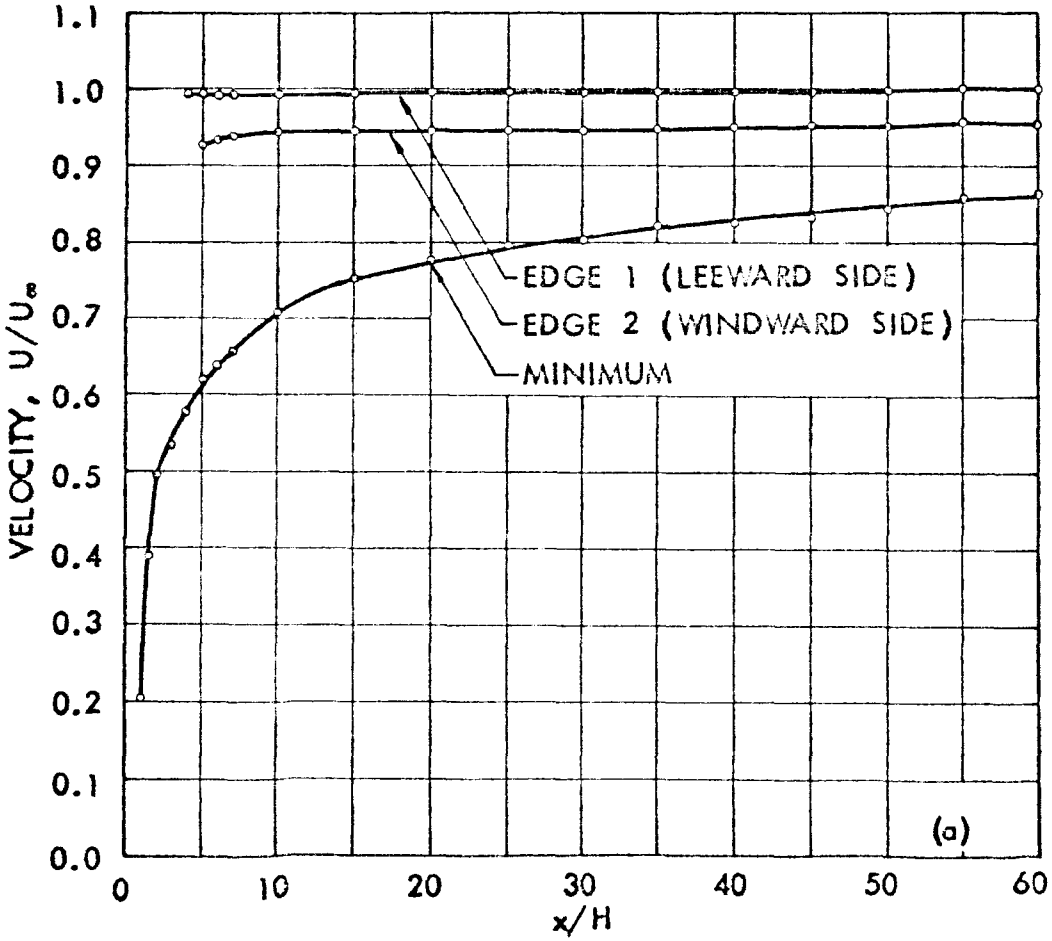

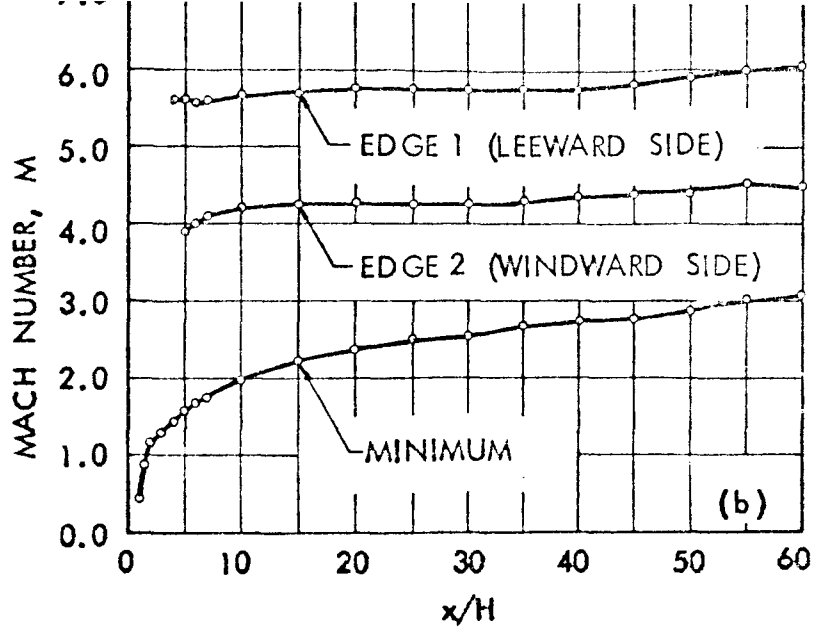

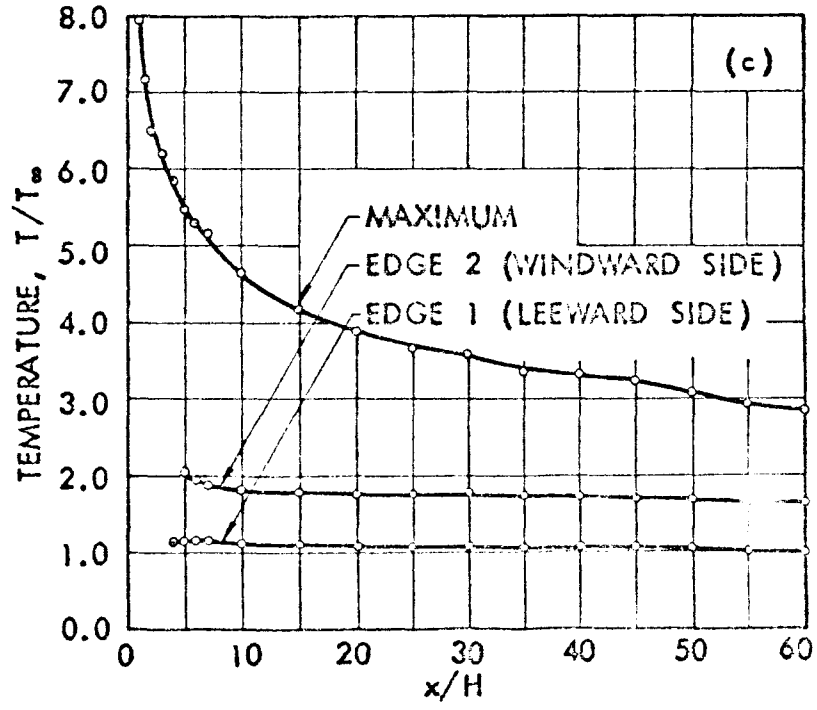

Fig. 14c STREAMWISE FLOW CHARACTERISTICS

MODEL : H = 0.15 in.

α = 20°

TEST CONDITION :

P_o = 10 psig M_∞ = 6.02

$Re_{\infty H}$ = 0.7 x 10^6

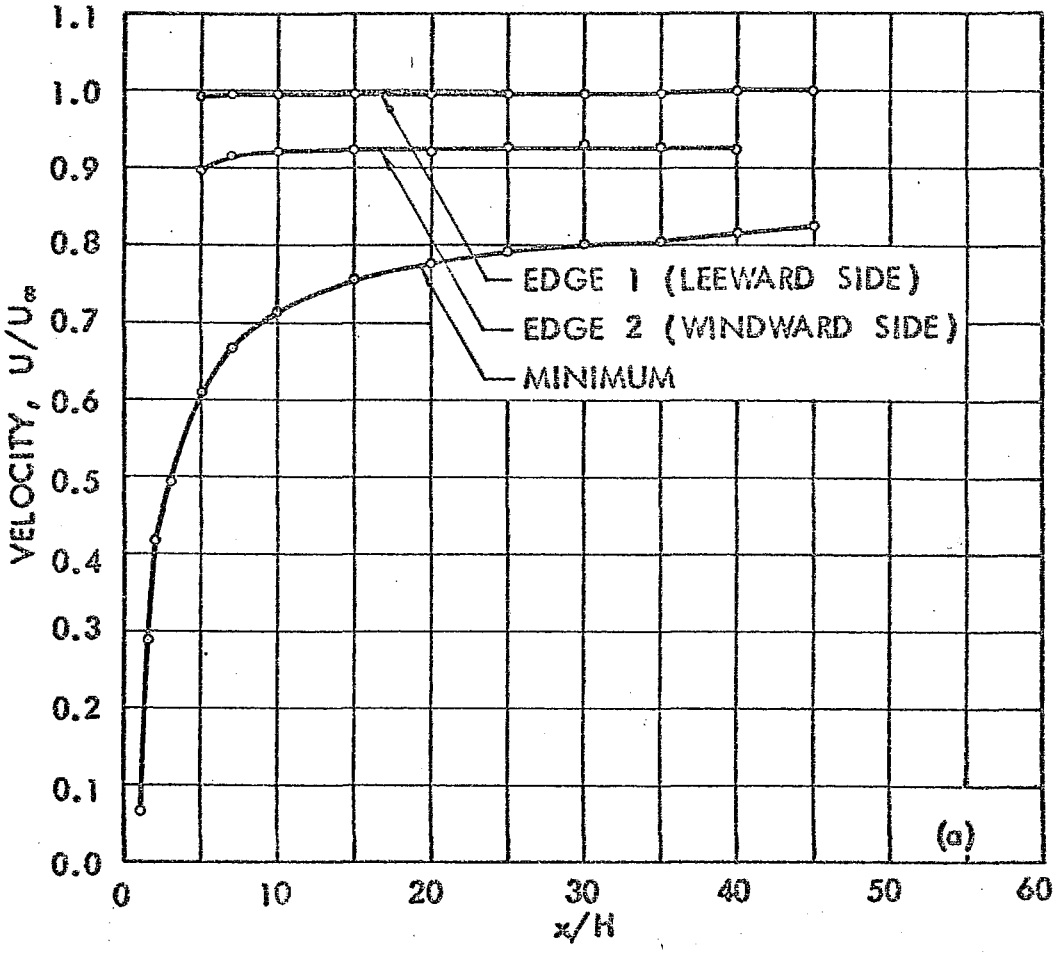

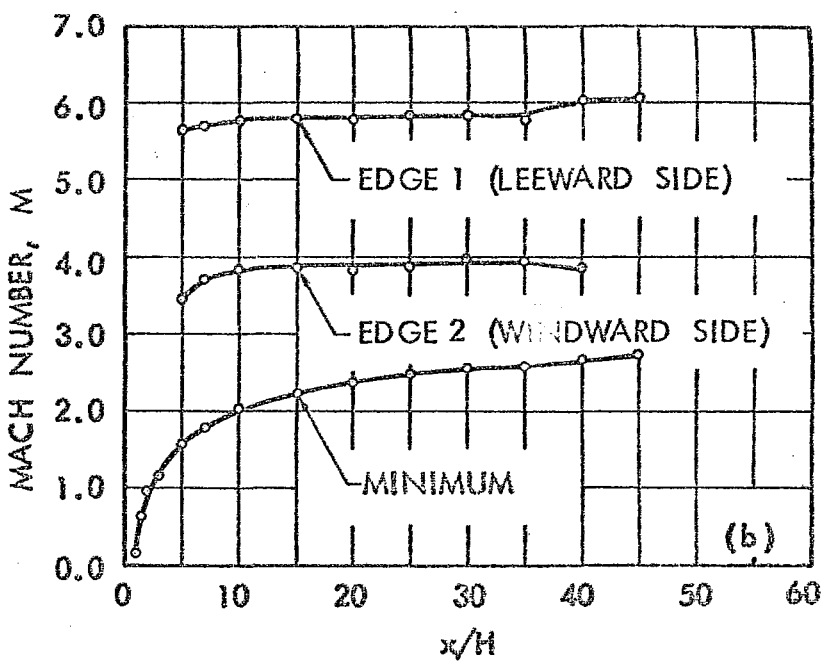

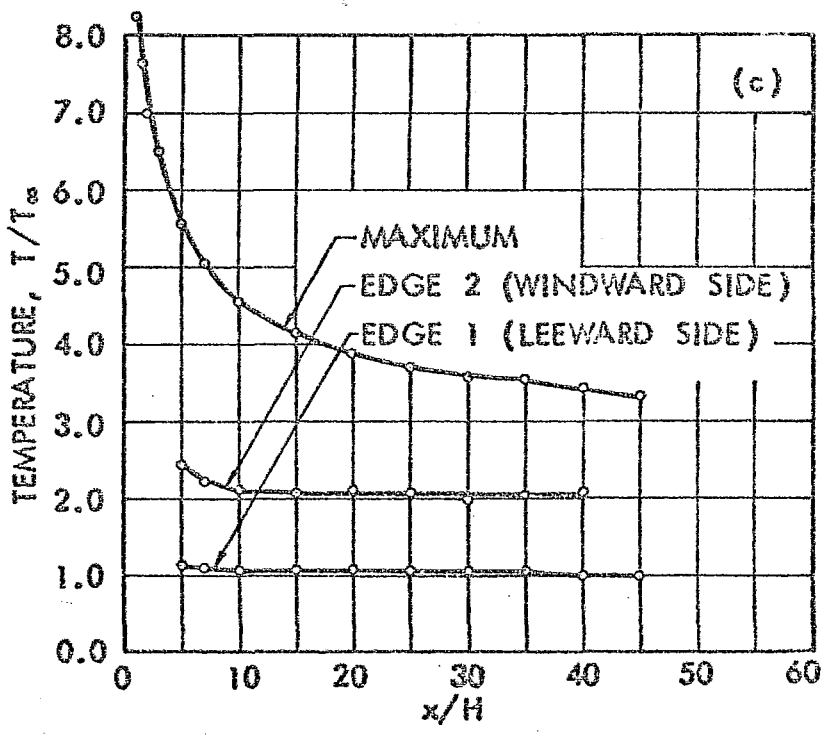

Fig. 14d STREAMWISE FLOW CHARACTERISTICS

MODEL : $H = 0.15$ in.

$\alpha = 25°$

TEST CONDITION :

$P_o = 10$ psig $\quad M_\infty = 6.02$

$Re_{\infty H} = 0.7 \times 10^6$

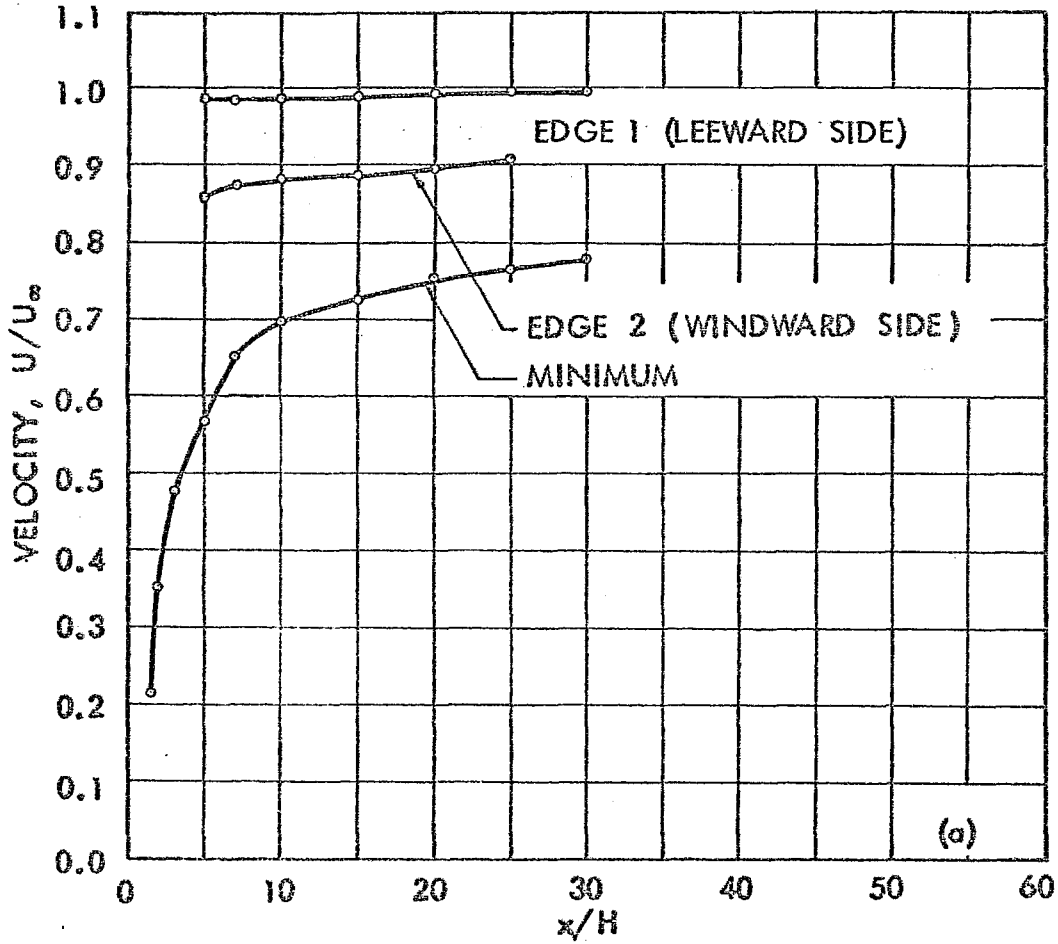

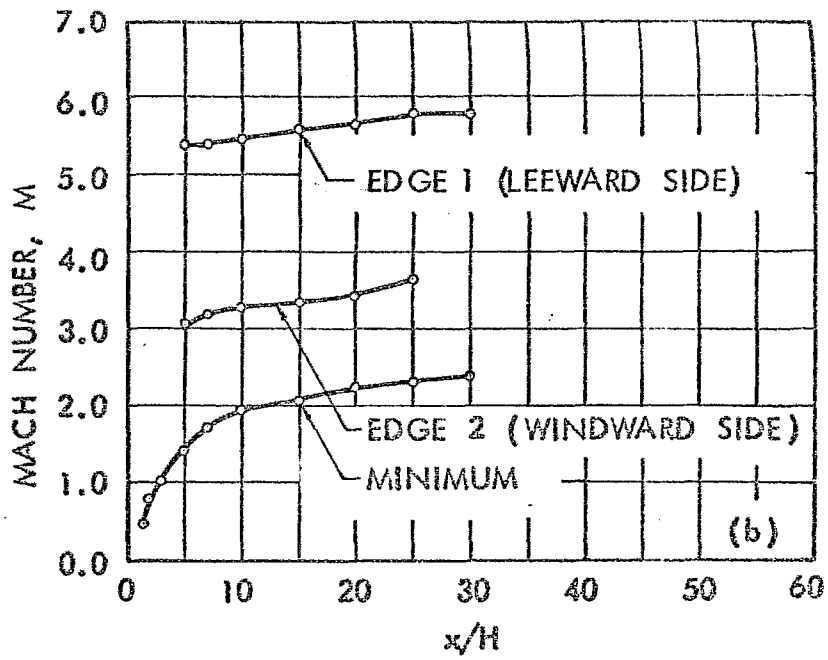

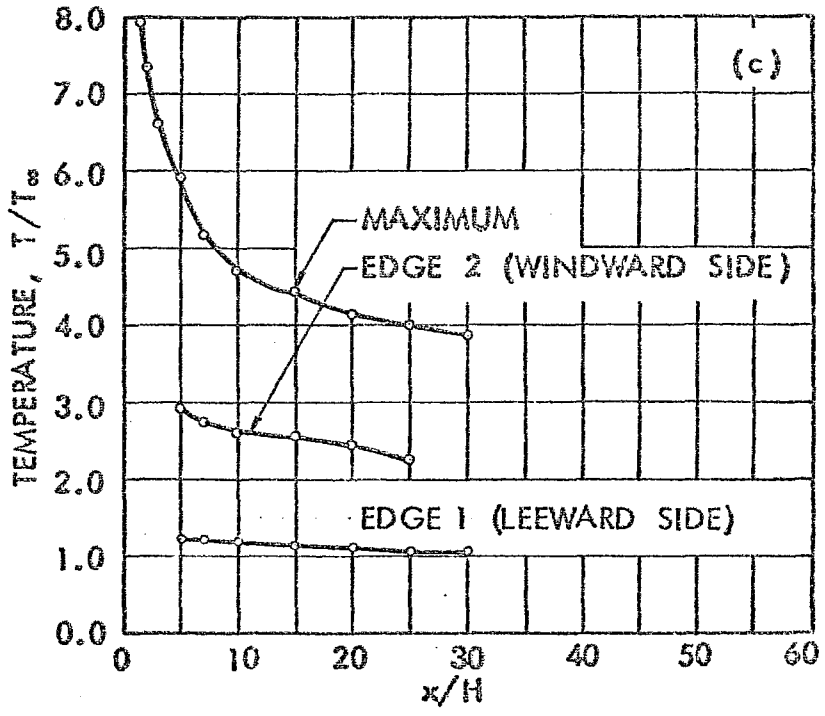

Fig. 14e STREAMWISE FLOW CHARACTERISTICS

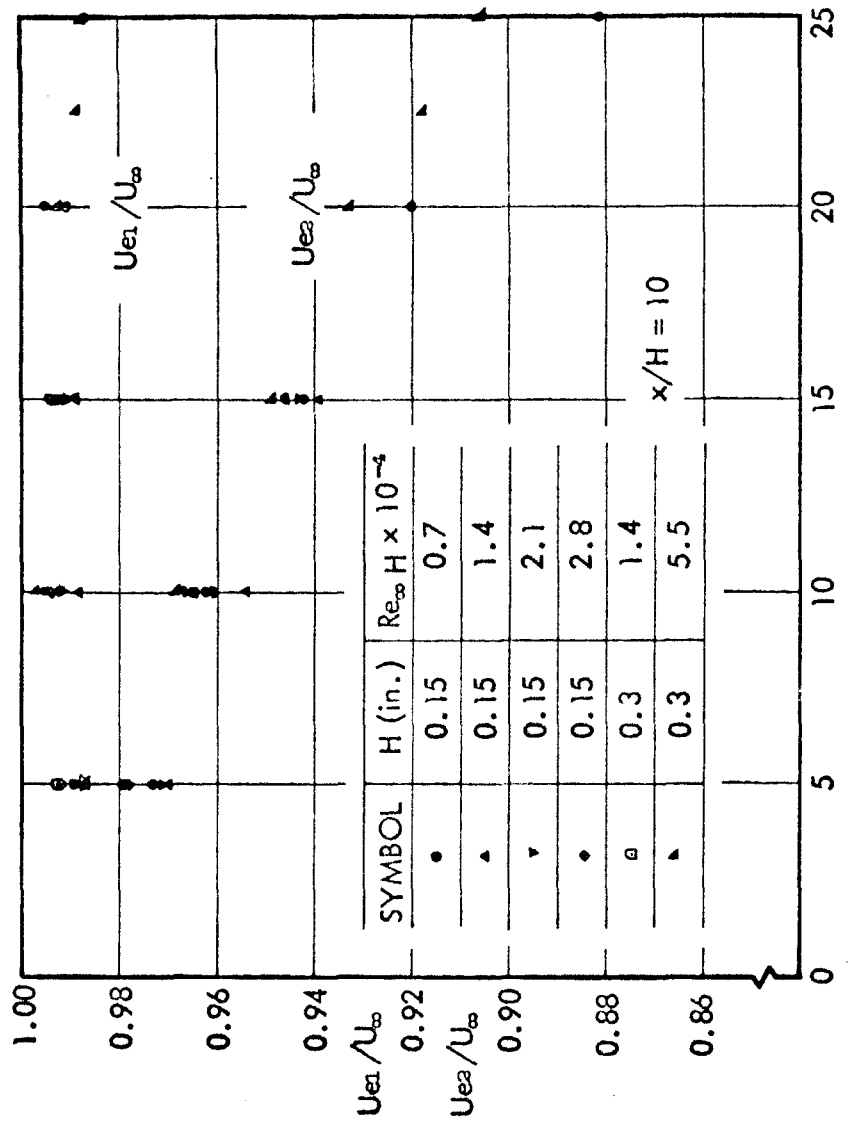

Fig. 15a VISCOUS WAKE EDGE VELOCITIES

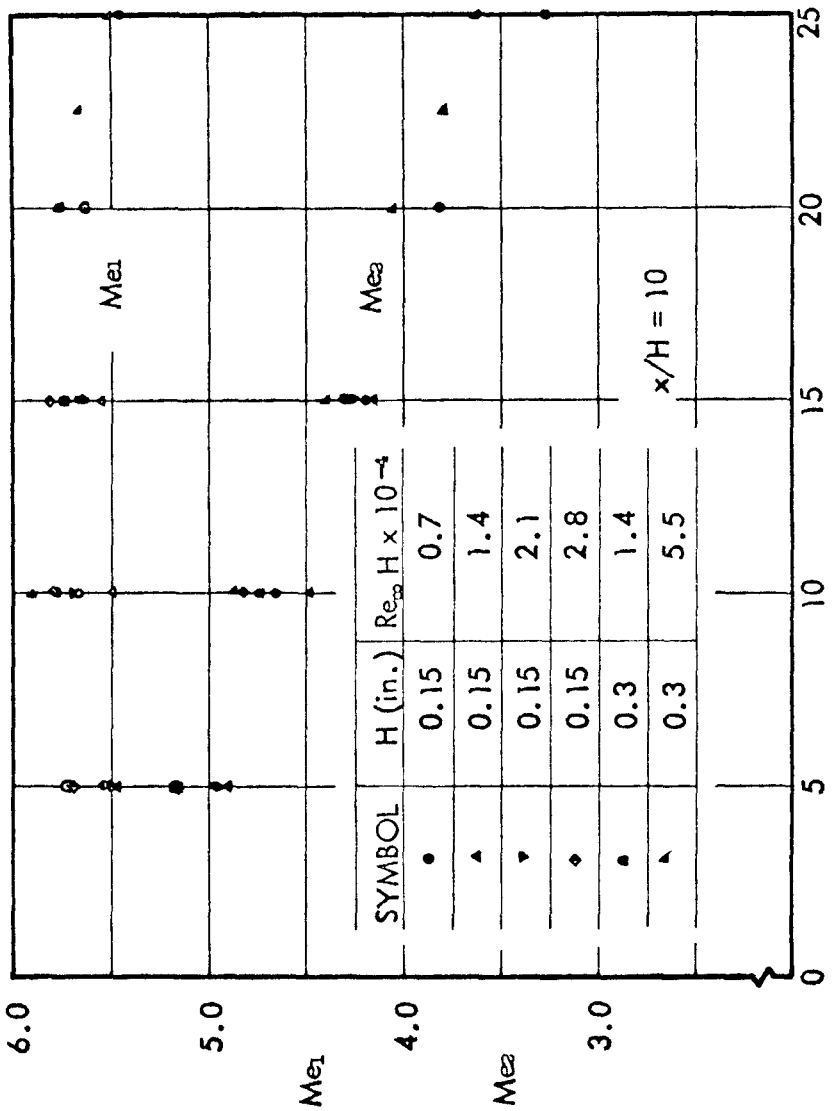

Fig. 15b VISCOUS WAKE EDGE MACH NUMBERS

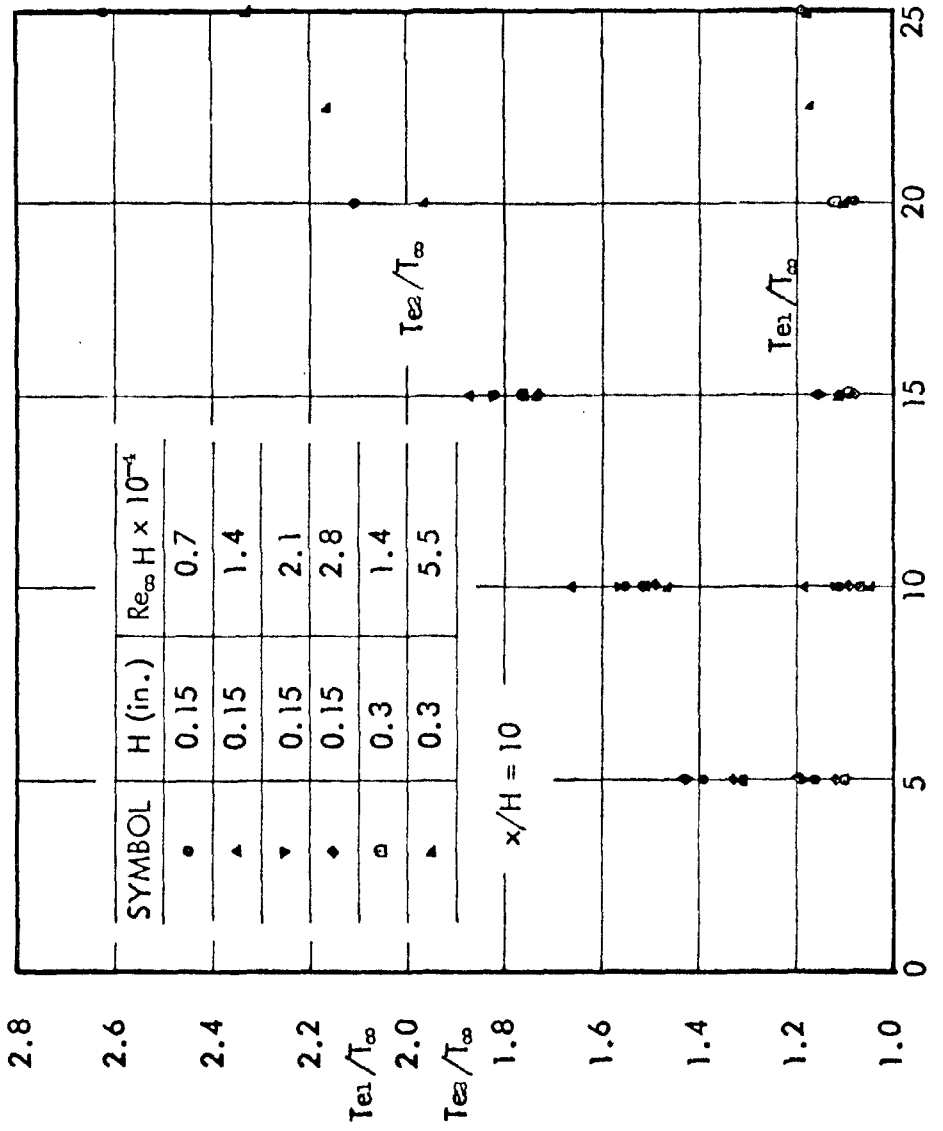

Fig. 15c VISCOUS WAKE EDGE TEMPERATURES

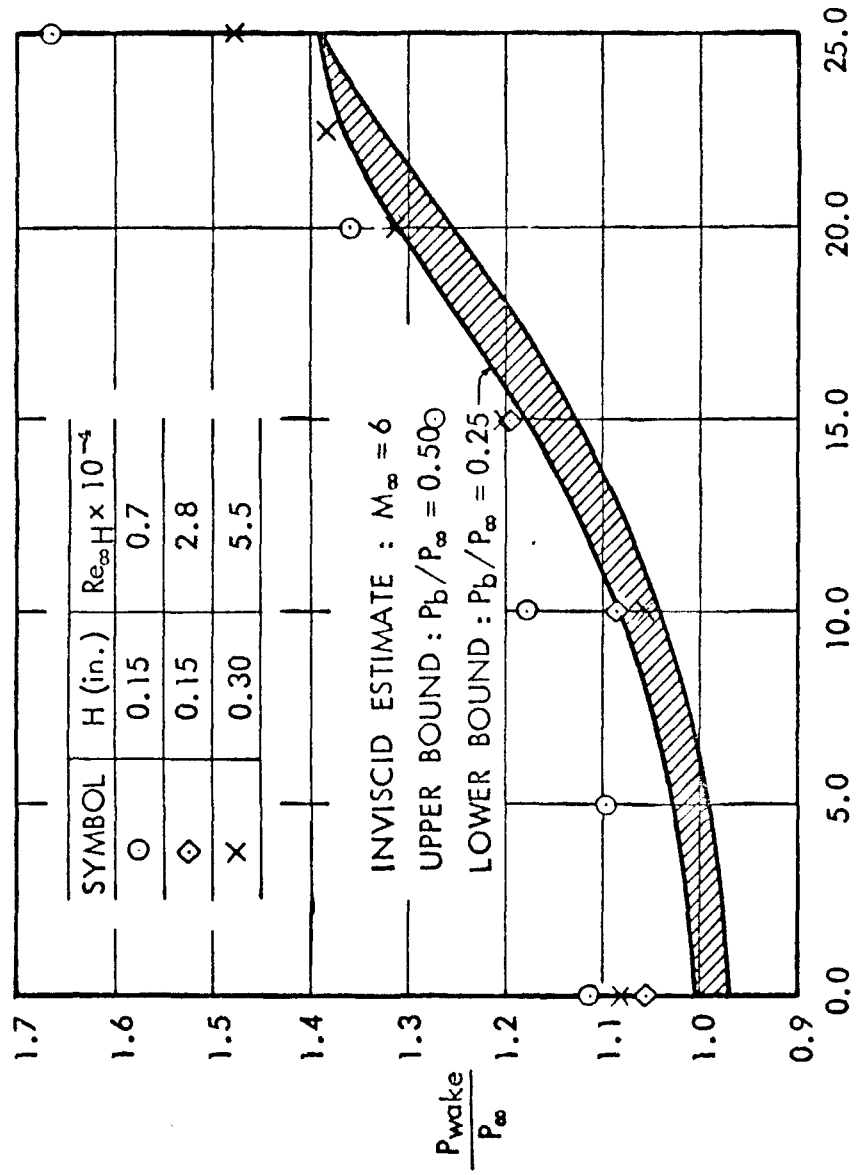

Fig. 16 FAR WAKE STATIC PRESSURE COMPARED TO RESULTS OF INVISCID ESTIMATE

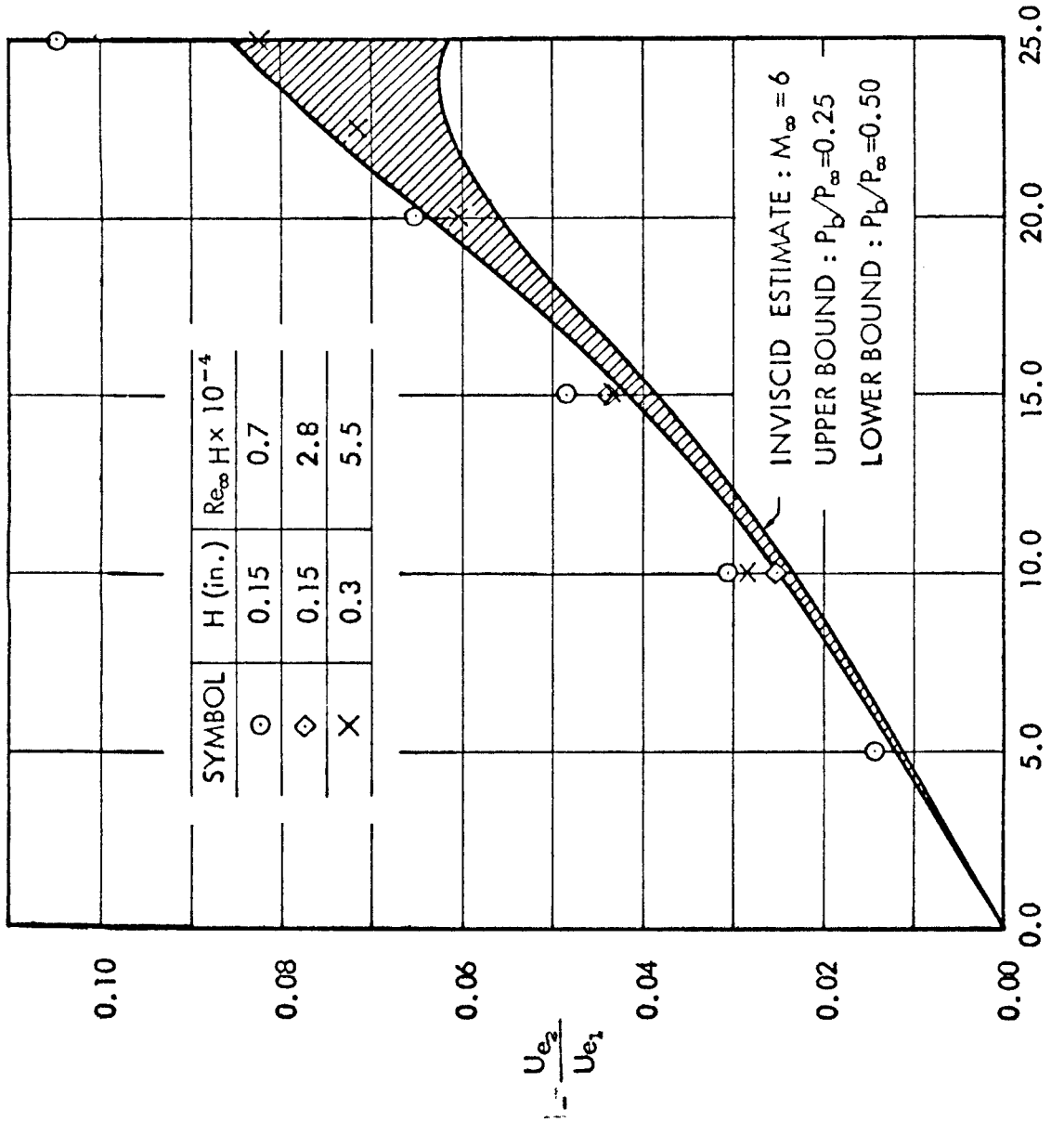

Fig. 17 NORMALIZED VELOCITY DIFFERENCE BETWEEN TWO VISCOUS WAKE EDGES

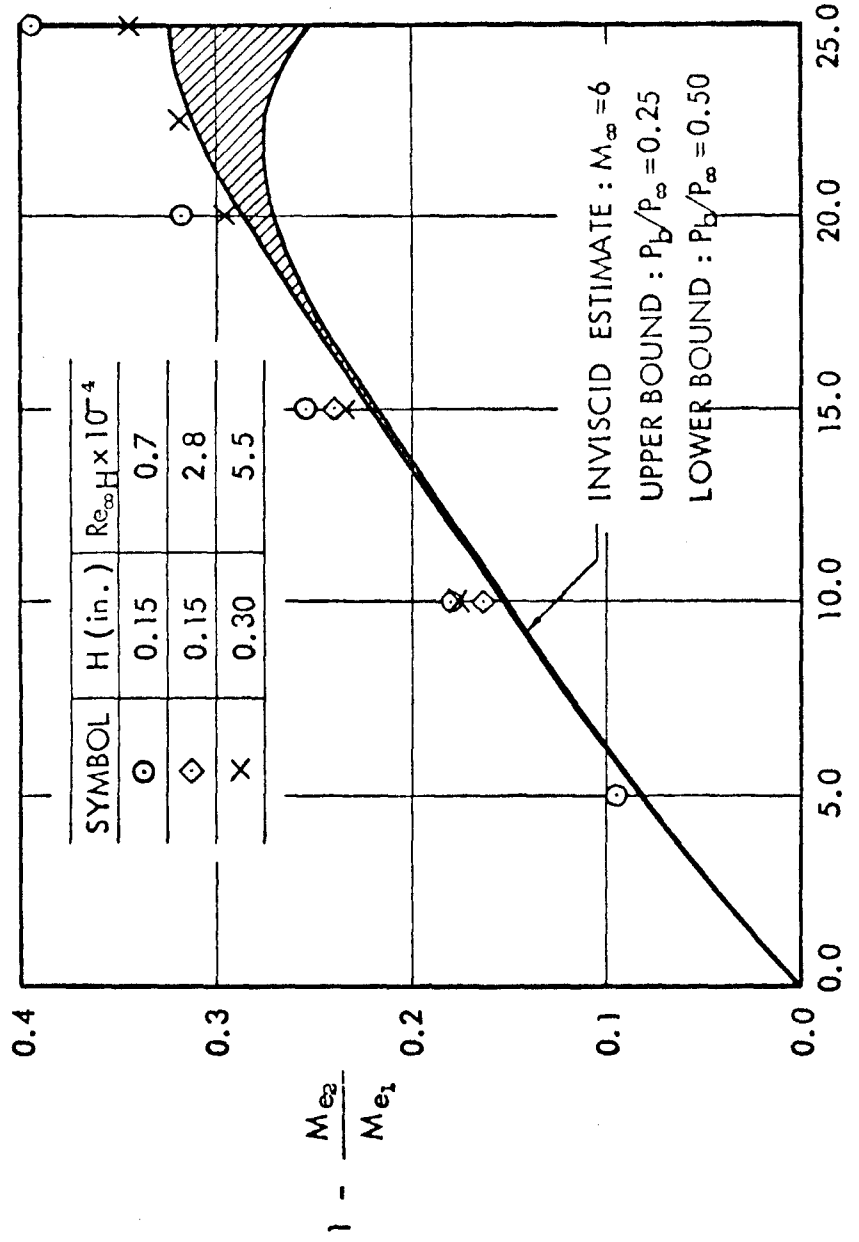

Fig. 18 NORMALIZED MACH NUMBER DIFFERENCE BETWEEN TWO VISCOUS WAKE EDGES

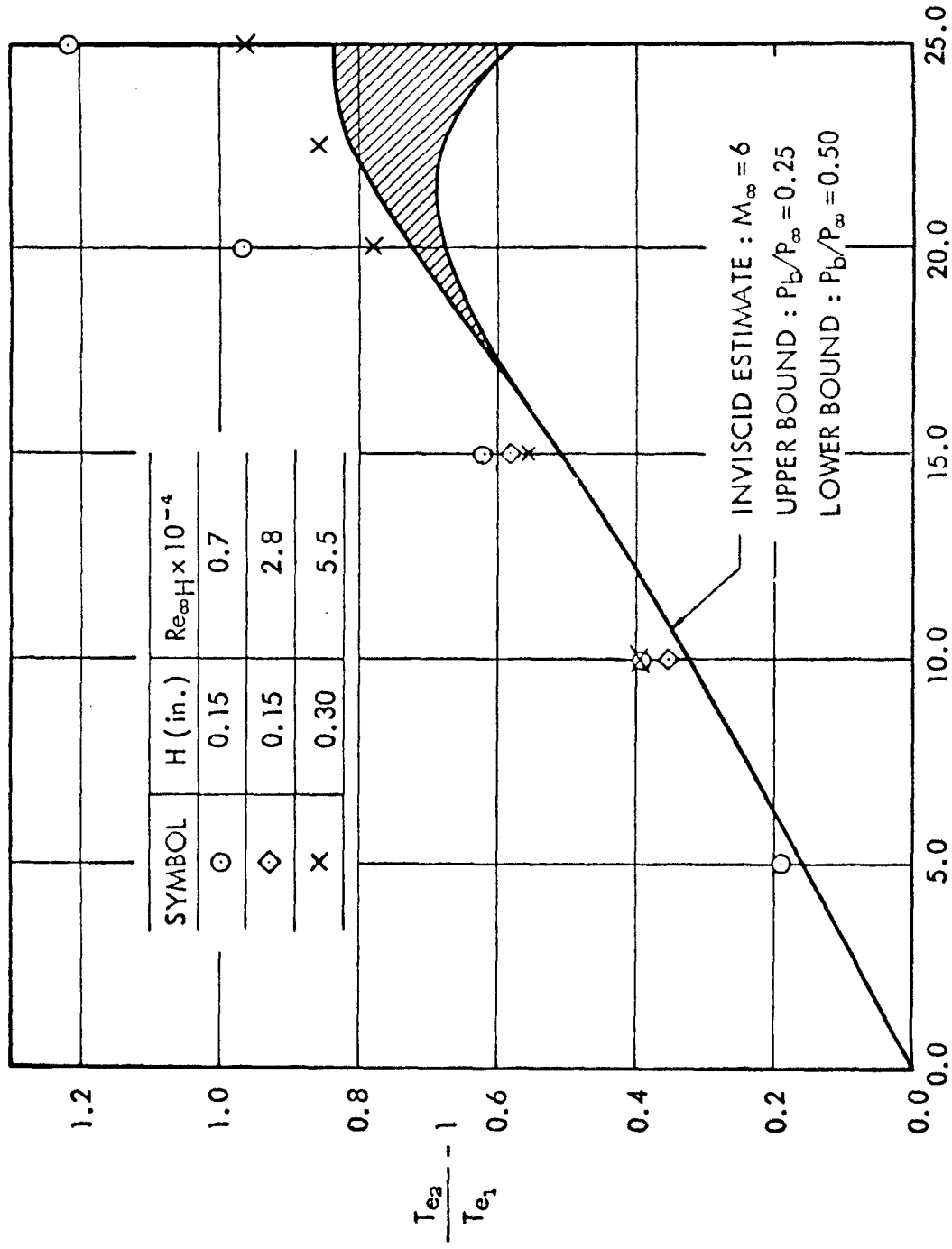

Fig. 19 NORMALIZED TEMPERATURE DIFFERENCE BETWEEN TWO VISCOUS WAKE EDGES

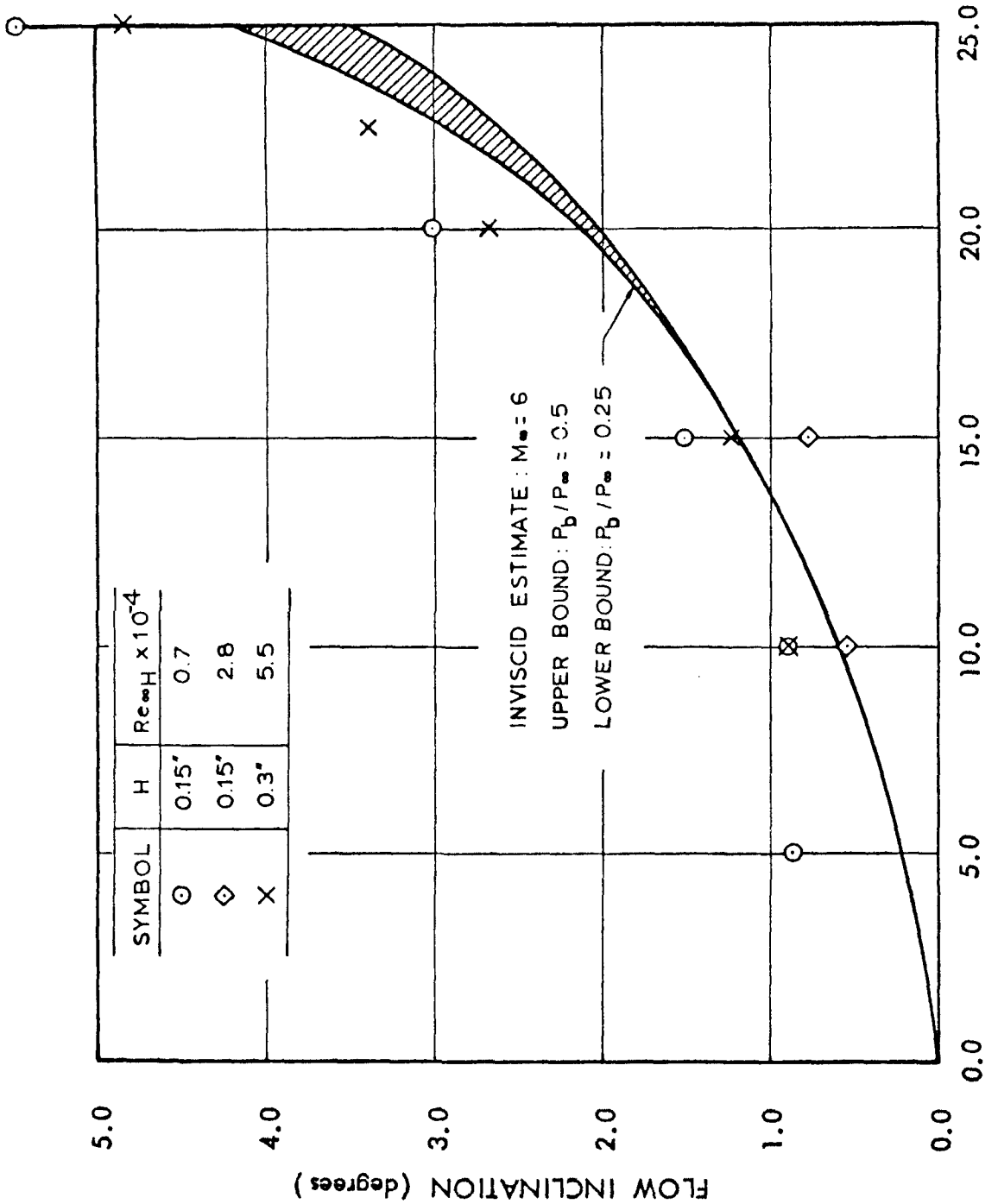

Fig. 20 FAR WAKE SLIPSTREAM INCLINATION

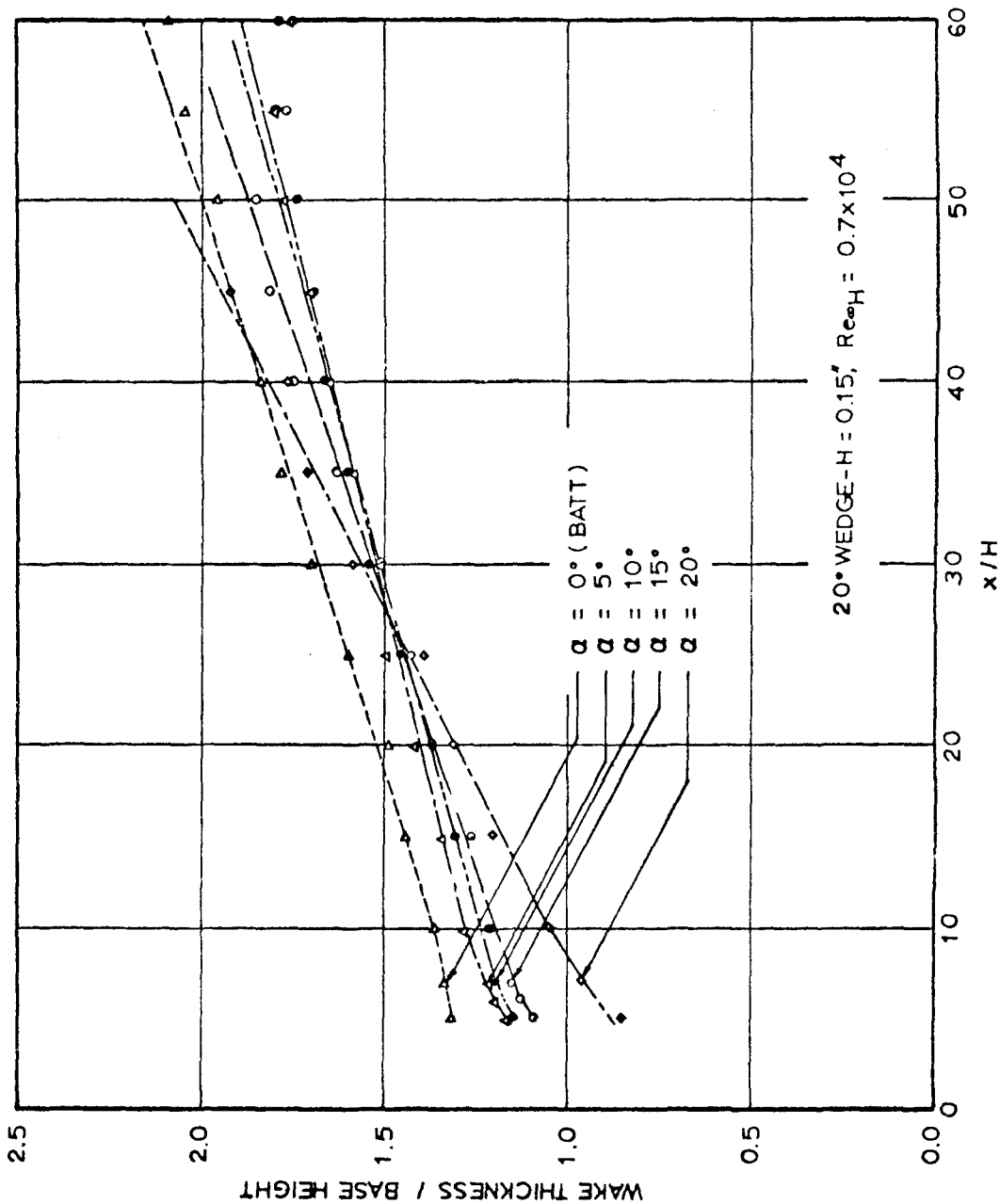

Fig. 21a WAKE THICKNESS

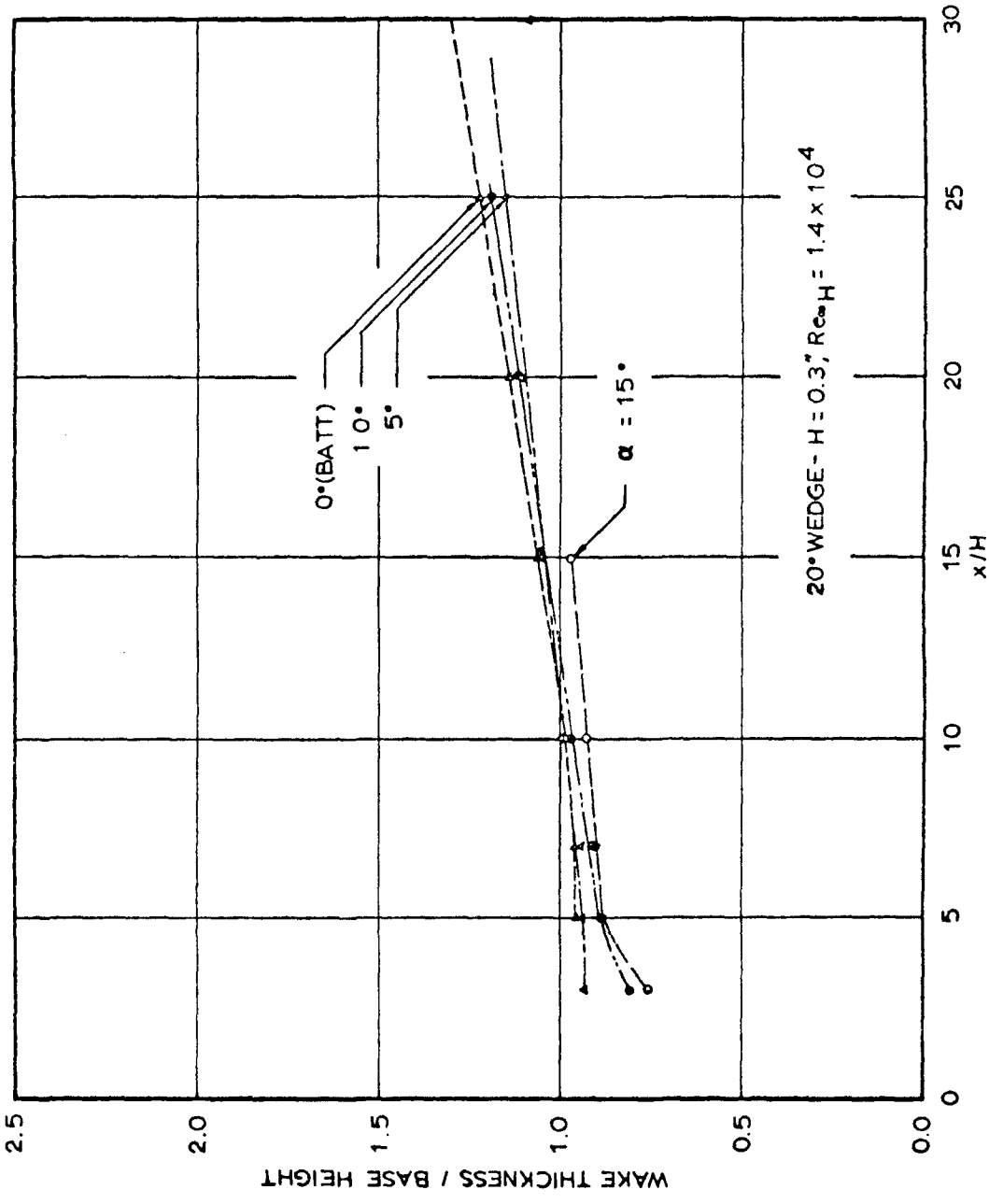

Fig. 21b WAKE THICKNESS

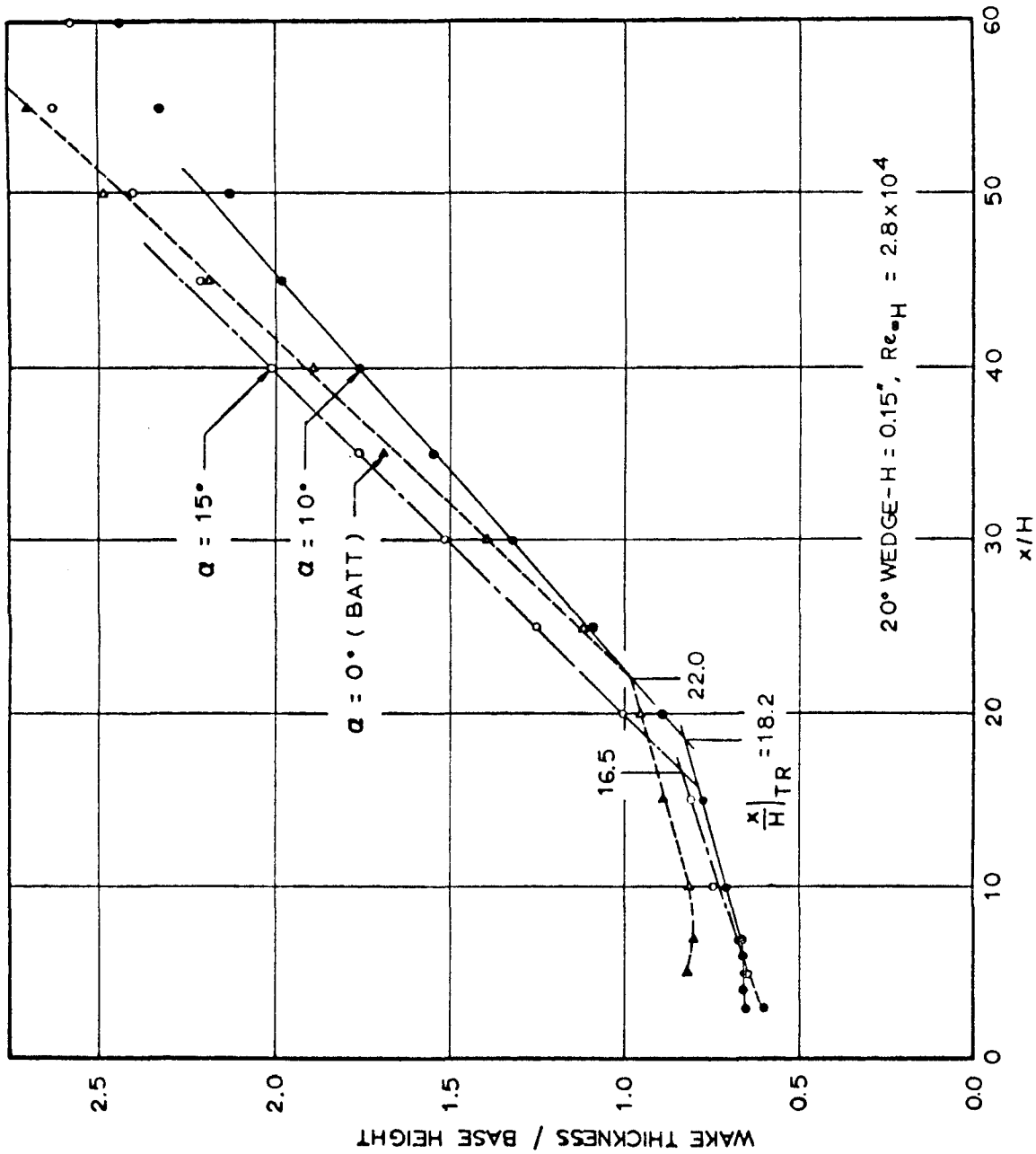

Fig. 21c WAKE THICKNESS

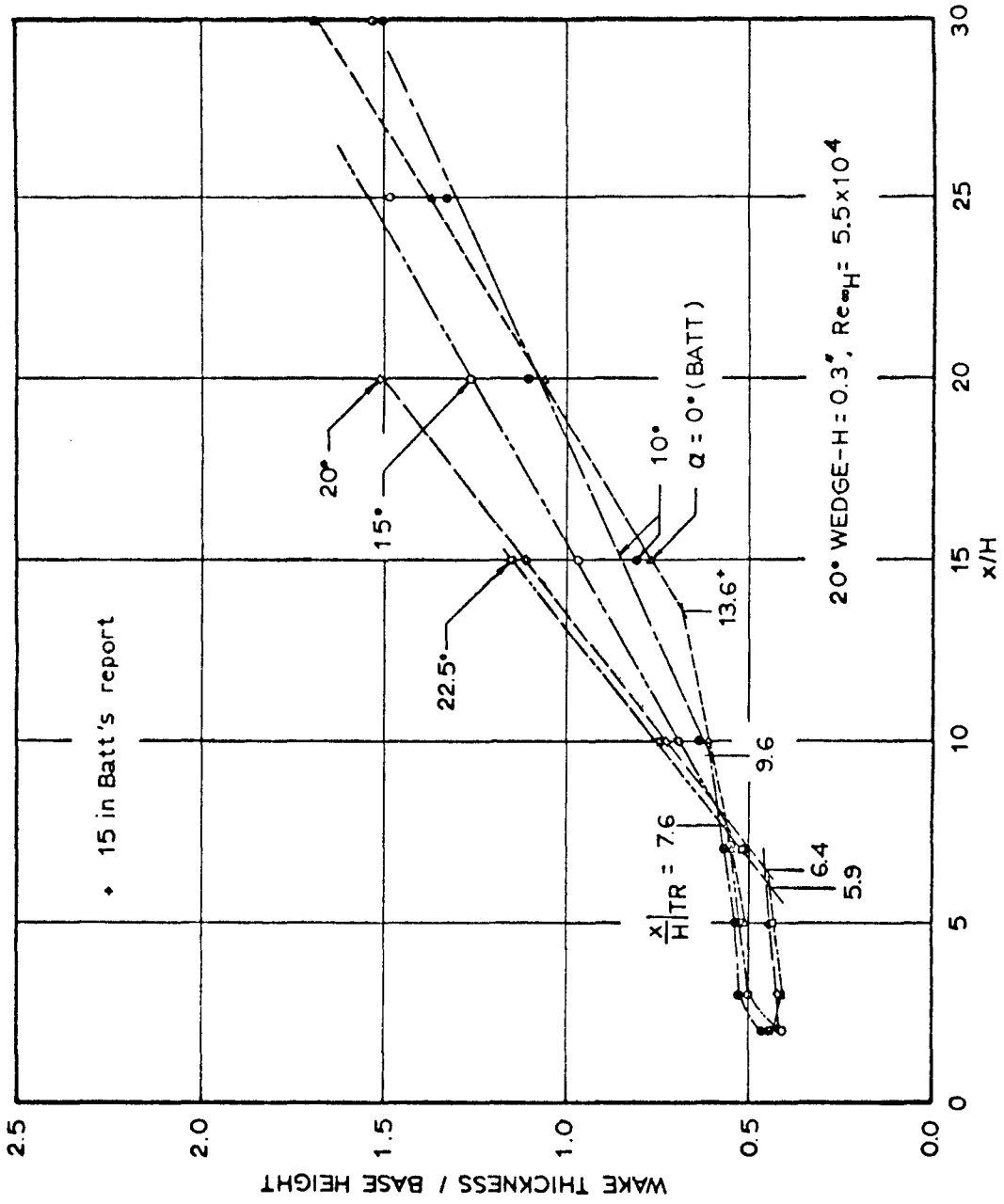

Fig. 21d WAKE THICKNESS

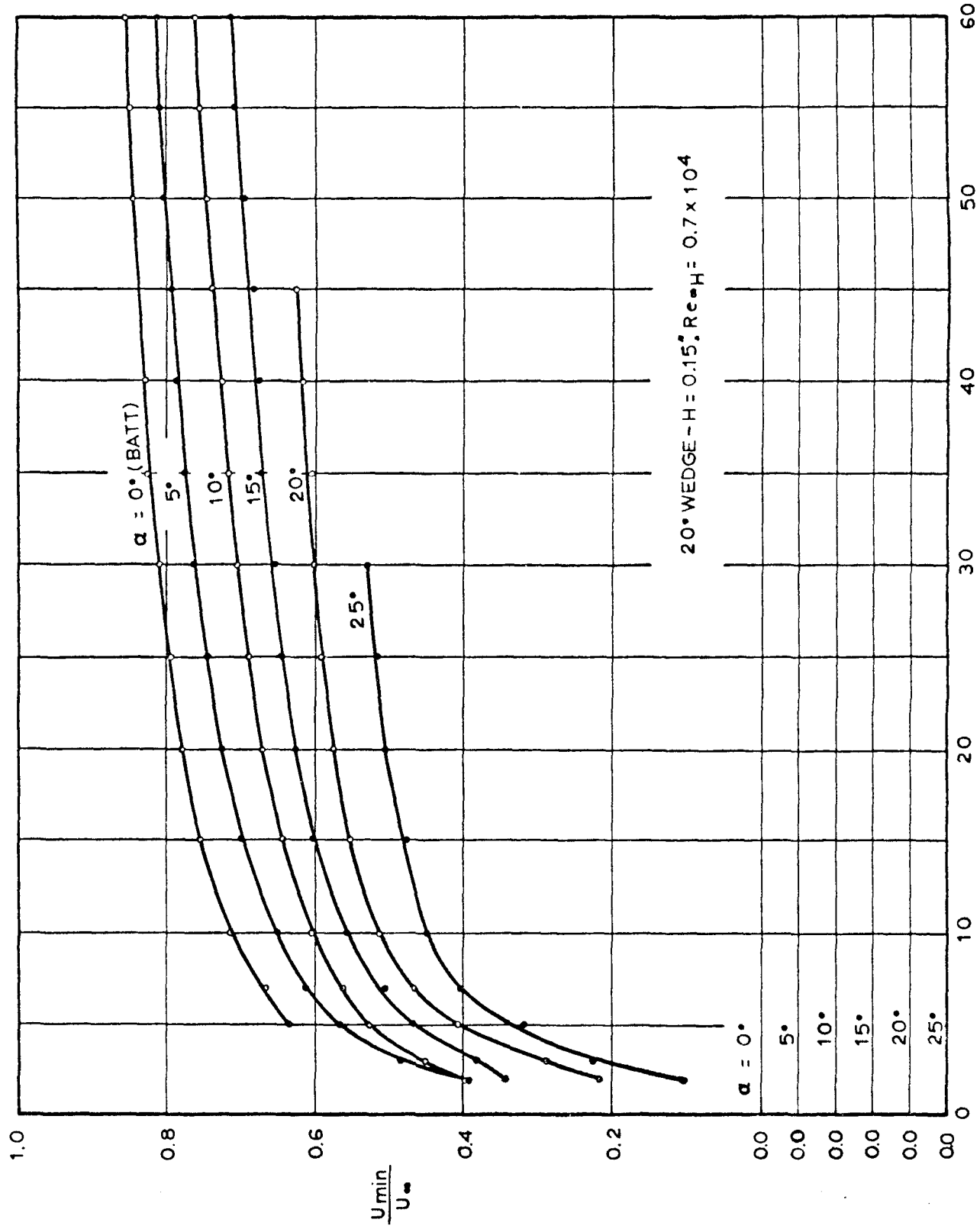

Fig. 22a VARIATION OF MINIMUM VELOCITY

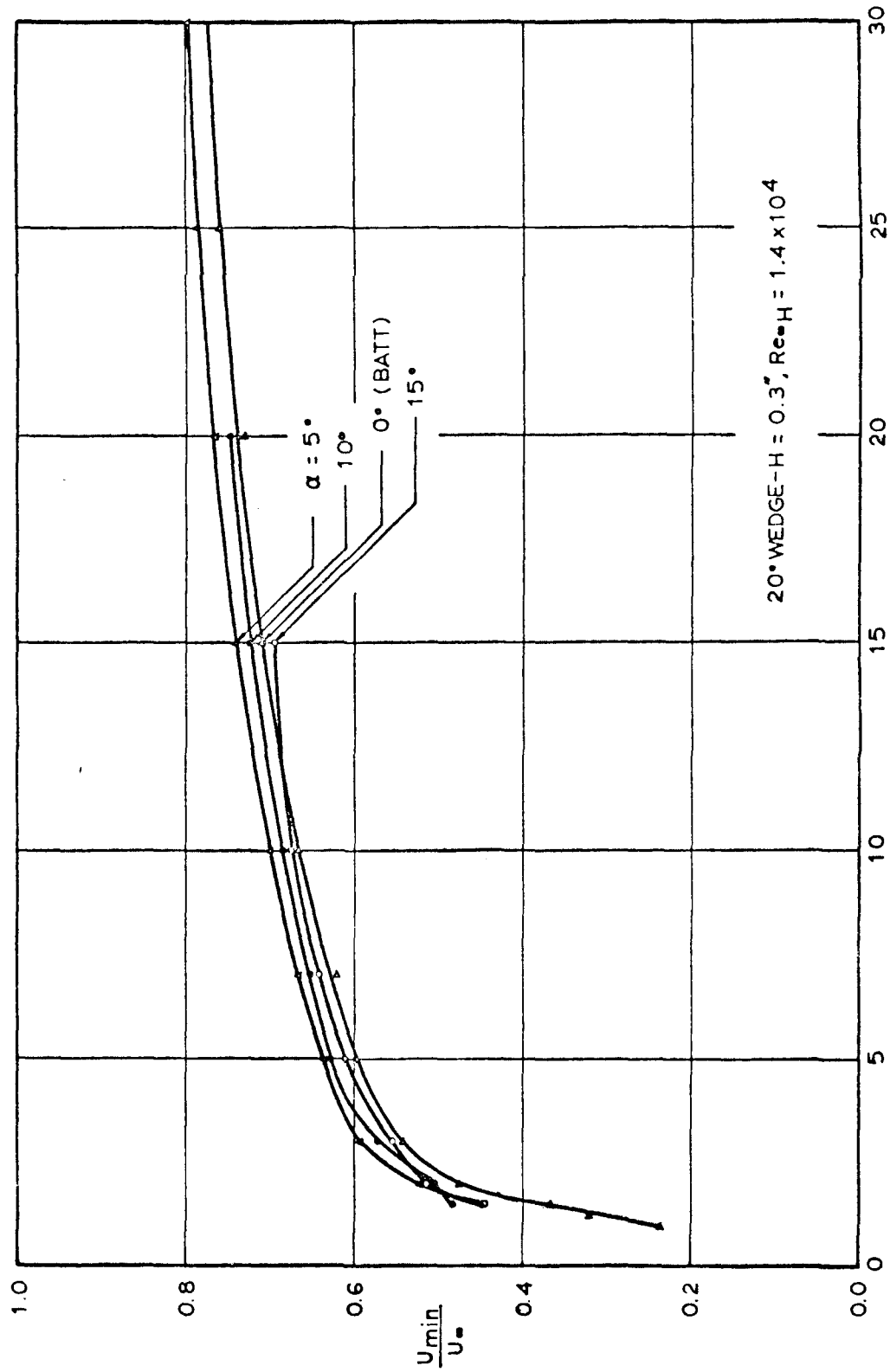

Fig. 22b VARIATION OF MINIMUM VELOCITY

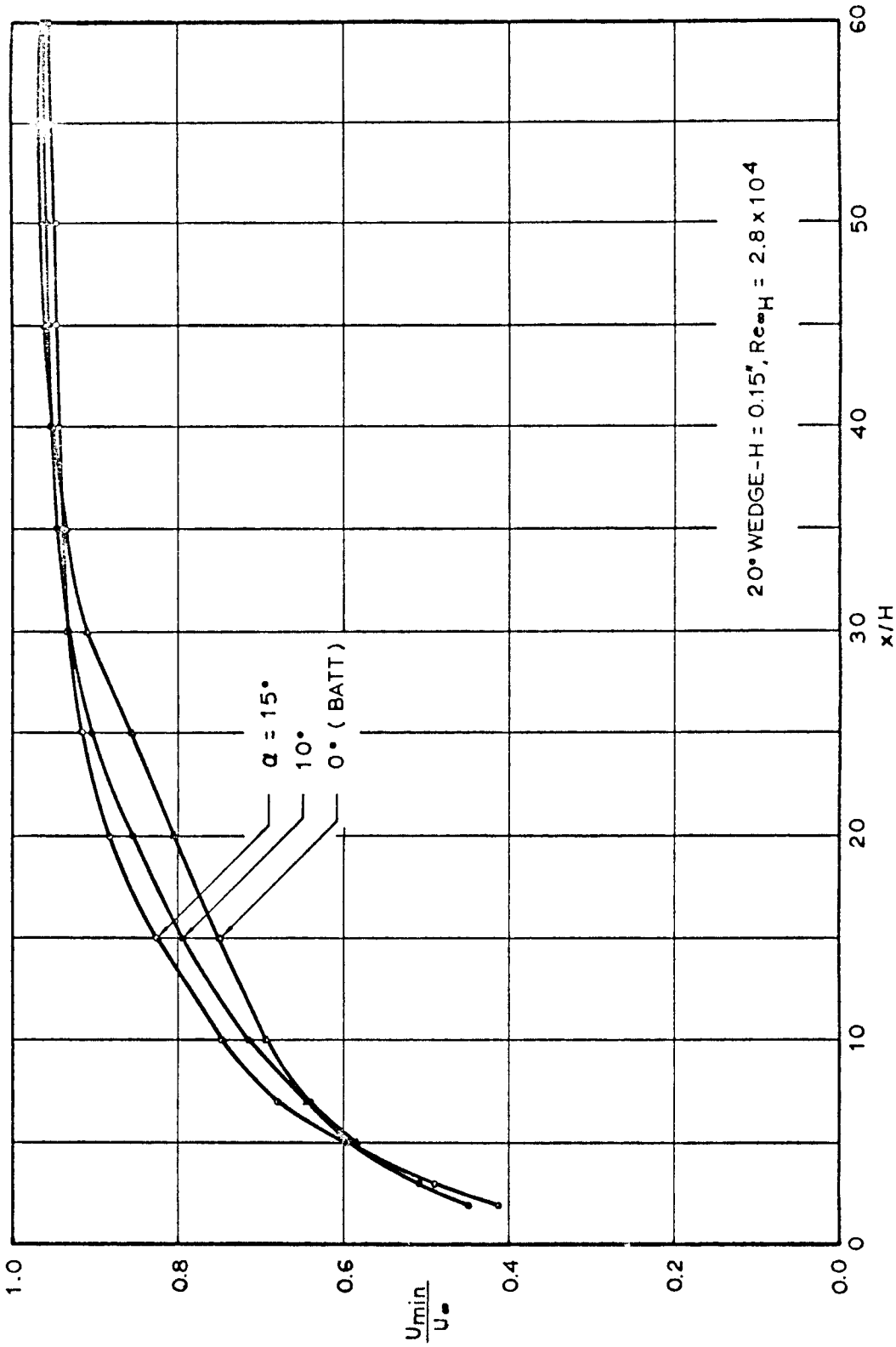

Fig. 22c VARIATION OF MINIMUM VELOCITY

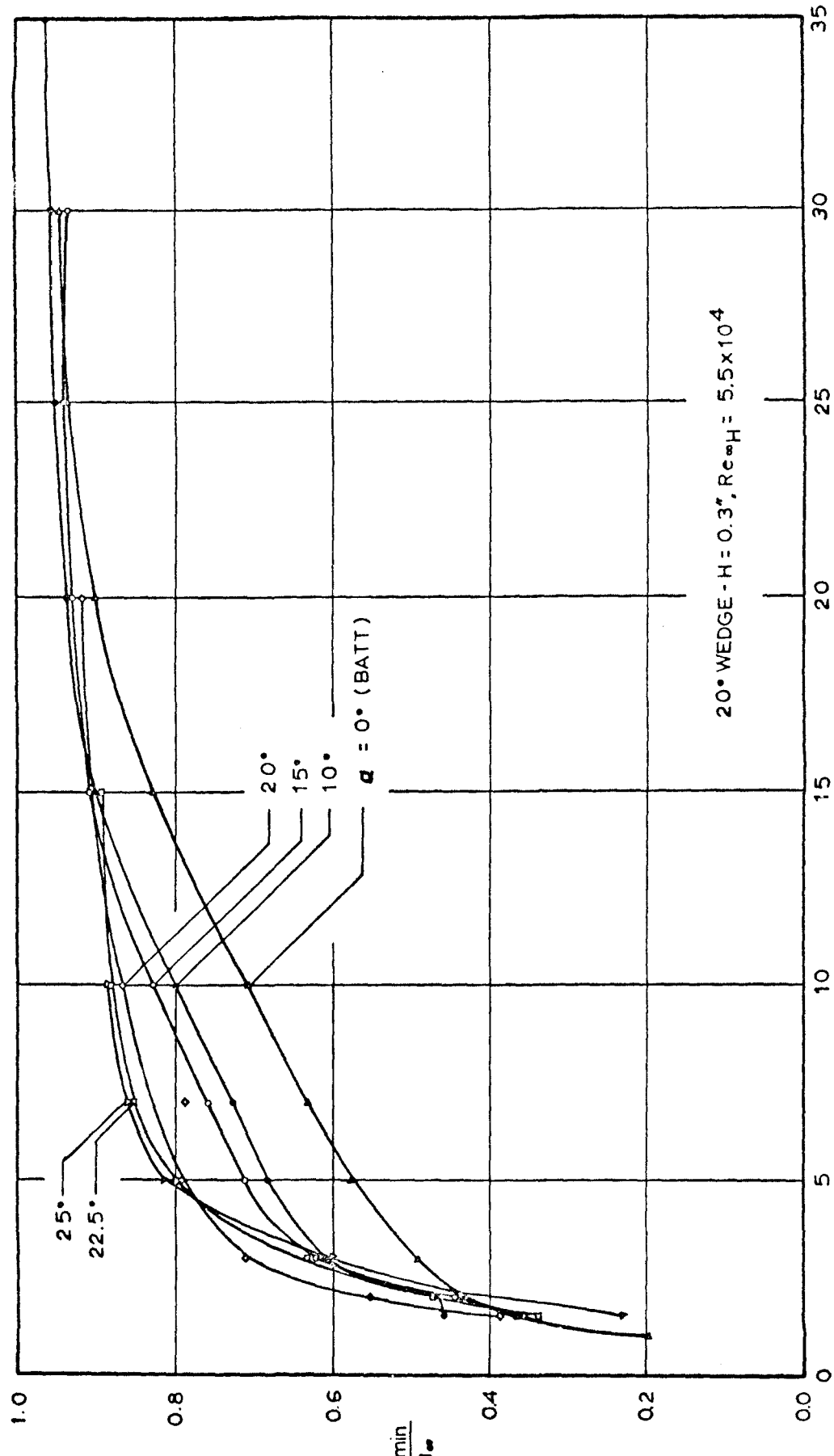

Fig. 22d VARIATION OF MINIMUM VELOCITY

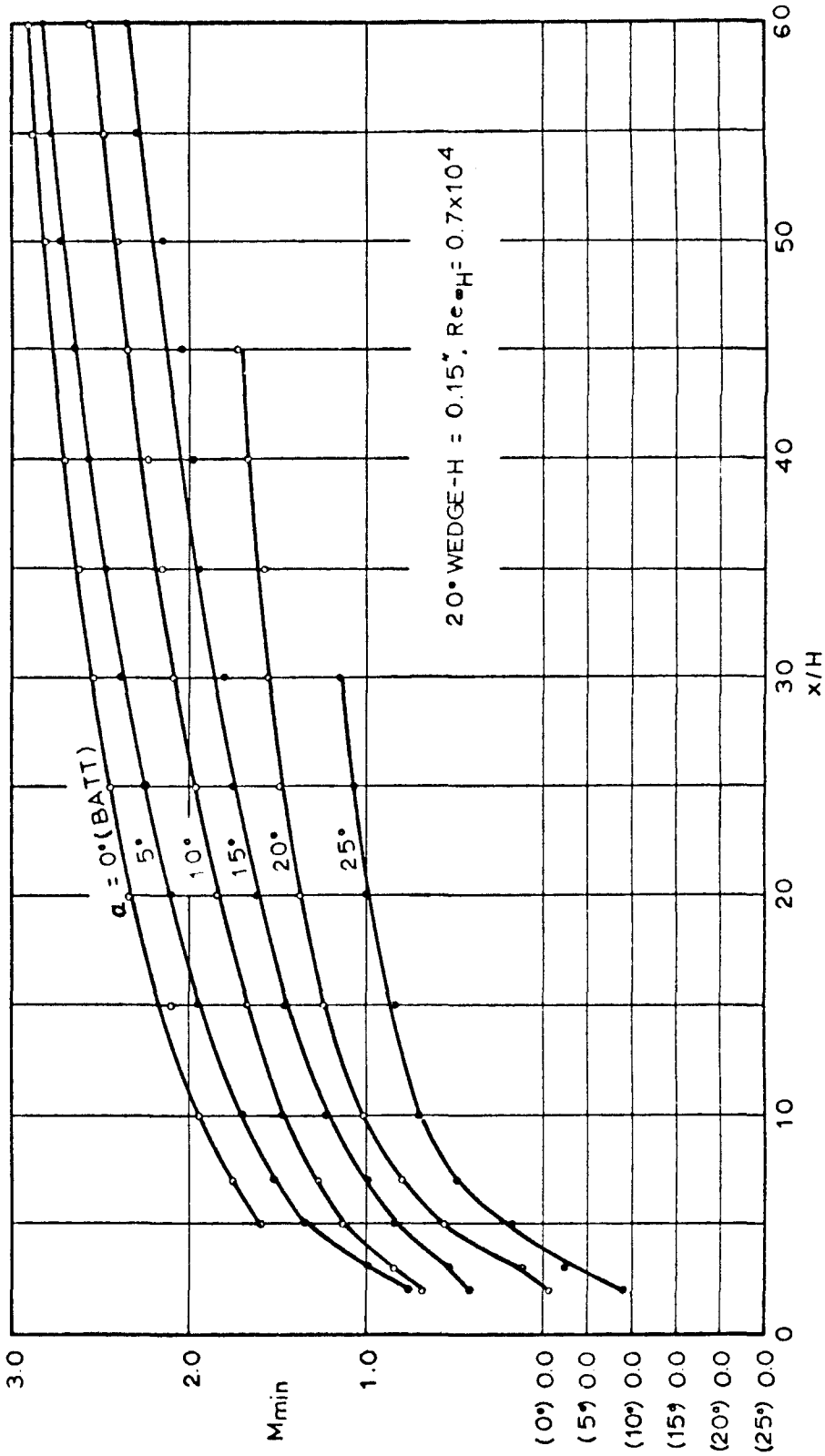

Fig. 23a VARIATION OF MINIMUM MACH NUMBER

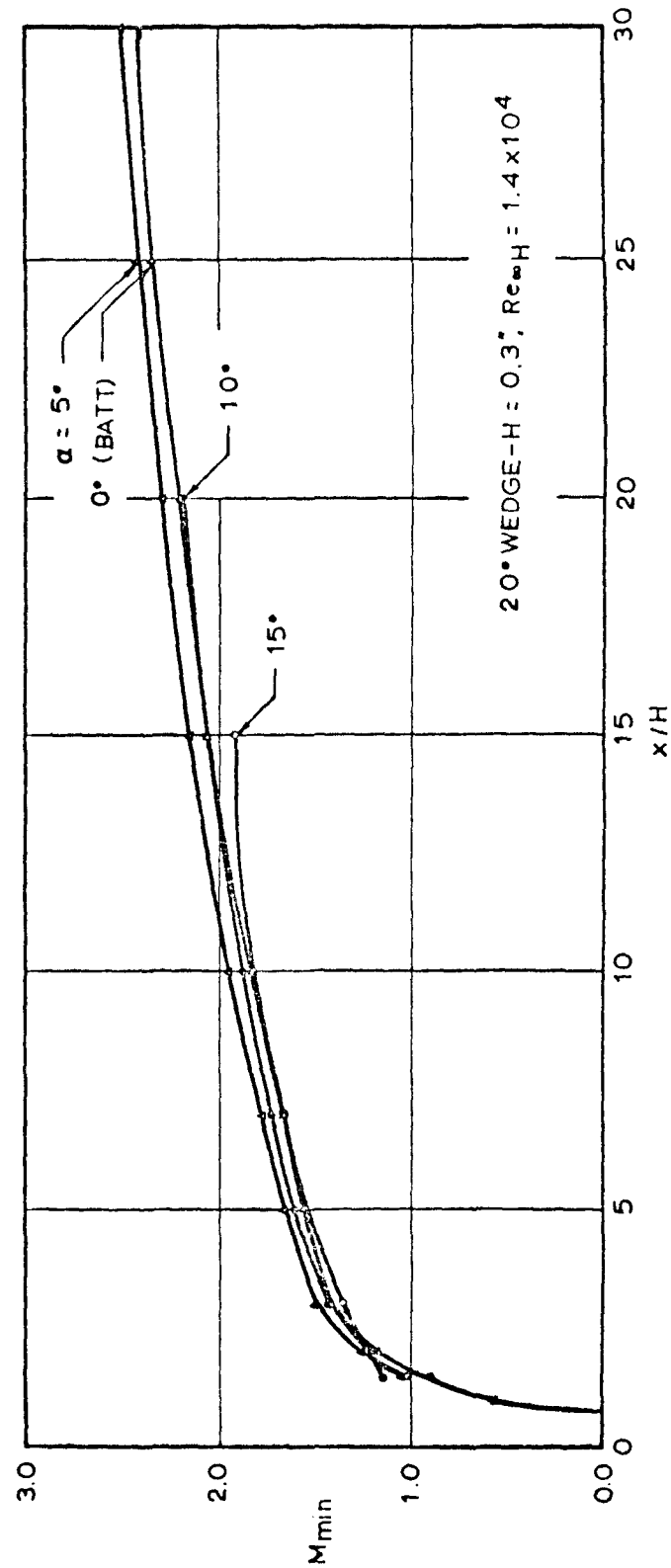

Fig. 23b VARIATION OF MINIMUM MACH NUMBER

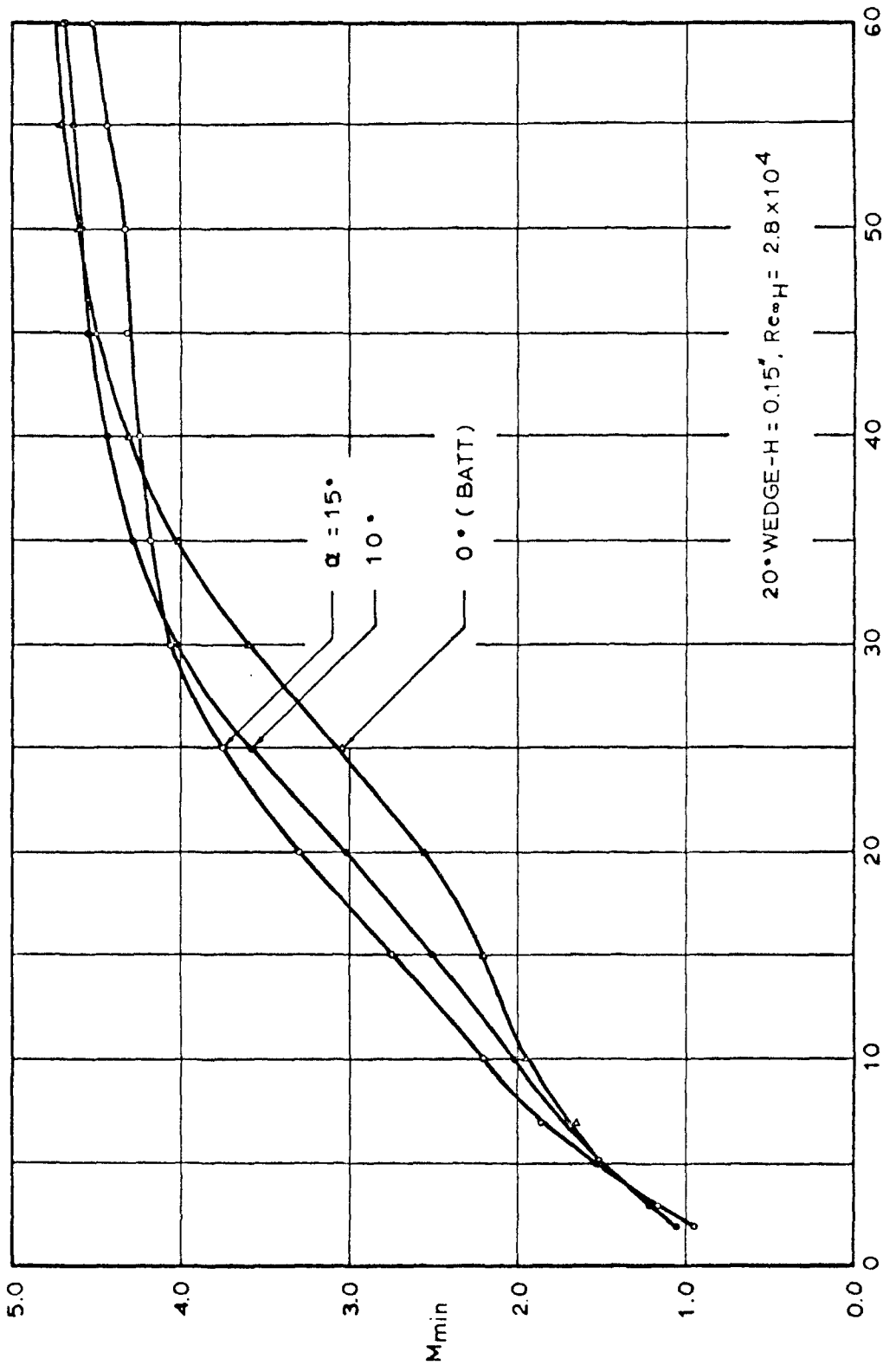

Fig. 23c VARIATION OF MINIMUM MACH NUMBER

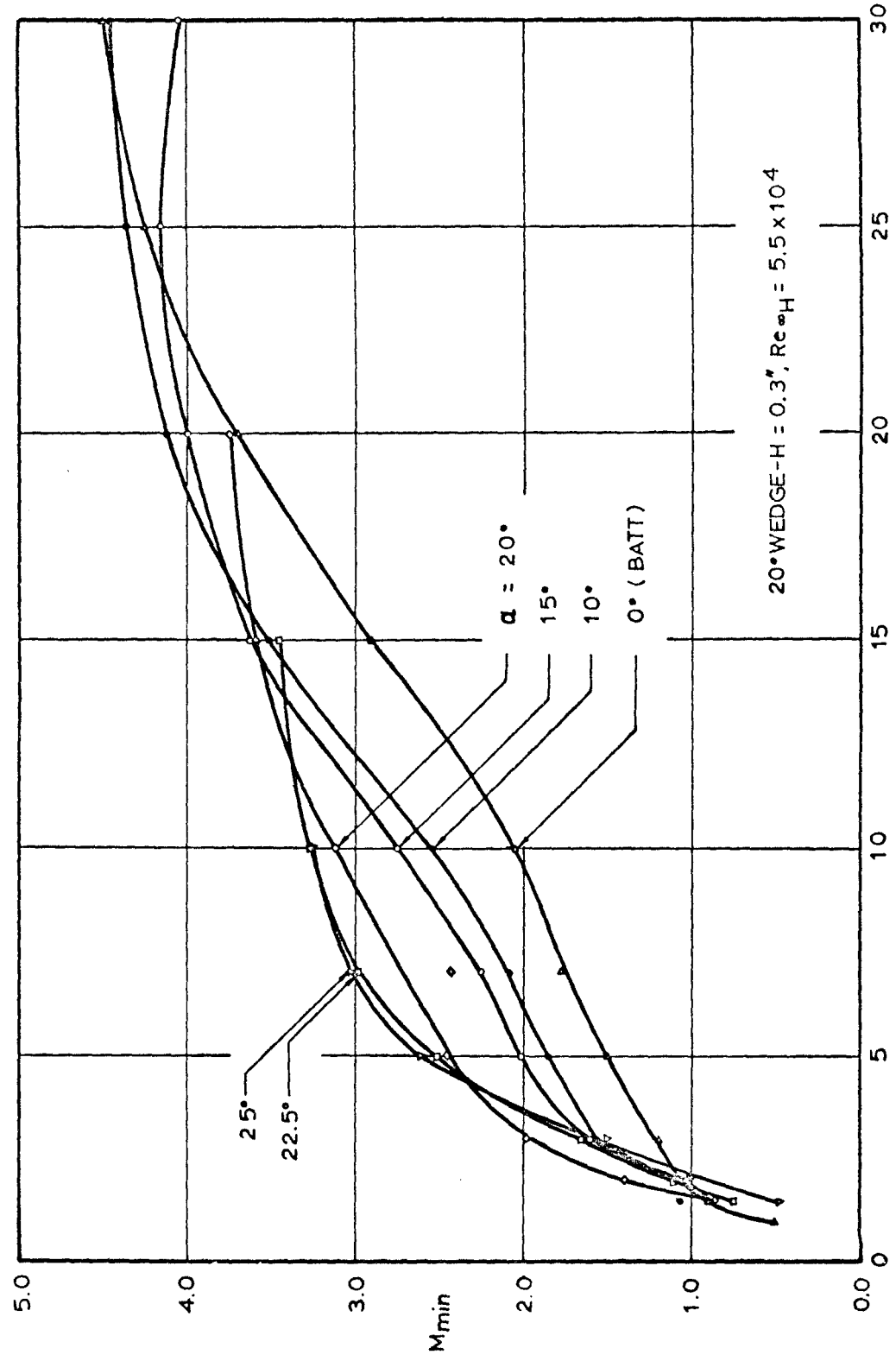

Fig. 23d VARIATION OF MINIMUM MACH NUMBER

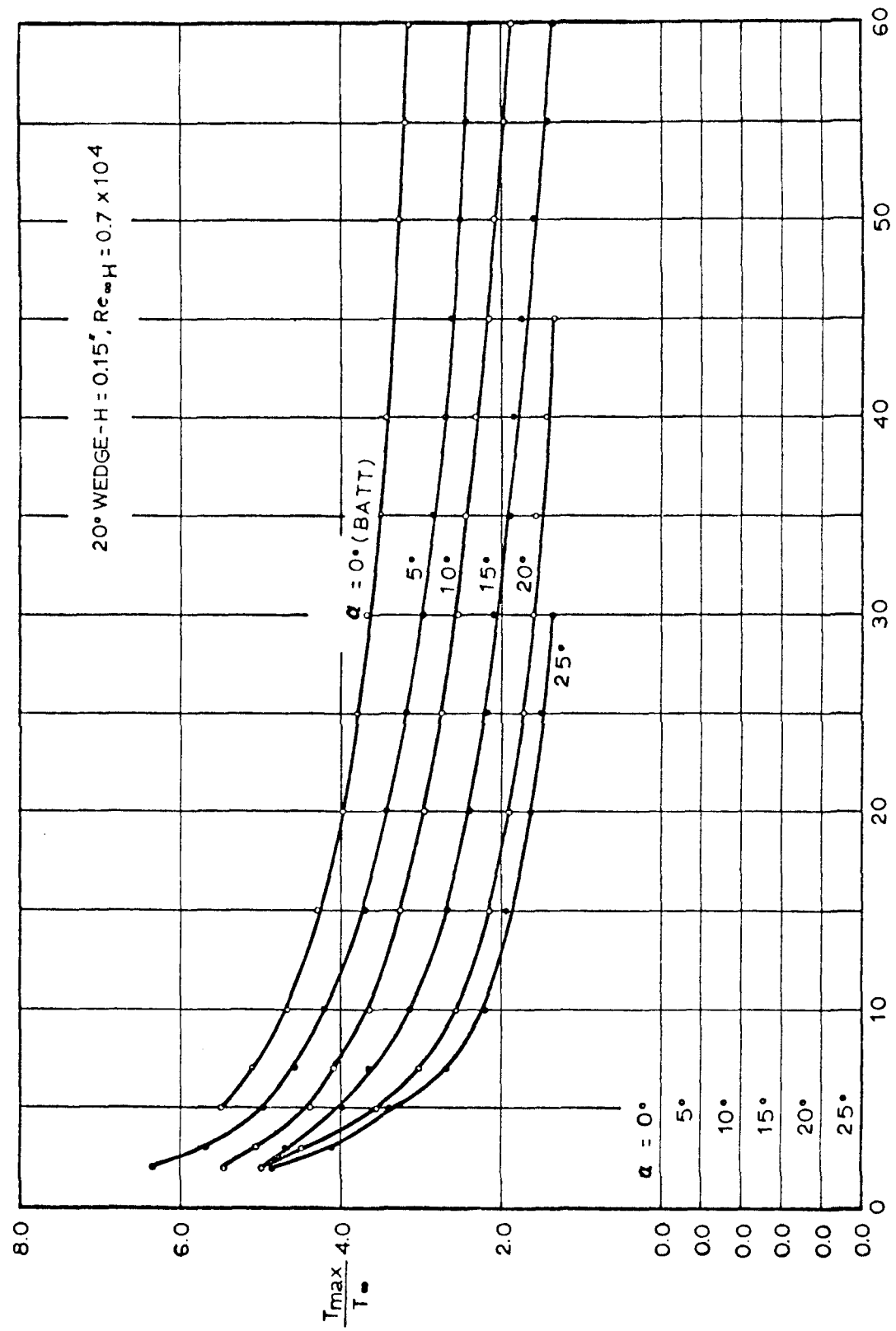

Fig. 24a VARIATION OF MAXIMUM TEMPERATURE

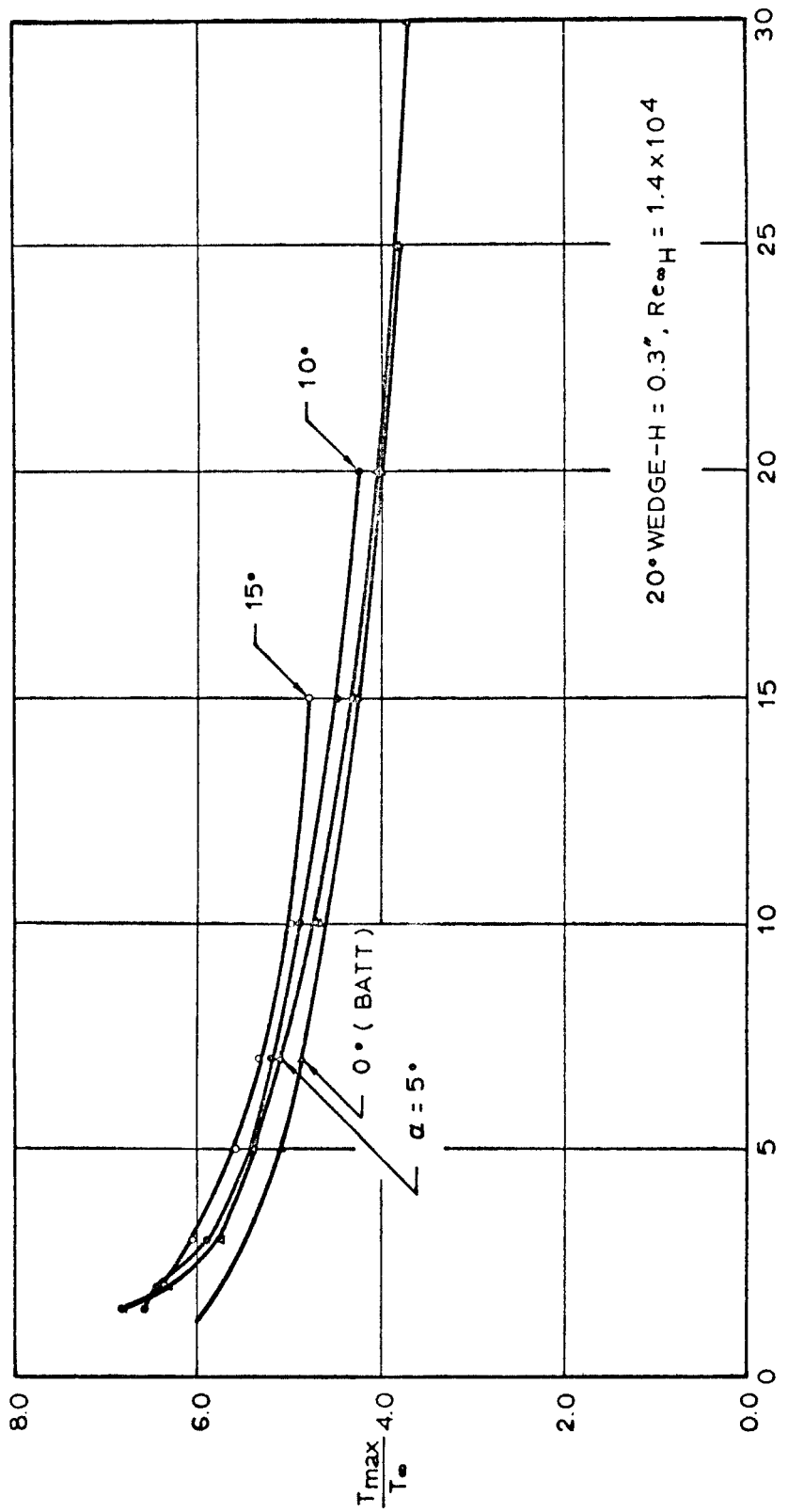

Fig. 24b VARIATION OF MAXIMUM TEMPERATURE

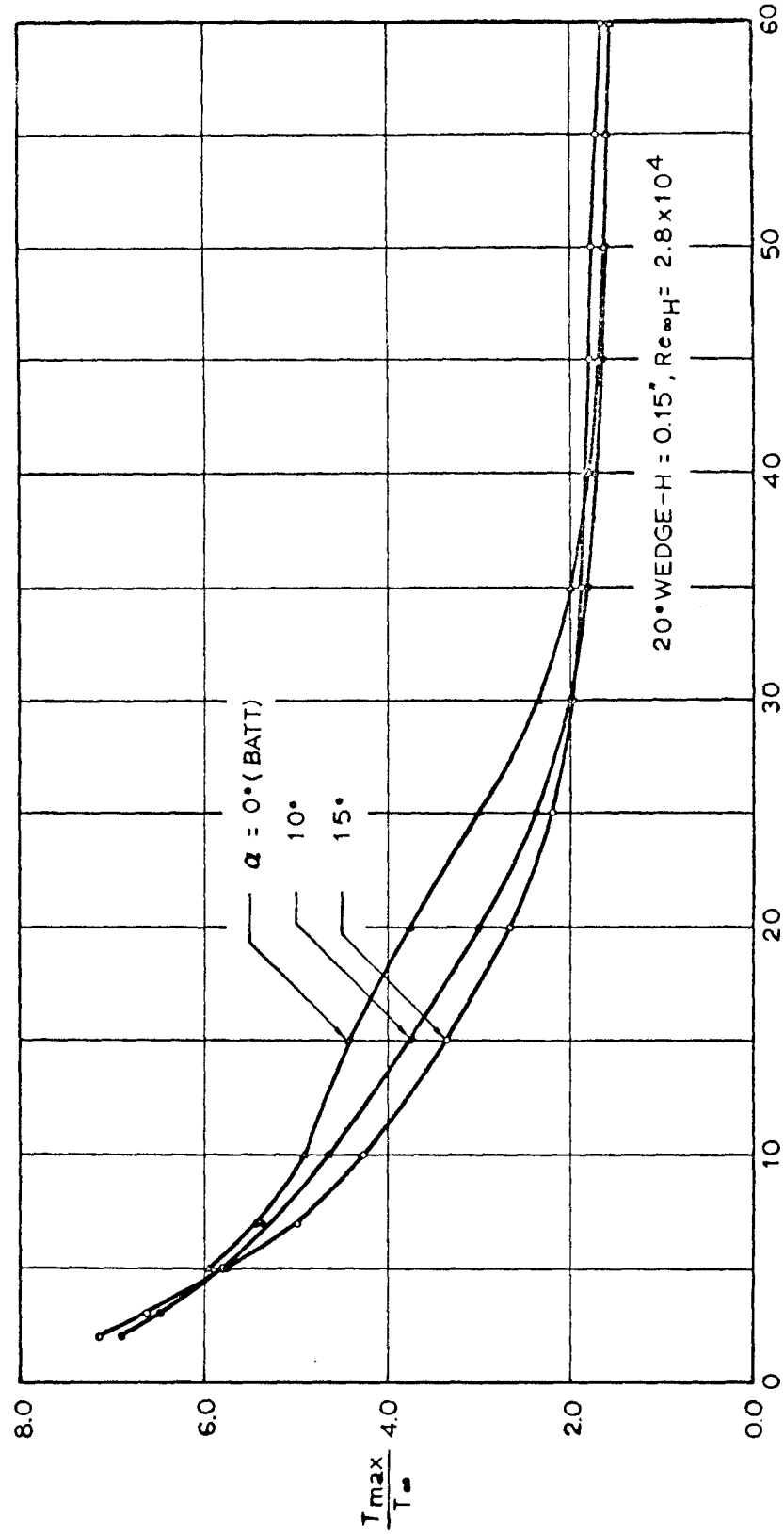

Fig. 24c VARIATION OF MAXIMUM TEMPERATURE

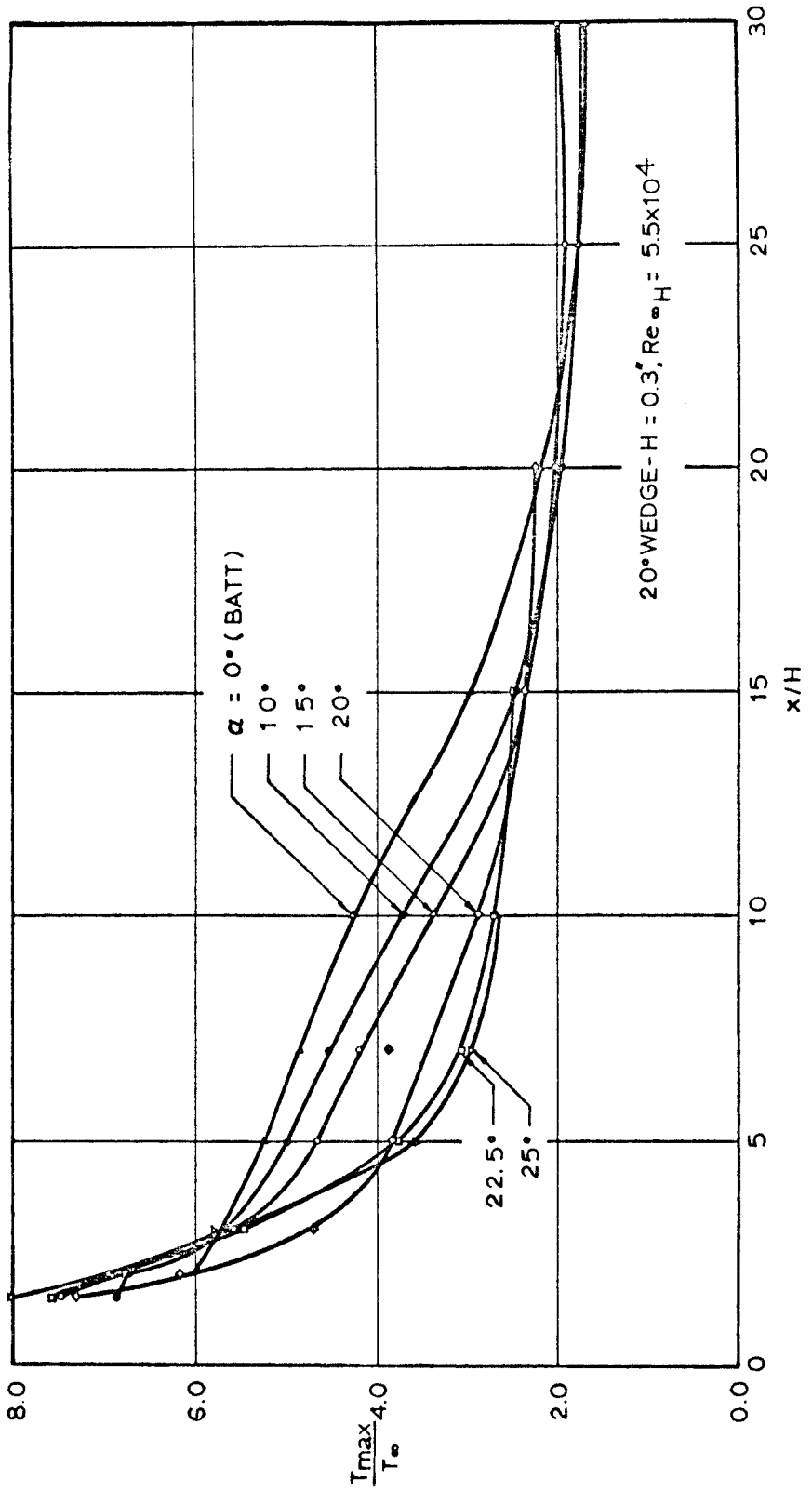

Fig. 24d VARIATION OF MAXIMUM TEMPERATURE

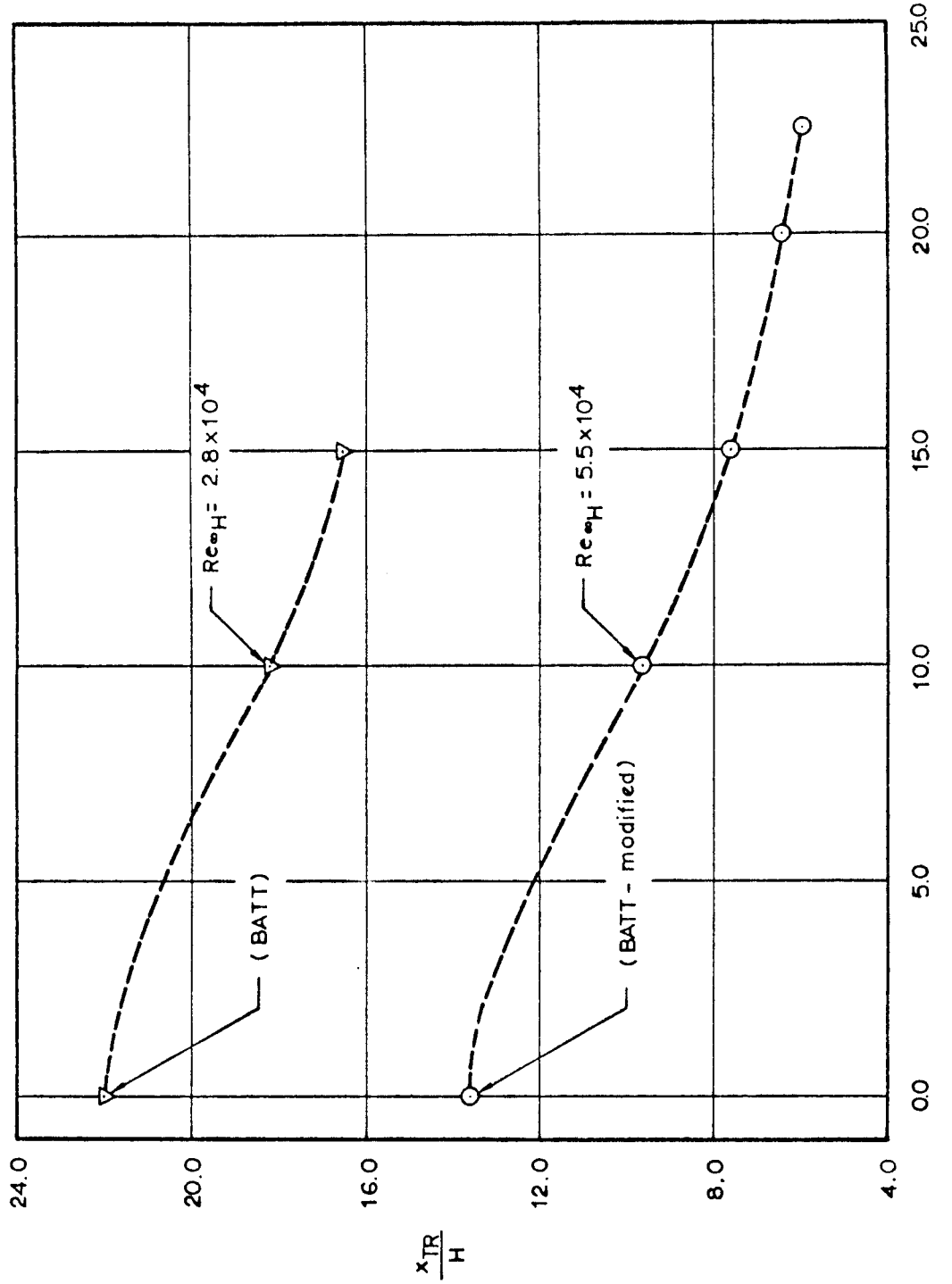

Fig. 25 TRANSITION ANALYSIS

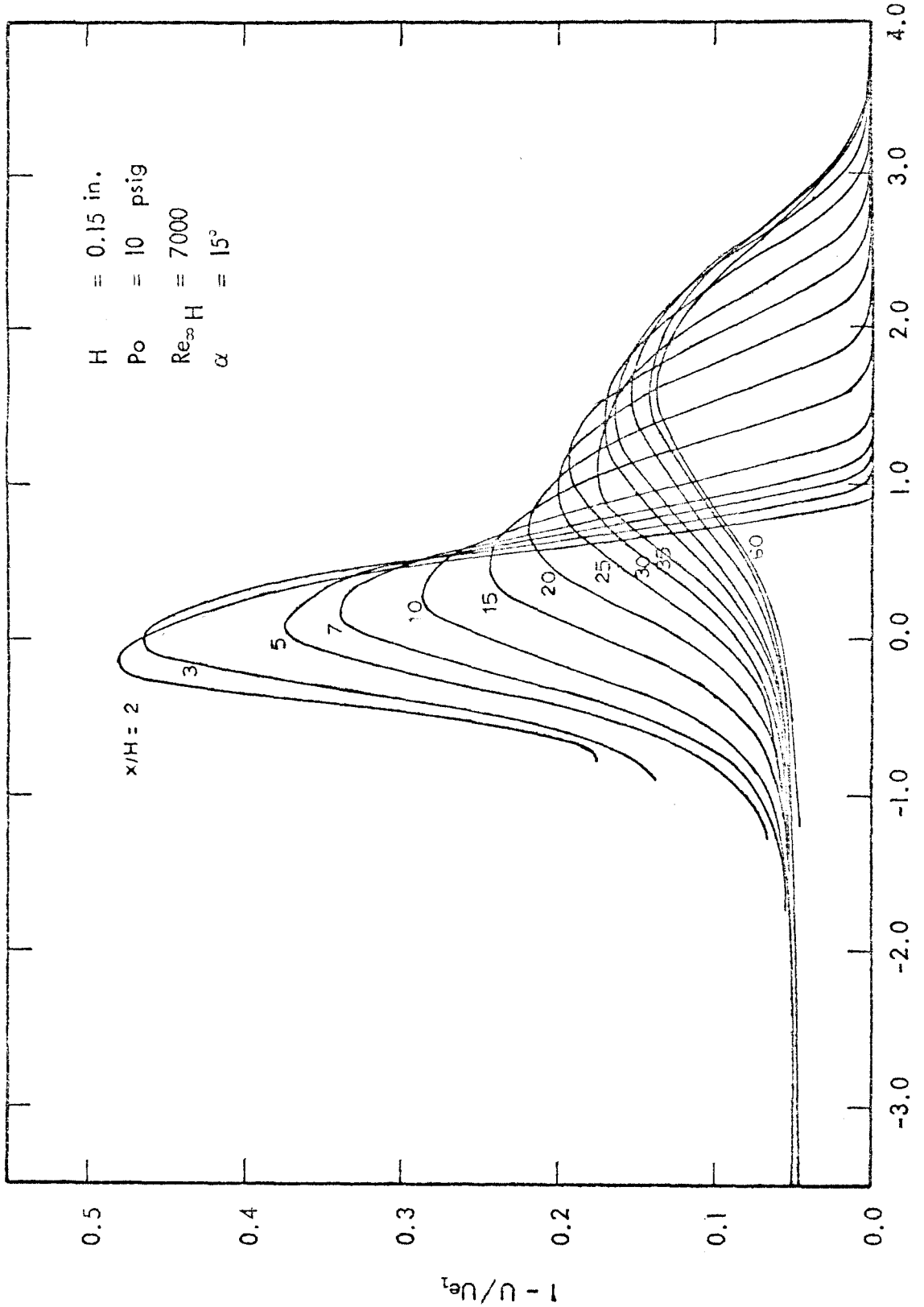

Fig. 26a NORMALIZED VELOCITY DEFECTS (LAMINAR WAKE)

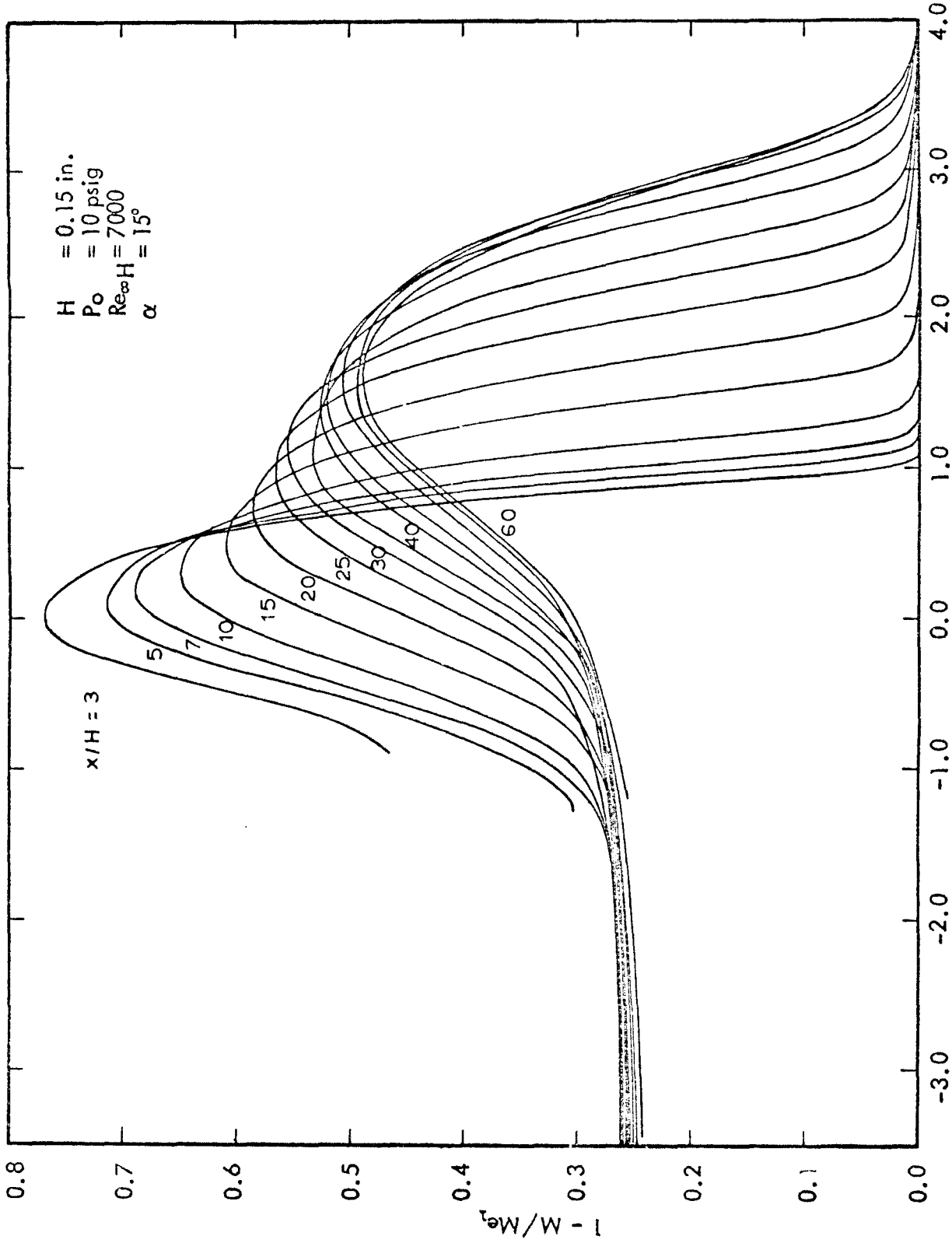

Fig. 26b NORMALIZED MACH NUMBER DEFECTS (LAMINAR WAKE)

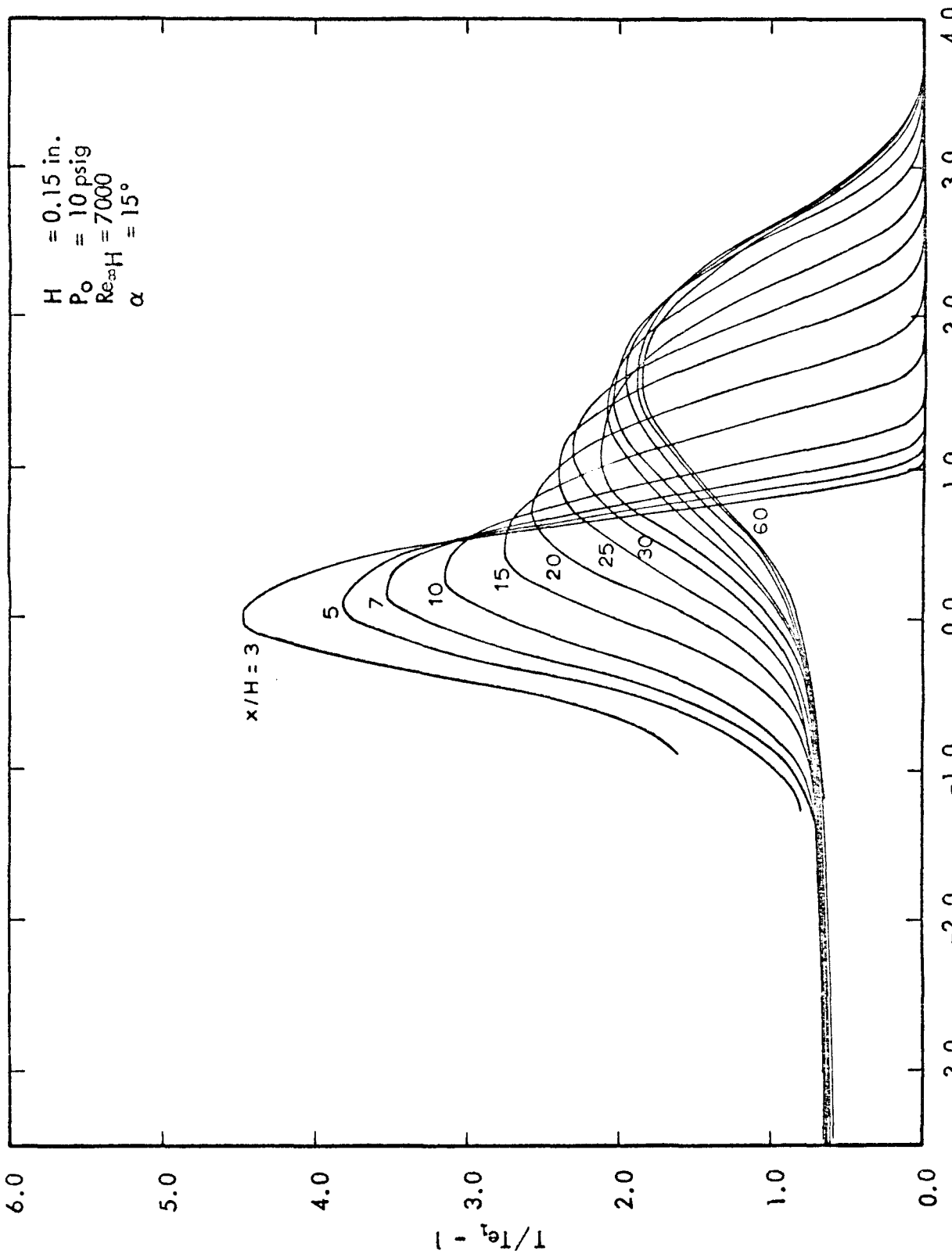

Fig. 26c NORMALIZED TEMPERATURE EXCESSES (LAMINAR WAKE)

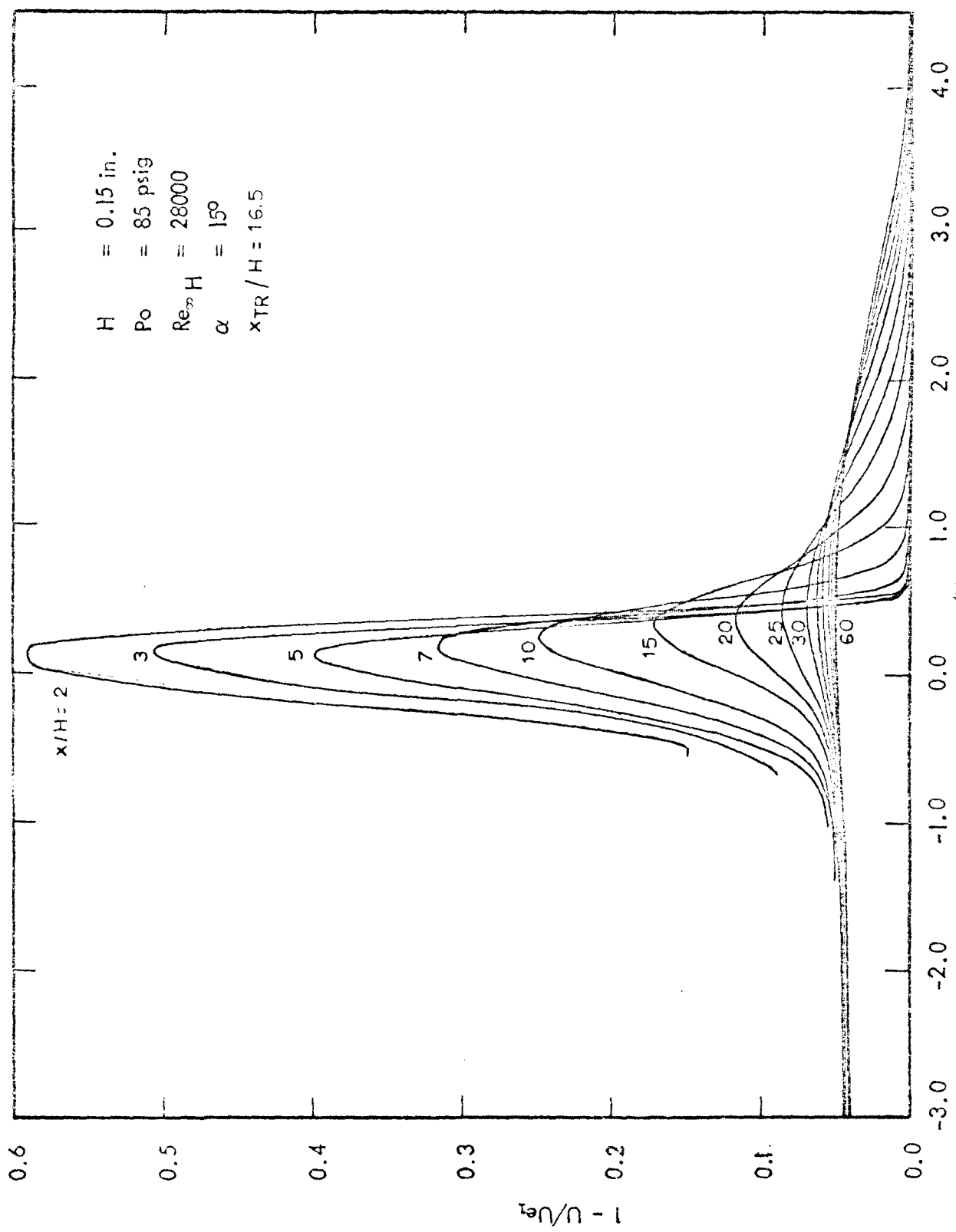

Fig. 27a NORMALIZED VELOCITY DEFECTS

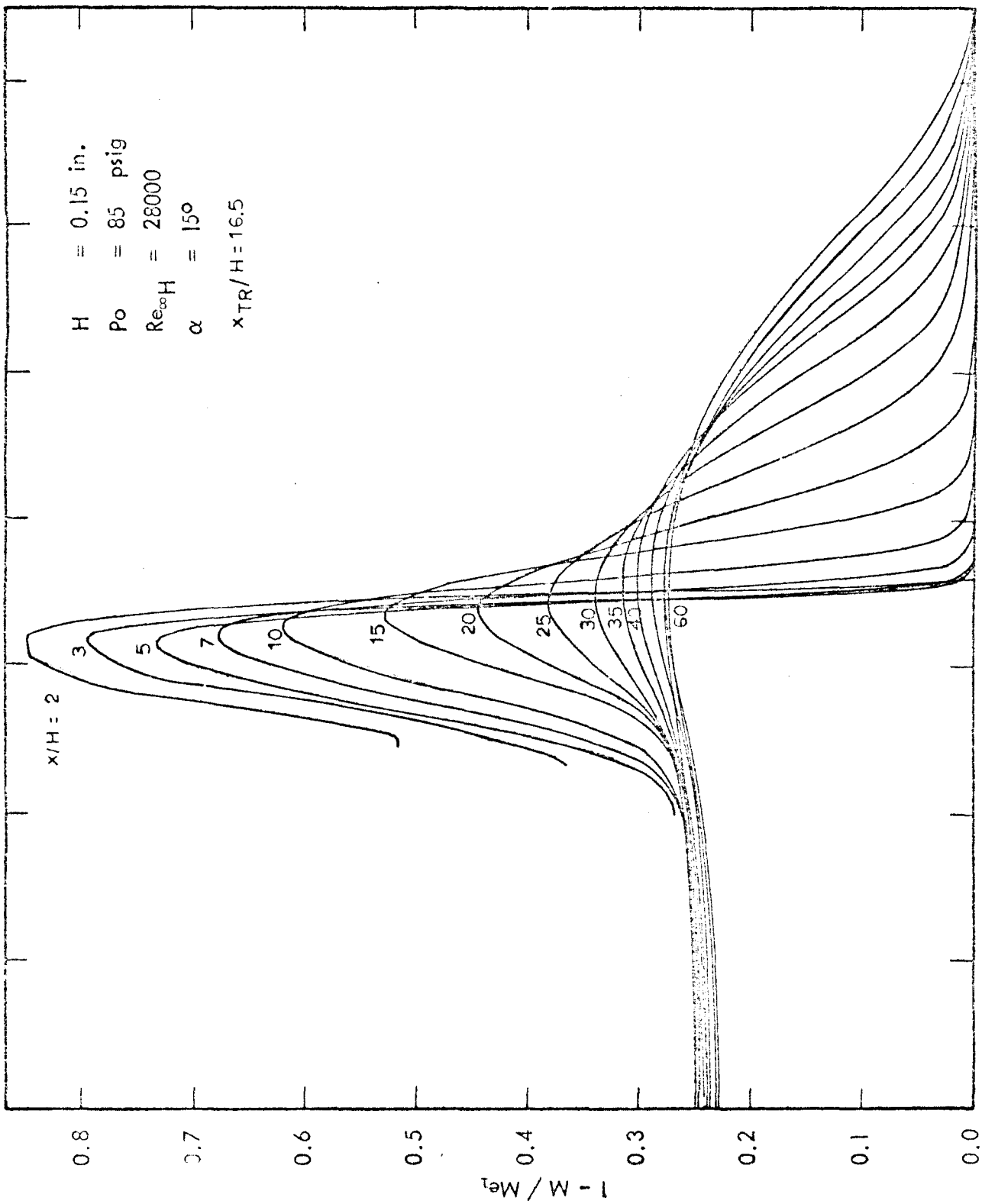

Fig. 27b NORMALIZED MACH NUMBER DEFECTS

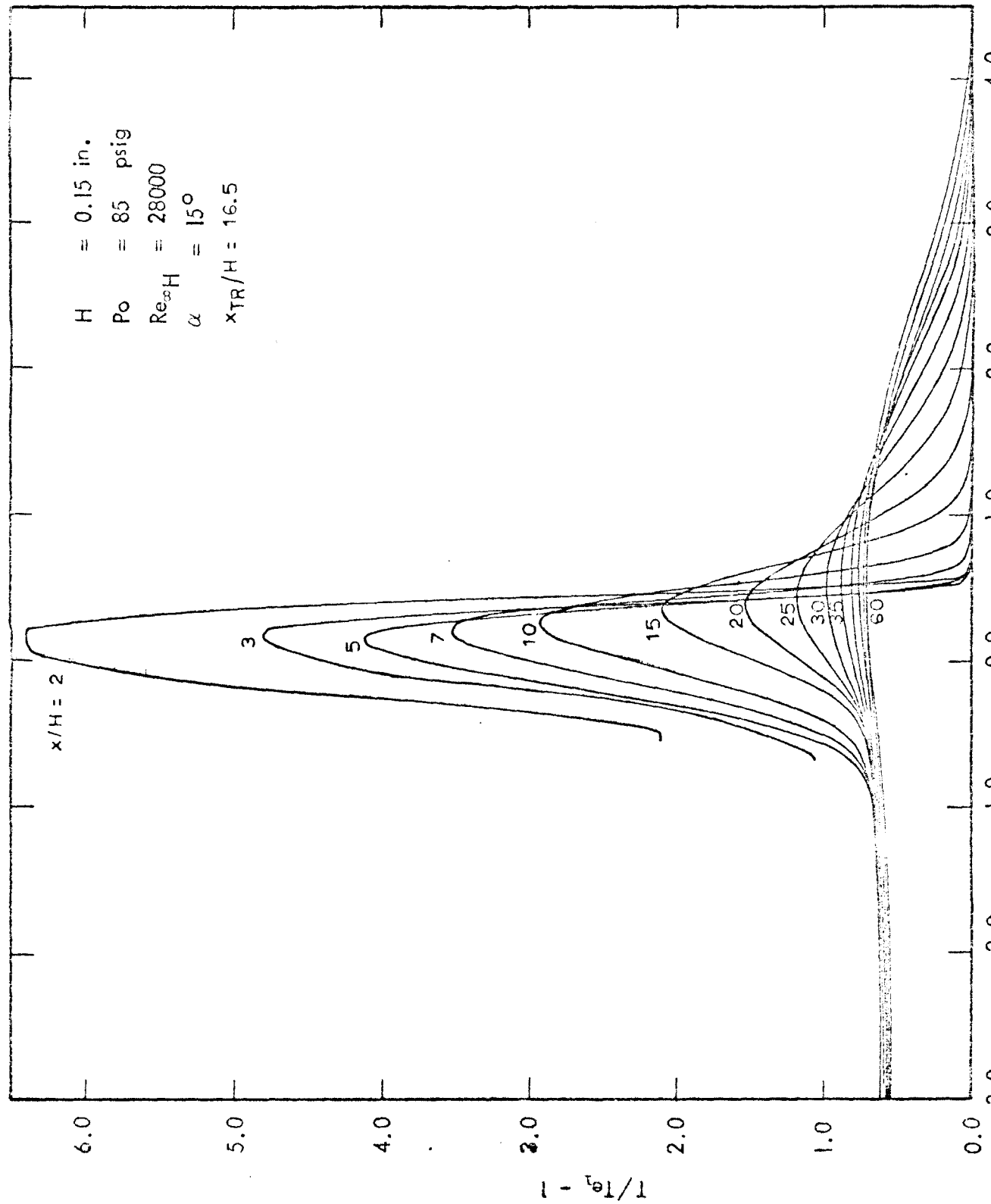

Fig. 27c NORMALIZED TEMPERATURE EXCESSES

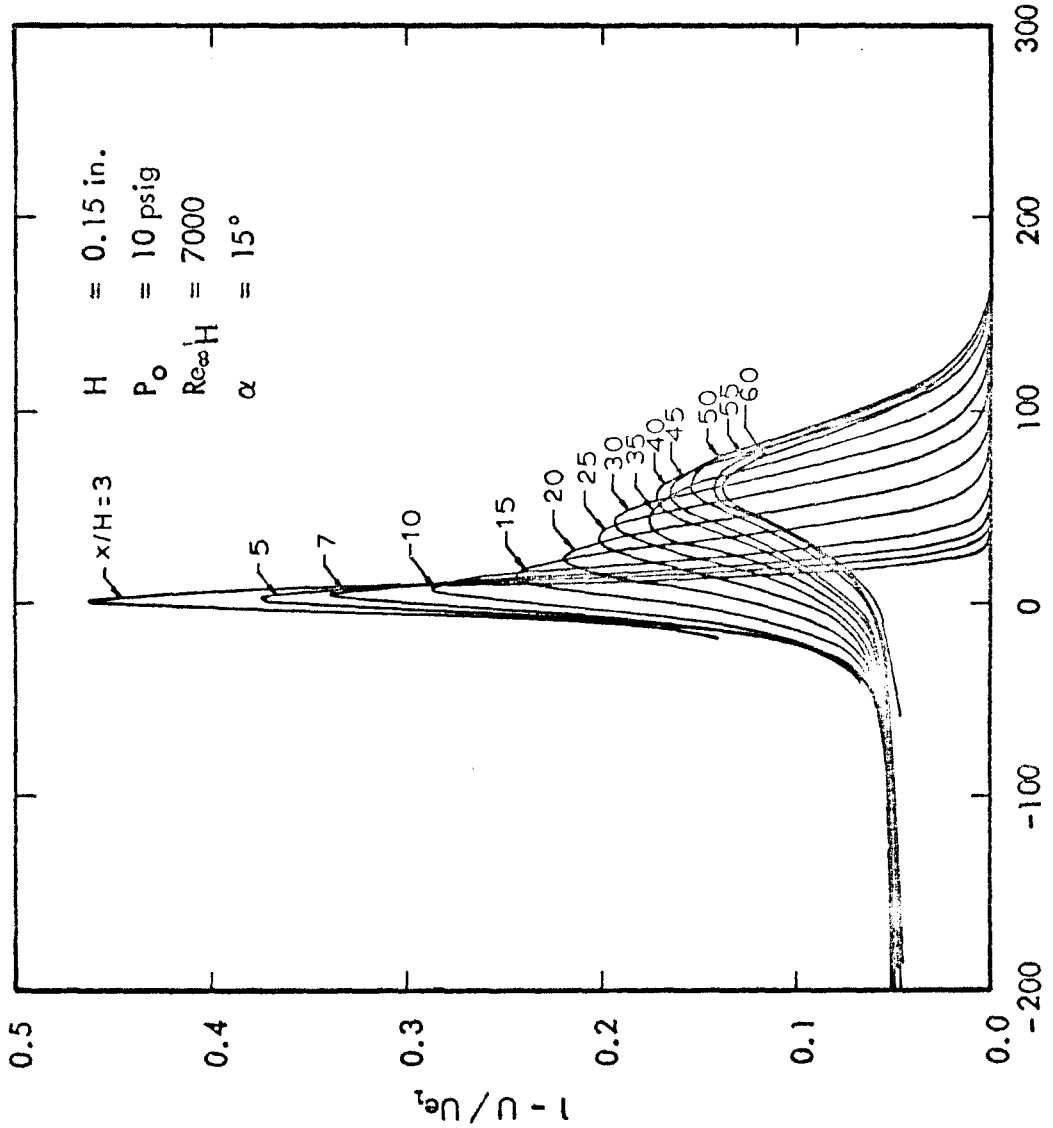

Fig. 28a VELOCITY DEFECTS PLOTTED IN TRANSFORMED Y - SCALE

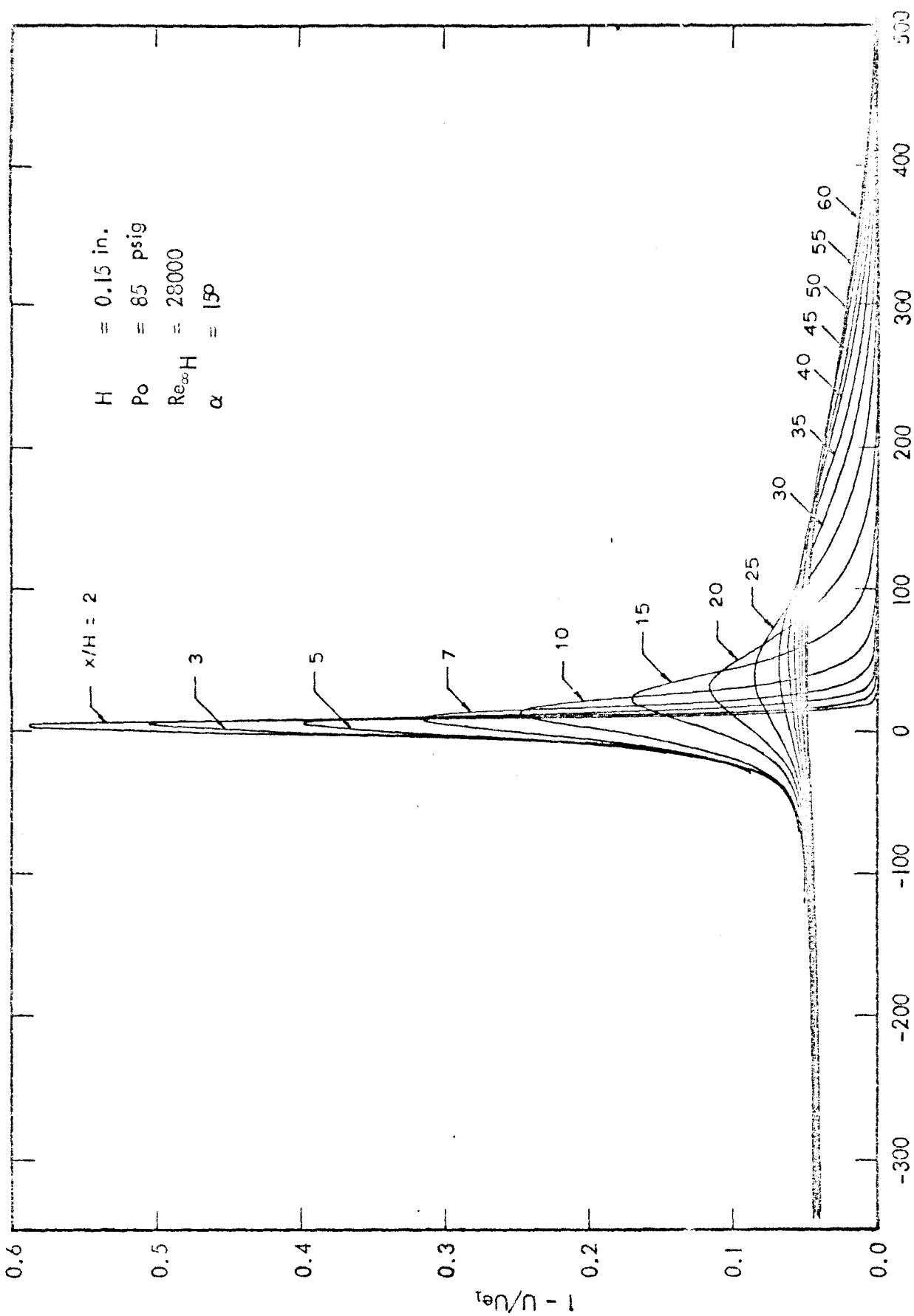

Fig. 28b VELOCITY DEFECTS PLOTTED IN TRANSFORMED y-SCALE

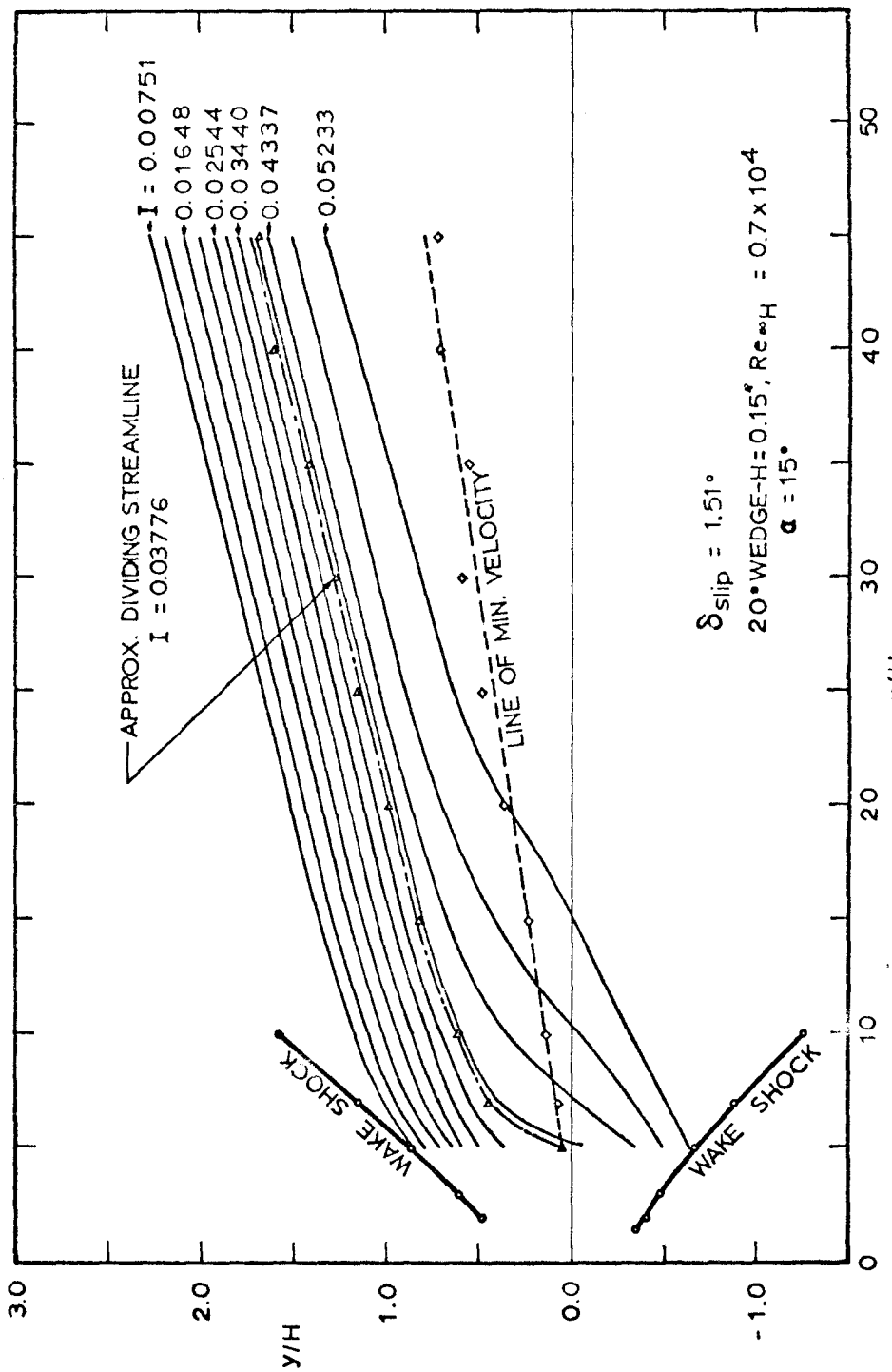

Fig. 29a FAR WAKE STREAMLINES

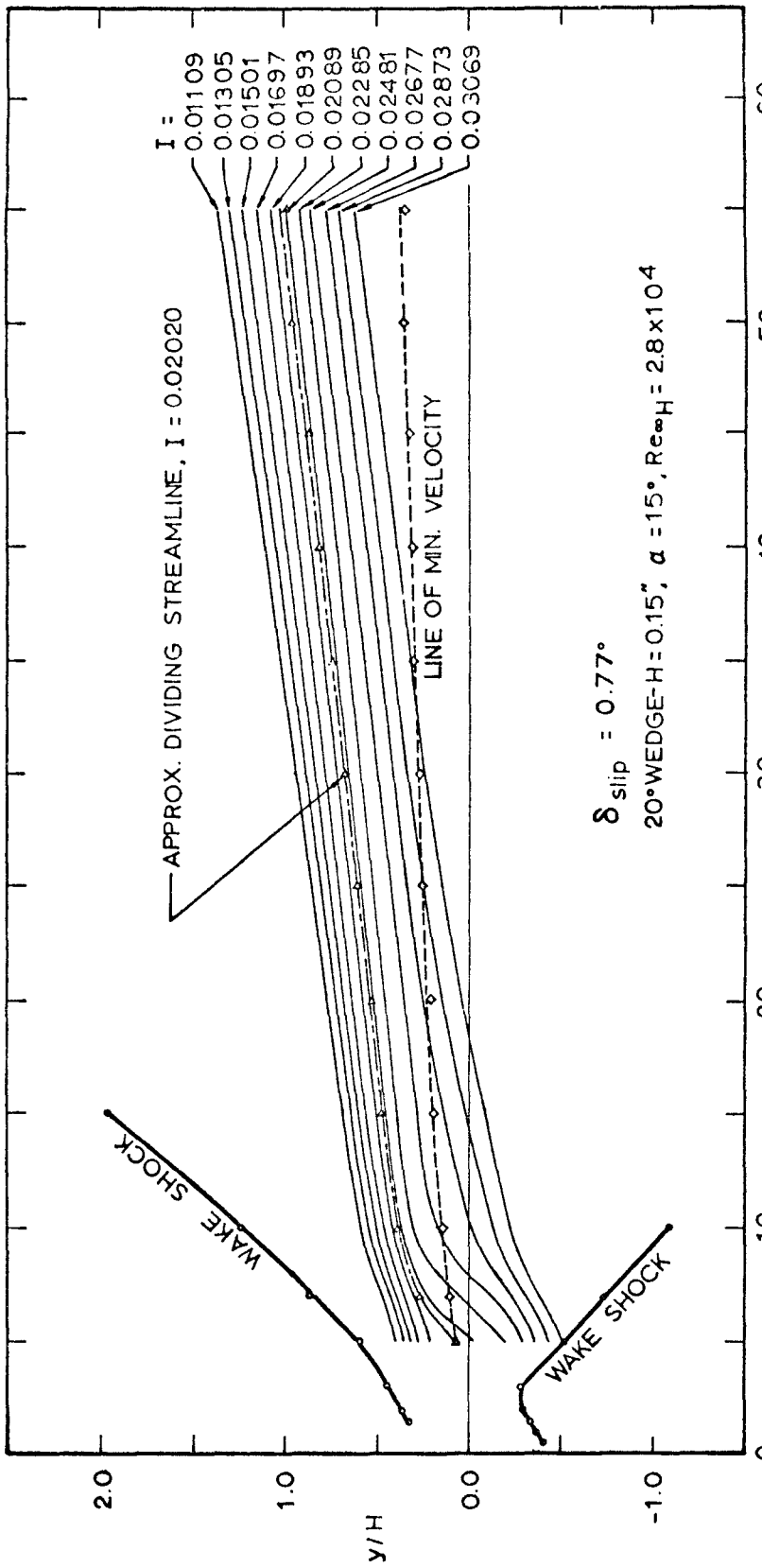

Fig. 29b FAR WAKE STREAMLINES

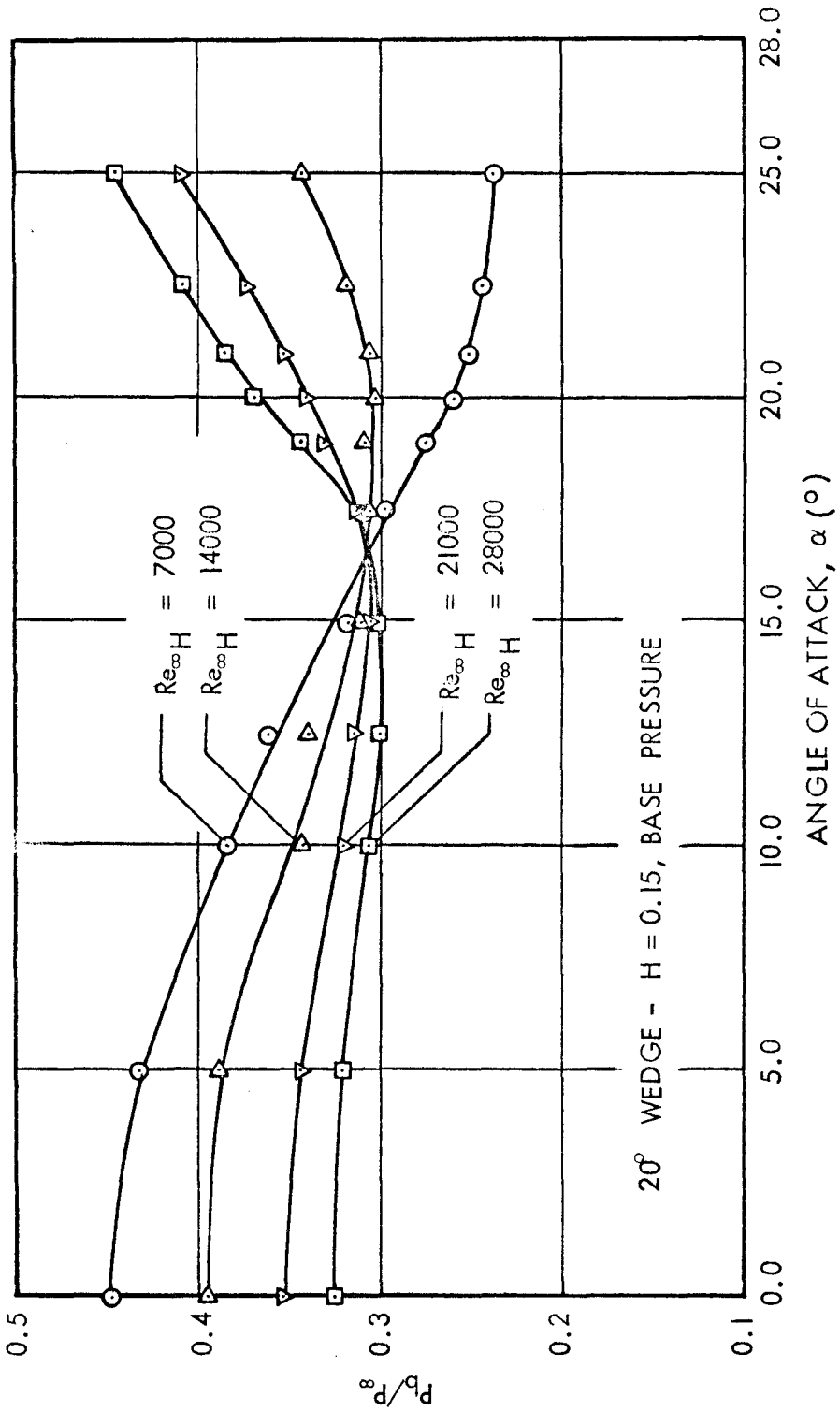

Fig. 30a BASE PRESSURE

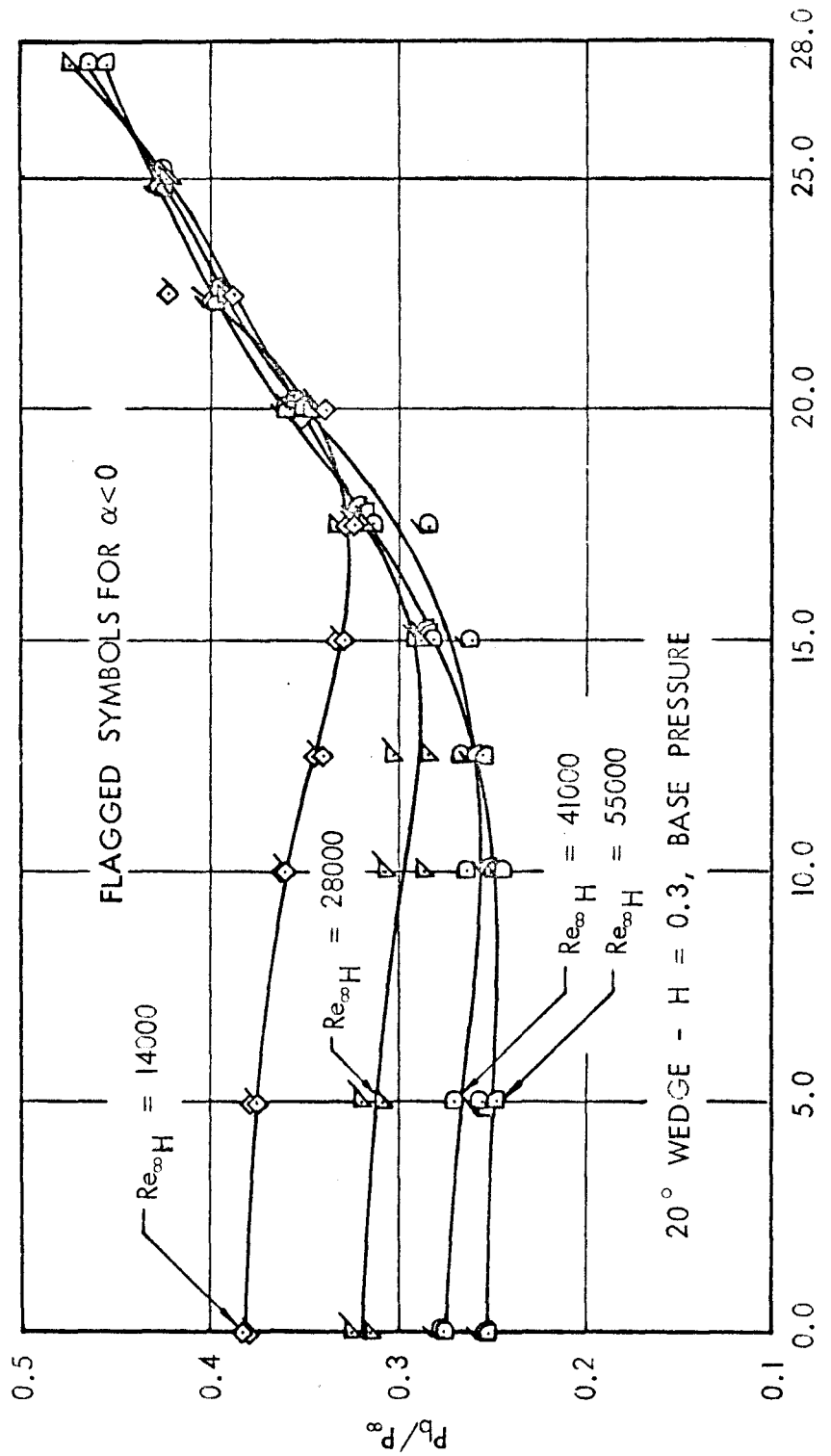

Fig. 30b BASE PRESSURE

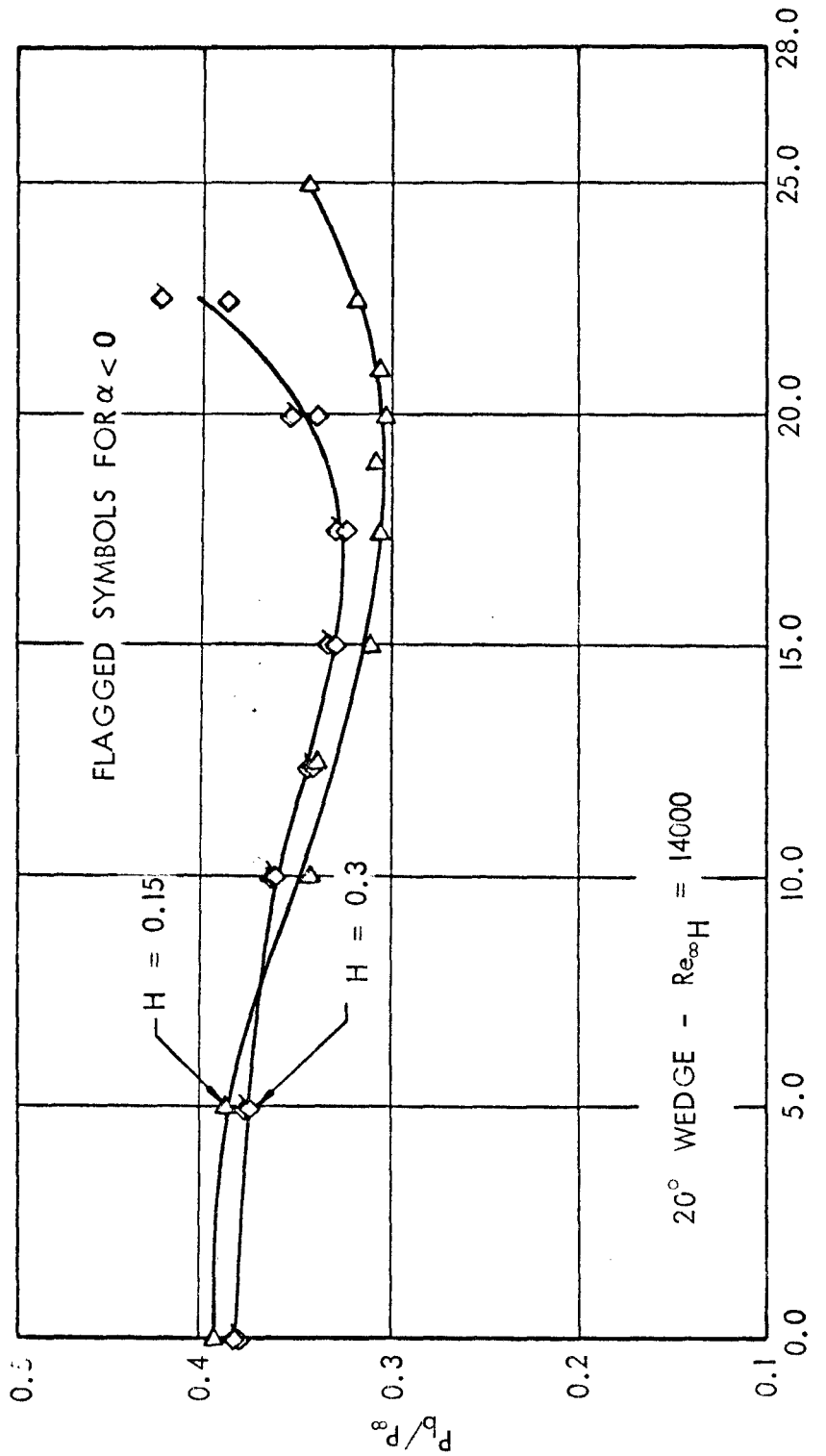

Fig. 31a CORRELATION OF BASE PRESSURE

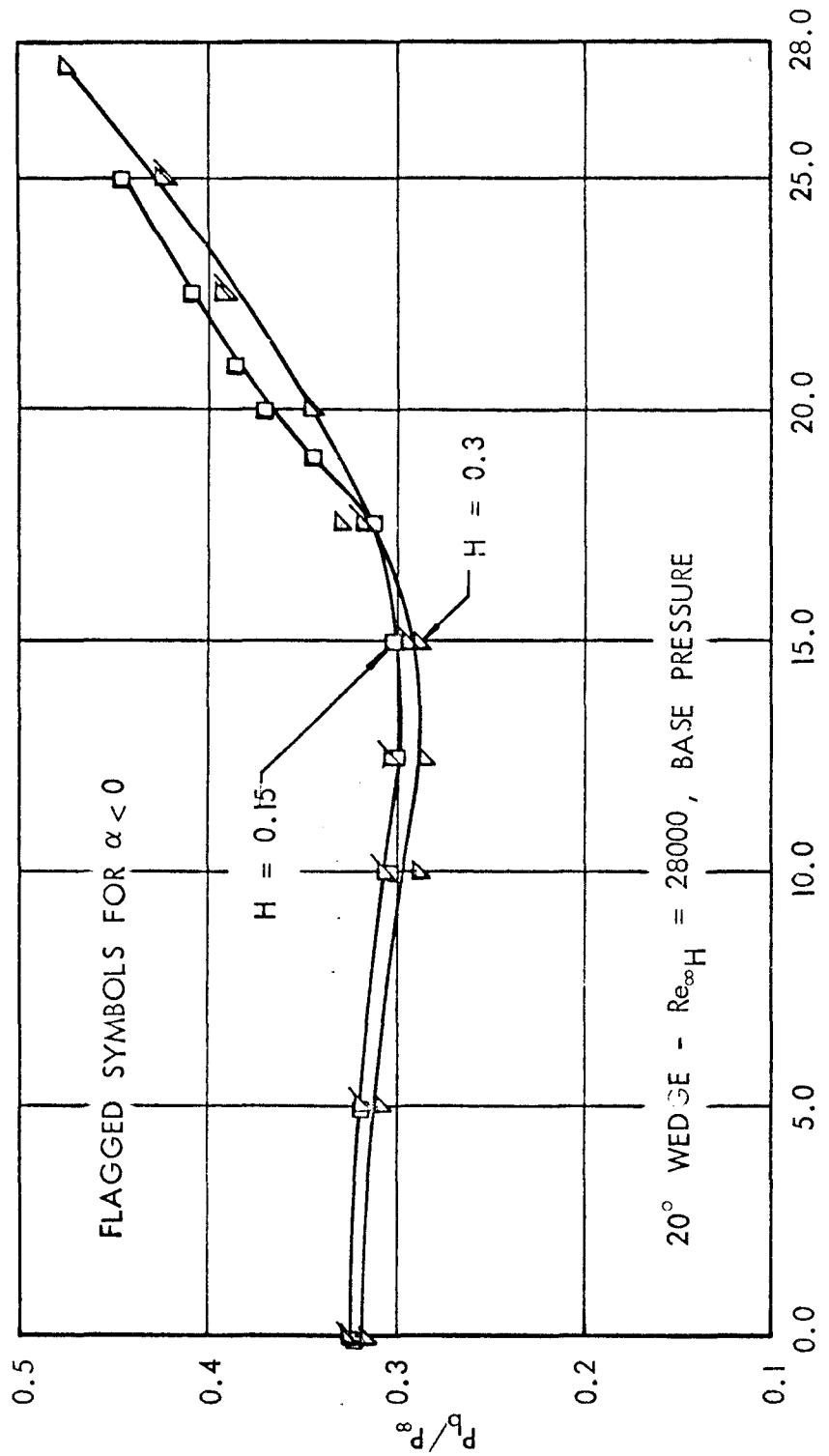

Fig. 31b CORRELATION OF BASE PRESSURE

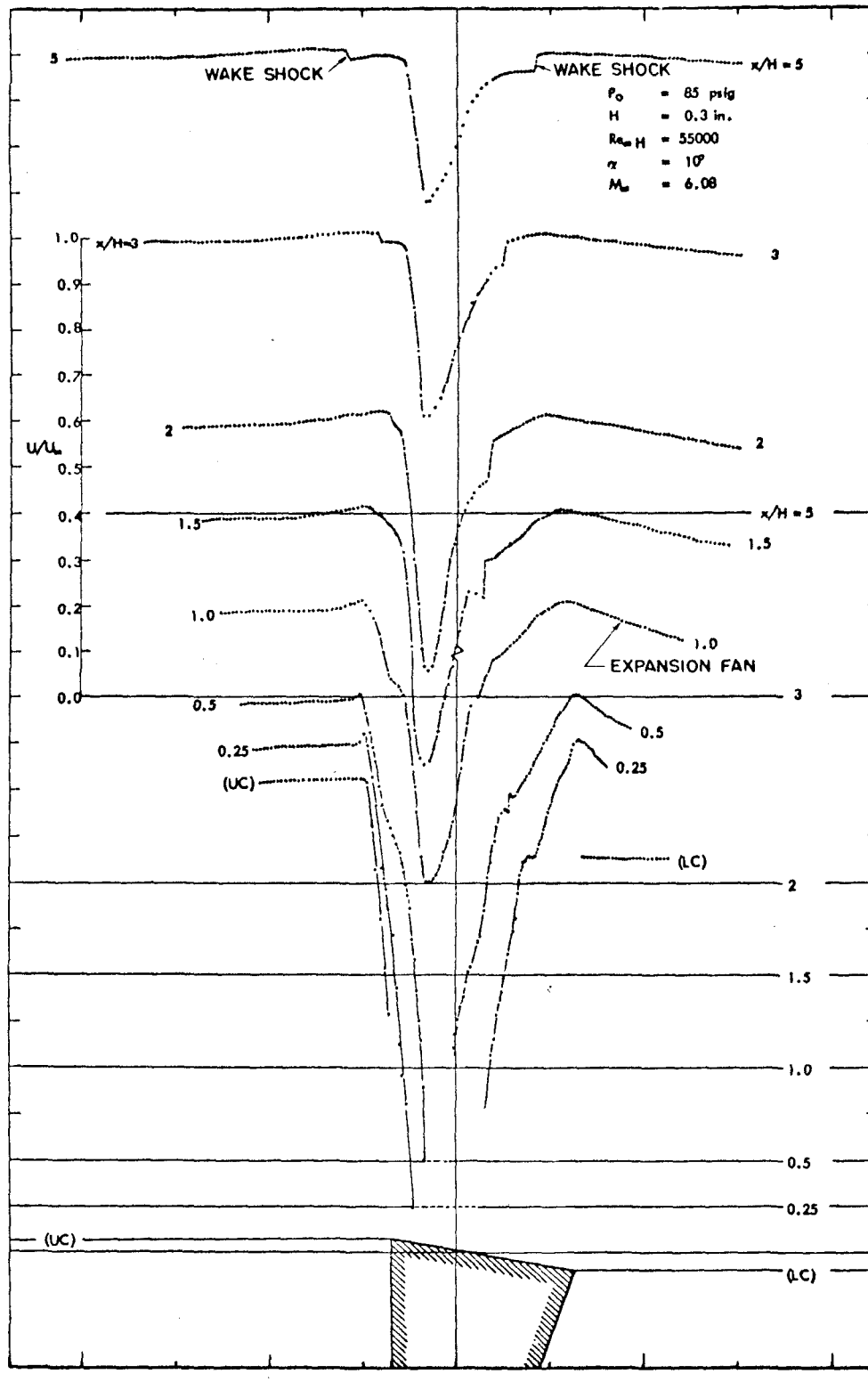

Fig. 32a NEAR WAKE VELOCITY PROFILES

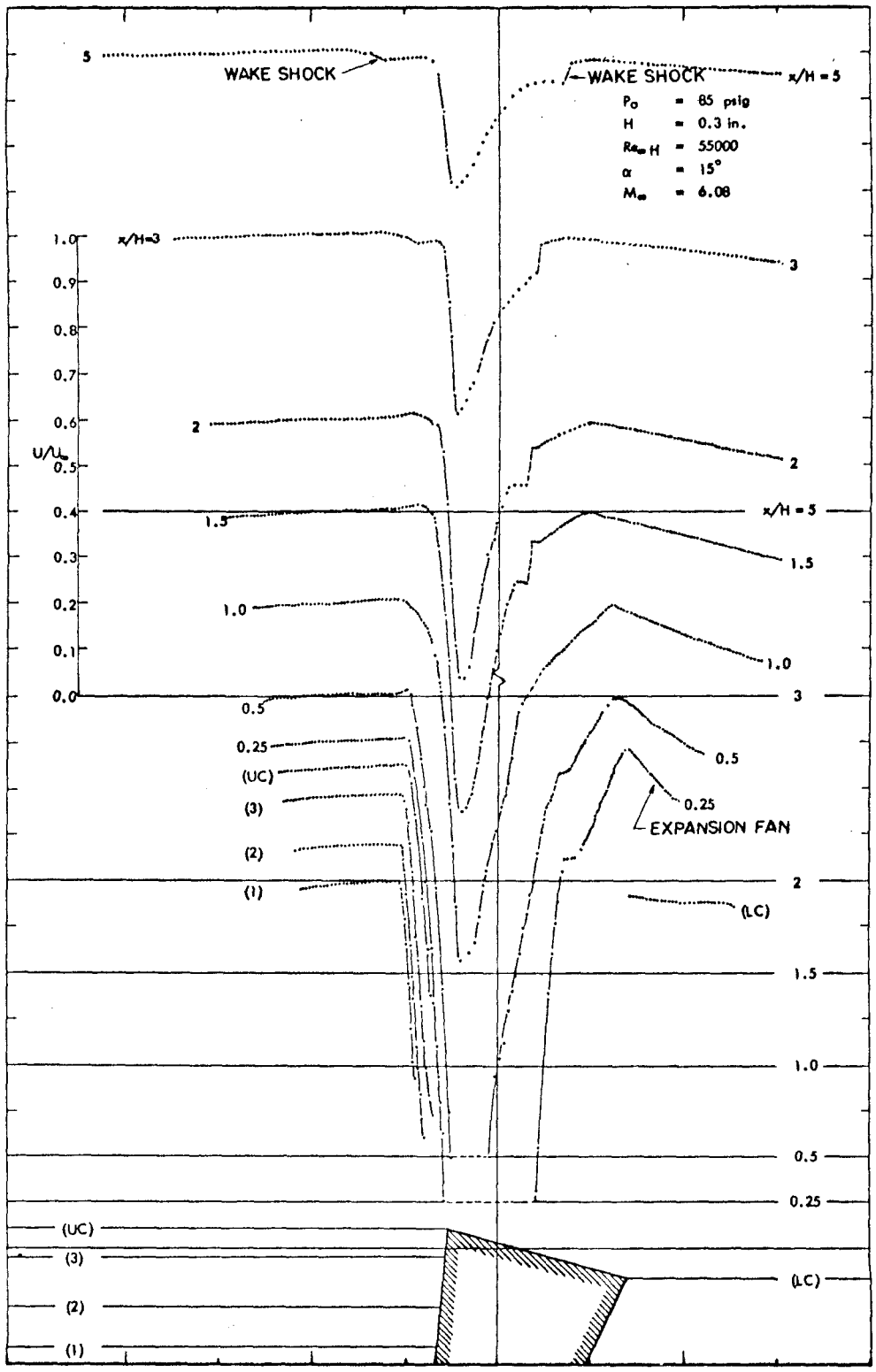

Fig. 32b NEAR WAKE VELOCITY PROFILES

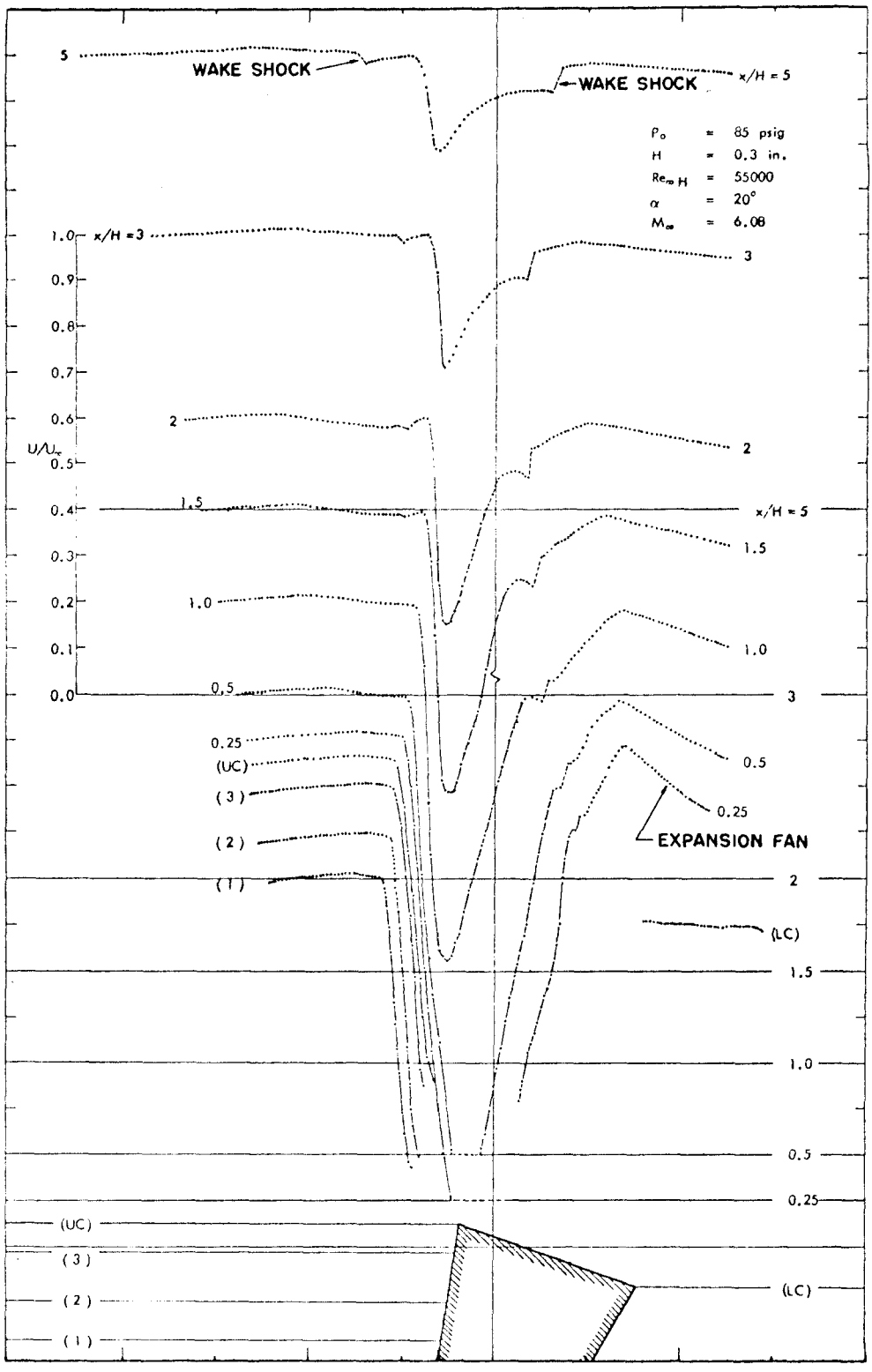

Fig. 32c NEAR WAKE VELOCITY PROFILES

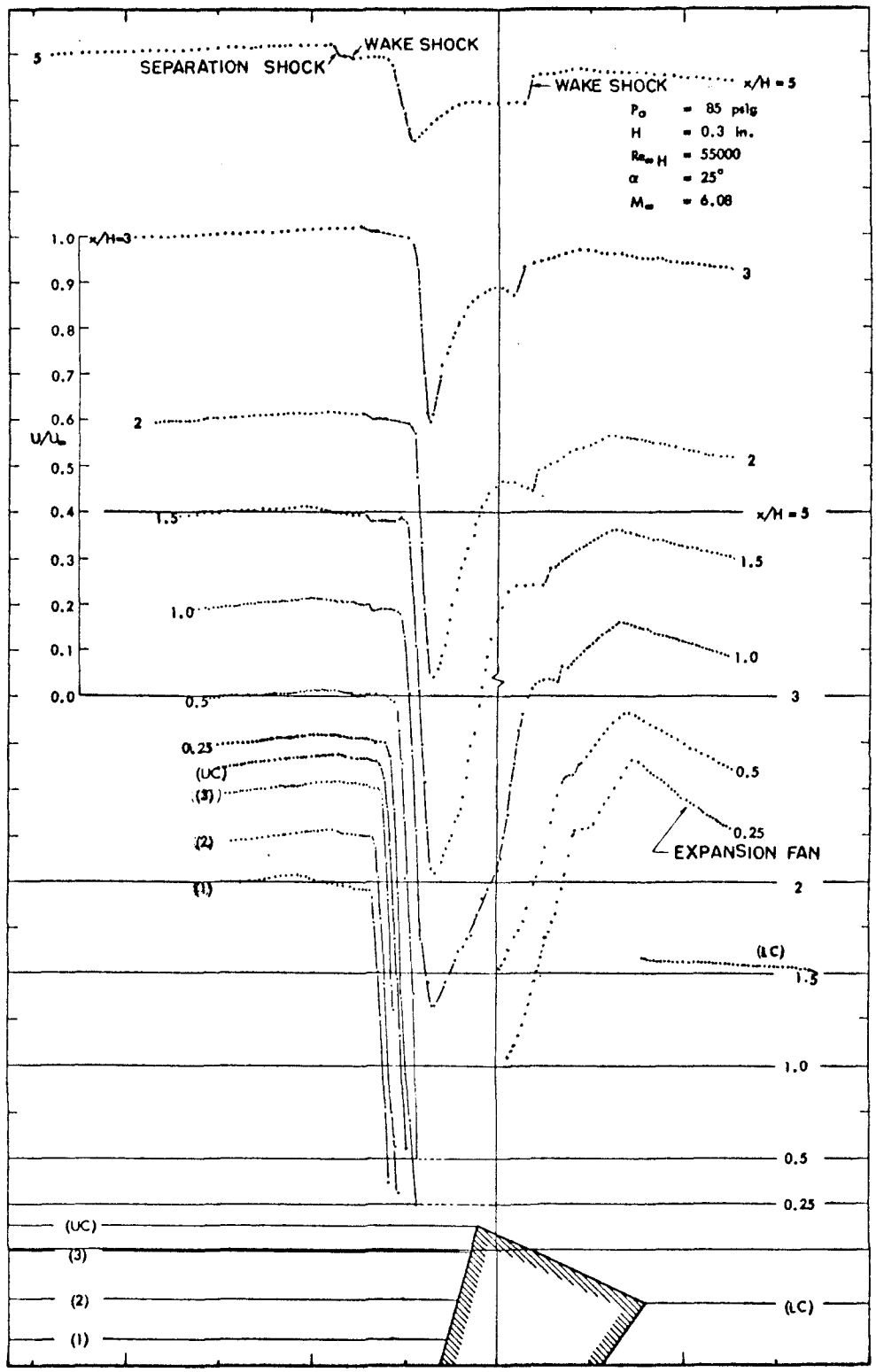

Fig. 32d NEAR WAKE VELOCITY PROFILES

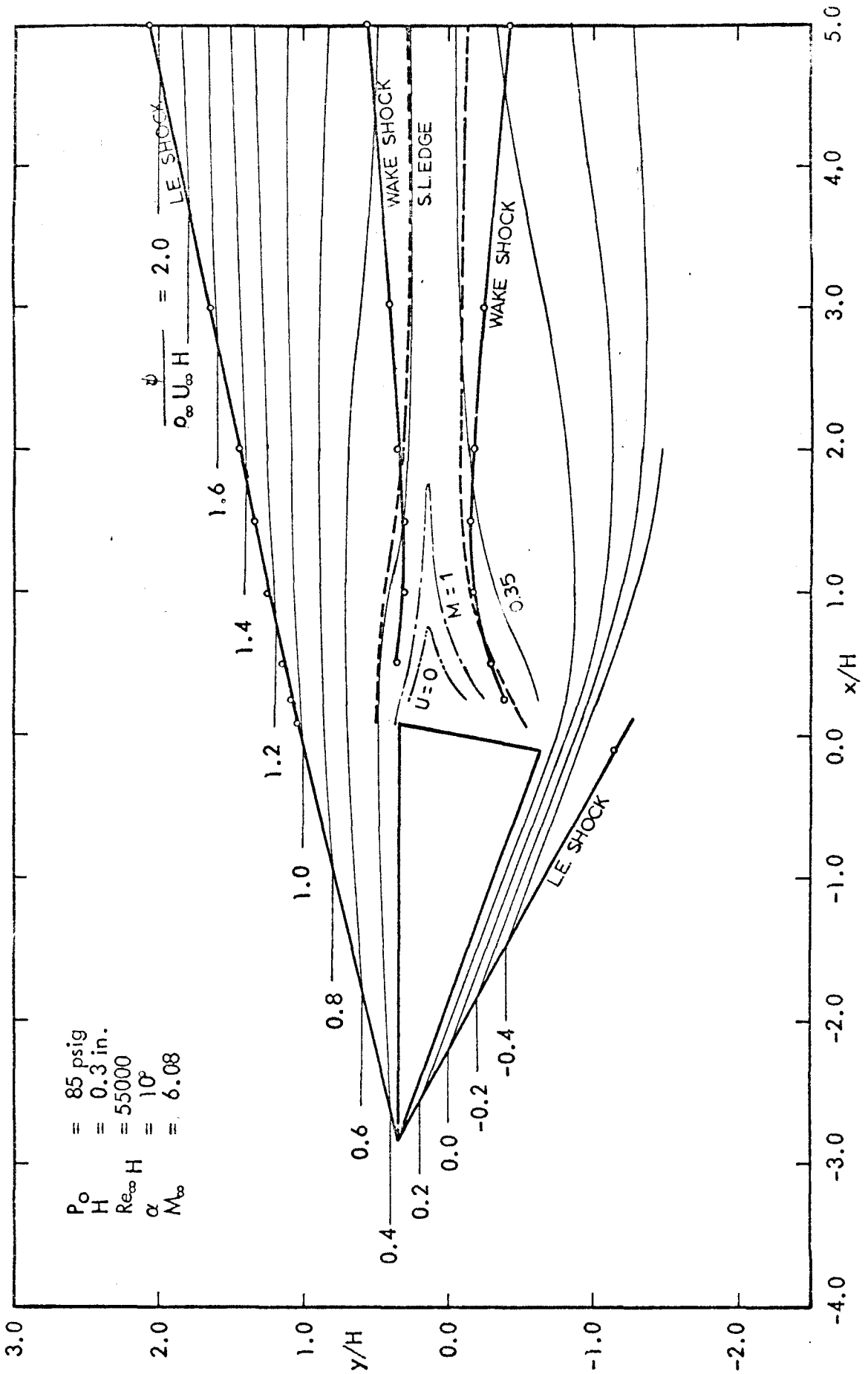

Fig. 33a NEAR WAKE FLOWFIELD

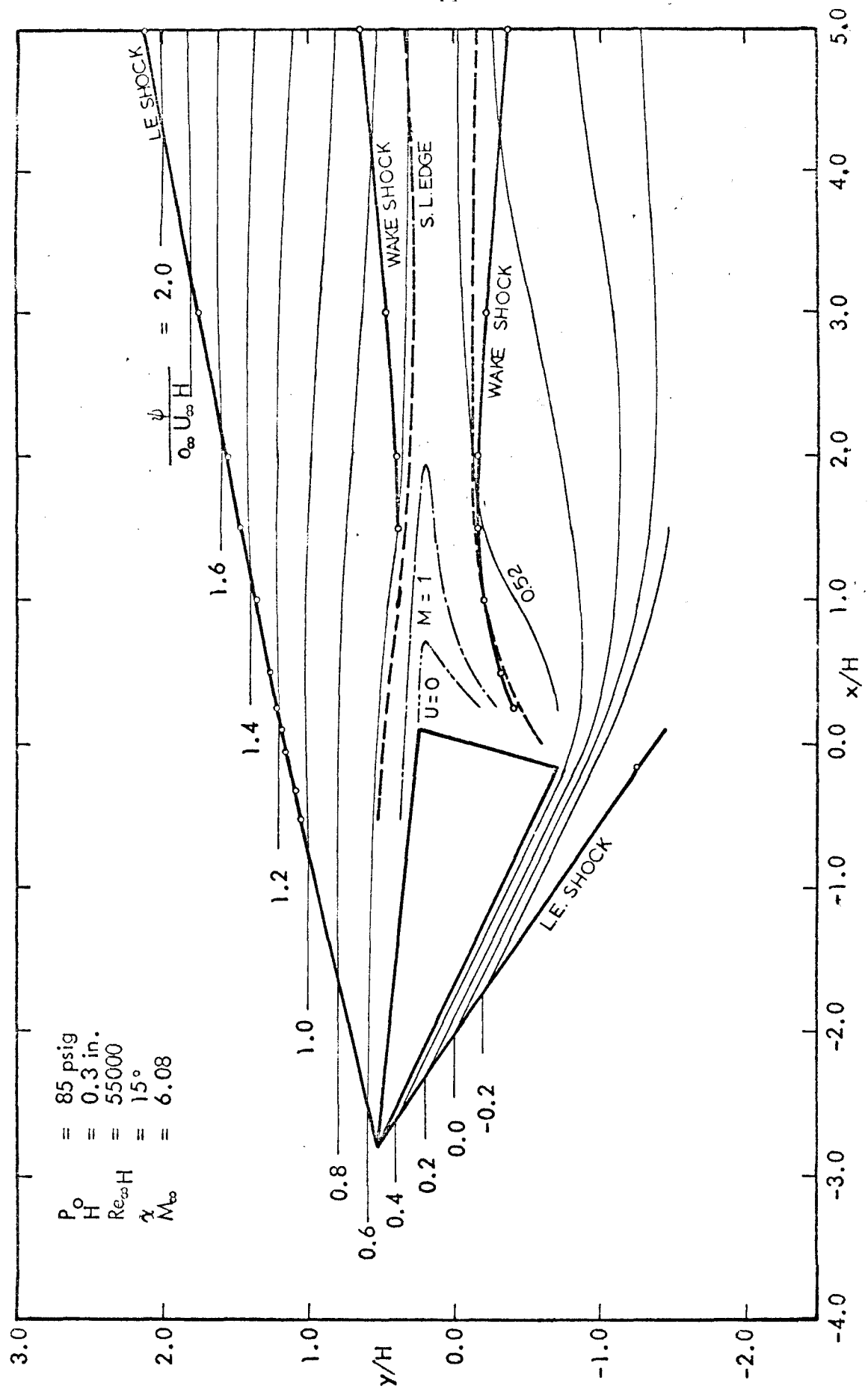

Fig. 33b NEAR WAKE FLOWFIELD

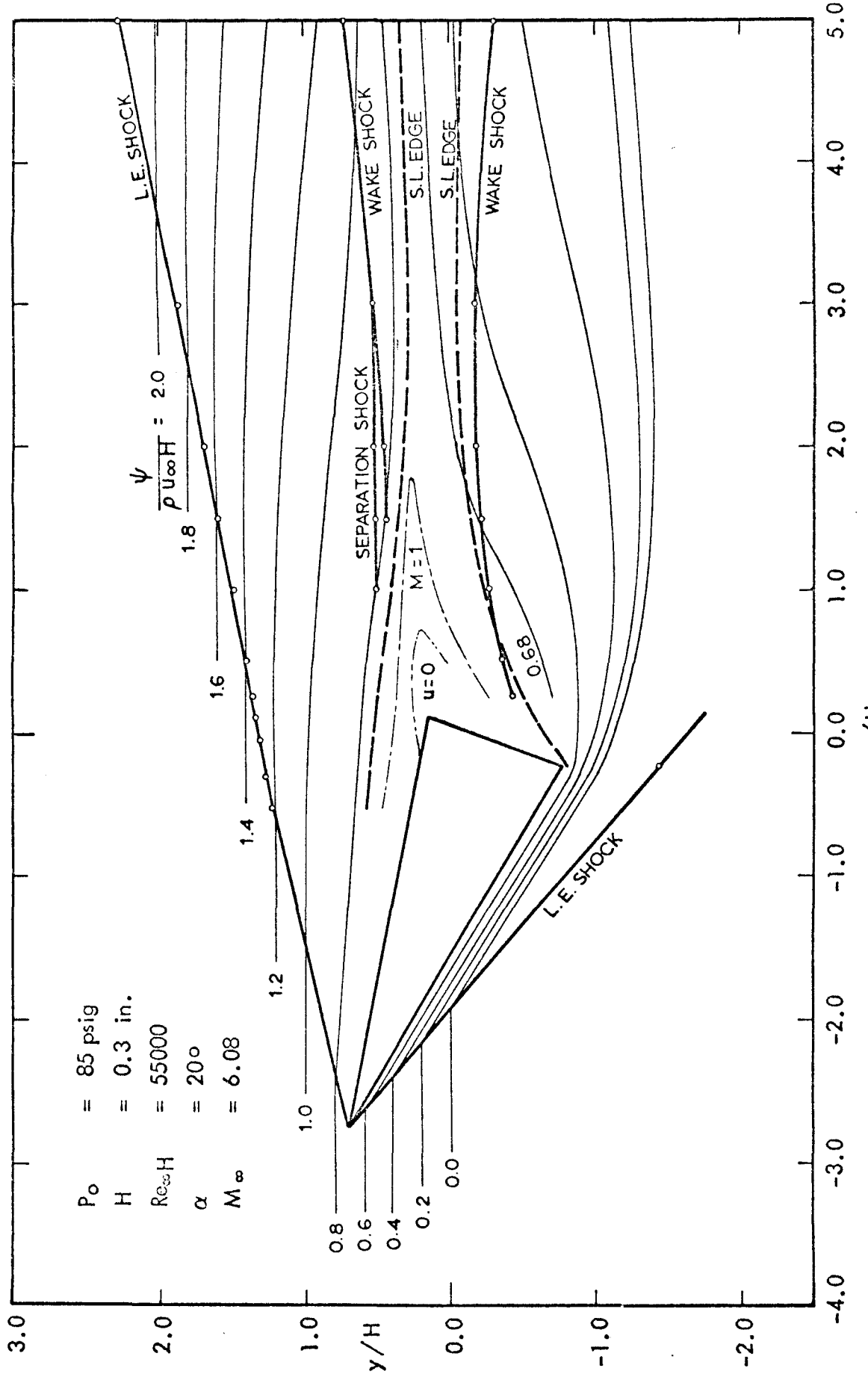

Fig. 33c NEAR WAKE FLOWFIELD

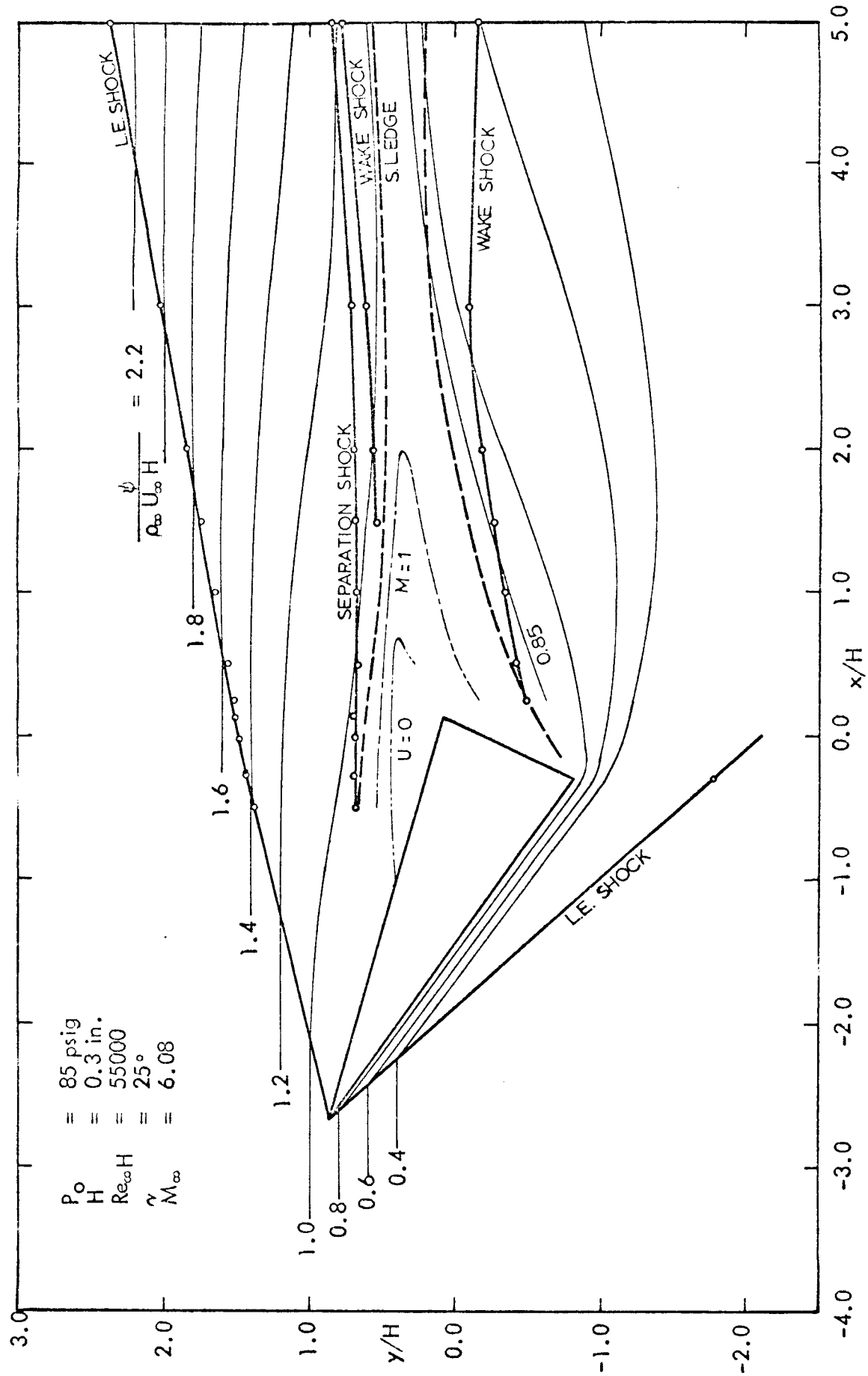

Fig. 33d NEAR WAKE FLOWFIELD